Ministry of Higher Education and Scientific Research
Hassiba Benbouali University of Chlef
Faculty of Technology
Department of Mechanical Engineering

# THESIS

to the fulfilment of the requirements for a

## DOCTORATE

Field : Science and Technology

Specialty : Mechanics and Energetic

By

**BILAL FETTAH**

---

# *Vibration Analysis Of A Shaft Supported By Two Ball Bearings With Metal Foam Damper*

---

Defended on 09/02/2023, in front of the jury composed of :

| | | | |
|---|---|---|---|
| MENDAS Mohamed | Professor | UHBChlef | President |
| BOUZIDANE Ahmed | Professor | UIK.Tiaret | Examiner |
| MERIEM BENZIANE Madjid | Professor | UHBChlef | Examiner |
| ZIDANE Ibrahim | Professor | UHBChlef | Examiner |
| ZAHLOUL Hamou | Professor | UHBChlef | Advisor |

**ACKNOWLEDGMENTS**

First of all, thanks to Allah for giving me the energy and the motivation to complete this thesis.

Second, I am extremely grateful to my supervisor, Professor. Zahloul Hamou for his invaluable advice, continuous support, and patience during my Doctoral study. His immense knowledge and plentiful experience have encouraged me in all the time of my academic research and my daily life.

I would like to thank all the jury members, namely, Pr. Mendas Mohammed, Pr. Bouzidane Ahmed, Pr. Merim Benziane Madjid, and Pr. Zidane Ibrahim, for accepting to examine my PhD thesis.

Last but not least, a special thank goes to my family and friends for their continuous support, patience and encouragements to finish this thesis. It would be impossible for me to complete my study without them.

Thank you for your helpful advice, your support during this period, for your cheerfulness, patience and love, thank you for always being on my side.

**ABSTRACT**

In rotating machinery, the adverse consequences of vibration are numerous, and these vibration problems cause the structure to fail. Therefore, the high response amplitudes of rotors should be minimized. The engineers used to add damping devices at bearing locations to decrease the vibration levels and dynamic loads. The objective of this work is to study a new design of a ball bearing with a metal foam damper in order to minimize vibration response amplitudes, transmitted forces, and sound emissions during the passage through resonance. The work consists of three aspects: firstly, we focus mainly on the metal foams and their applications in different industrial sectors; secondly, an experimental study is carried out to determine the dynamic characteristics such as stiffness and damping of aluminum foams; and, finally, a numerical study based on the finite element method of a rotor made of a flexible shaft, a disc, and two ball bearings is achieved to identify the effect of the addition of a metal foam damper on the modal response. The obtained results show that the use of metal foam as damper in a system has a good impact in the rotor vibrations.

**Key words:** metal foams,ball bearings,damping,vibration analysis,transmissibility, Finite Element Method

**RESUME**

Dans les machines tournantes, les conséquences néfastes des vibrations sont nombreuses, et ces problèmes vibratoires entraînent la défaillance de la structure. Par conséquent, les amplitudes de réponse élevées des rotors doivent être minimisées. Les ingénieurs avaient l'habitude d'ajouter des dispositifs d'amortissement aux emplacements des roulements pour réduire les niveaux de vibration et les charges dynamiques. L'objectif de ce travail est d'étudier une nouvelle conception d'un roulement à billes avec un amortisseur en mousse métallique afin de minimiser les amplitudes de réponse vibratoire, les forces transmises et les émissions sonores lors du passage en résonance. Le travail comporte trois volets : premièrement, nous nous concentrons principalement sur les mousses métalliques et leurs applications dans différents secteurs industriels ; deuxièmement, une étude expérimentale est menée pour déterminer les caractéristiques dynamiques telles que la rigidité et l'amortissement des mousses d'aluminium ; et, enfin, une étude numérique basée sur la méthode des éléments finis d'un rotor composé d'un arbre flexible, d'un disque et de deux roulements à billes est réalisée pour identifier l'effet de l'ajout d'un amortisseur en mousse métallique sur la réponse modale. Les résultats obtenus montrent que l'utilisation de mousse métallique comme amortisseur dans un système a un bon impact sur les vibrations du rotor.

**Mots clés:** mousses métalliques, roulements à billes, amortissement, analyse des vibrations, transmissibilité, méthode des éléments finis

## ملخص

**في الآلات الدوارة ، تكون العواقب السلبية للاهتزاز عديدة ، وتتسبب مشاكل الاهتزاز هذه في فشل الهيكل. لذلك ، يجب تقليل سعة الاستجابة العالية للاعمدة الدوارة. اعتاد المهندسون على إضافة أجهزة التخميد في مواقع التحميل لتقليل مستويات الاهتزاز والأحمال الديناميكية. الهدف من هذا العمل هو دراسة تصميم جديد لمحمل كروي مع مخمد رغوي معدني من أجل تقليل اتساع استجابة الاهتزاز ، والقوى المرسلة ، والانبعاثات الصوتية أثناء المرور عبر الرنين. يتكون العمل من ثلاثة جوانب: أولاً ، نركز بشكل أساسي على الرغاوي المعدنية وتطبيقاتها في القطاعات الصناعية المختلفة ؛ ثانيًا ، تم إجراء دراسة تجريبية لتحديد الخصائص الديناميكية مثل الصلابة والتخميد لرغاوي الألومنيوم ؛ وأخيرًا ، تم إجراء دراسة عددية تعتمد على طريقة العناصر المحدودة لدوار مصنوع من عمود مرن وقرص واثنين من المحامل الكروية لتحديد تأثير إضافة مثبط الرغوة المعدني على الاستجابة النموذجية. تظهر النتائج التي تم الحصول عليها أن استخدام الرغوة المعدنية كمخمد في النظام له تأثير جيد في اهتزازات الدوار.**



**الكلمات الرئيسية: الرغاوي المعدنية ، الكرات ، التخميد ، تحليل الاهتزاز ، القابلية للانتقال ، طريقة العناصر المحدودة**

**CONTENTS**

ACKNOWLEDGMENTS ..... I

ABSTRACT ..... II

RESUME ..... III

ملخص ..... IV

CONTENTS ..... V

INDEX OF FIGURES ..... VIII

INDEX OF TABLES ..... X

ABREVIATIONS AND SYMBOLS ..... XI

INTRODUCTION ..... 1

CHAPTER 01:LITERATURE REVIEW ..... 3

1-1 INTRODUCTION ..... 3

1-2 ROTORDYNAMICS ..... 3

1-2-1 RIGID AND FLEXIBLE ROTOR DEFINITION ..... 3

1-2-2 OBJECTIVES OF ROTORDYNAMICS ANALYSIS ..... 4

1-2-3 CAUSES OF VIBRATION ..... 4

1-2-3-1 MOTORS ..... 4

1-2-3-2 TURBINES ..... 5

1-2-3-3 ROTORS ..... 6

1-2-4 CONTROL OF VIBRATION ..... 6

1-2-4-1 ACTIVE VIBRATION CONTROL ..... 6

1-2-4-2 SEMI-ACTIVE VIBRATION CONTROL ..... 8

1-2-4-3 PASSIVE VIBRATION CONTROL ..... 9

1-2-5 BEARINGS AND THEIR EFFECT ON ROTORDYNAMICS ..... 9

1-2-5-1 SQUEEZE FILM DAMPER ..... 9

1-2-5-2 HYDROSTATIC BEARING ..... 10

1-2-5-3 HYDRODYNAMIC BEARINGS ..... 12

1-2-5-4 WIRE MESH BEARING ..... 13

1-2-6 INTELIGENT MATERIALS IN VIBRATION CONTROL ..... 15

1-2-6-1 ELECTRORHOLOGICAL FLUIDS DAMPER ..... 15

1-2-6-2 MAGNETORHOLOGICAL FLUIDS DAMPER ..... 16

1-3 METAL FOAMS ..... 17
1-3-1 DEFINITION OF METAL FOAMS ..... 17
1-3-2 TYPE OF METAL FOAMS ..... 18
1-3-2-1 CLOSED CELL METAL FOAMS ..... 18
1-3-2-2 OPEN CELL METAL FOAMS ..... 19
1-3-3 PROPERTIES OF METAL FOAMS ..... 19
1-3-3-1 MECHANICAL PROPERTIES ..... 19
1-3-1-2 THERMAL AND PHYSICAL PROPERTIES ..... 21
1-3-4 DAMPING IN METAL FOAMS ..... 25
1-4 CONCLUSION ..... 27
CHAPTER 02: EXPERIMENTAL STUDY ..... 28
2-1 INTRODUCTION ..... 28
2-2 EXPERIMENTAL STUDY ..... 28
2-2-1 ROTOR KIT DESCRIPTION ..... 29
2-2-2 EXPERIMENTAL SET-UP ..... 29
2-2-2-1 PROPOSED MODIFICATION AT BEARING ADAPTER ..... 38
2-2-3 TRANSMISSIBILITY RESULTS ..... 40
2-2-4 ISOLATION RESULTS ..... 43
2-3 CONCLUSION ..... 45
CHAPTER 03: NUMERICAL ANALYSIS ..... 46
3-1 INTRODUCTION ..... 46
3-2FINITE ELEMENT MODELING OF A FLEXIBLE SHAFT SUPPORTED BY TWO BALL BEARINGS ..... 46
3-2-1 ROTATING COORDINATE SYSTEM ..... 46
3-2-2 DISK ELEMENTS MODEL ..... 49
3-2-3 SHAFT MODEL ..... 51
3-2-4 BEARINGS MODEL ..... 54
3-2-5 ASSEMBLY OF THE FULL EQUATIONS OF MOTION ..... 57
3-2-6 CALCULATION OF THE STIFFNESS K AND THE VDAMPING C OF THE FOAM DAMPER ..... 58

3-2-6-1 DAMPING COEFFICIENT $\xi$ ..... 59
3-2-6-2 CALCULATION OF EQUIVALENT STIFFNESS AND DAMPING COEFFICIENTS ..... 60
3-3FREE LATERAL RESPONSE OF A FLEXIBLE SHAFT SUPPORTED BY TWO BALL BEARINGS WITHOUT METAL FOAM DAMPER ..... 61
3-3-1 MODELLING EXAMPLE ..... 61
3-4 FREE LATERAL RESPONSE OF A FLEXIBLE SHAFT SUPPORTED BY TWO BALL BEARINGS WITH METAL FOAM DAMPER ..... 65
3-4-1 RUNNING THROUGH CRITICAL SPEED ..... 65
3-5 ANALYSE OF THE RESULTS ..... 70
3-6 CONCLUSION ..... 70
GENERAL CONCLUSION AND FUTURE WORKS ..... 71
REFERENCES ..... 74
APPENDIX A: SOFTWARE EXAMPLE OF SIMPLE JEFFCOTT ROTOR ..... 84
APPENDIX B: CALCULATION OF MAPS OF CRITICAL SPEEDS AND ASSOCIATED MODE SHAPES. ..... 86
APPENDIX C: CALCULATES THE MASS, STIFFNESS AND DAMPING MATRICES FOR THE BEARINGS ..... 92
APPENDIX D: CALCULATES THE CRITICAL SPEEDS FOR THE ROTOR SYSTEM.. 94

**INDEX OF FIGURES**

**Figure 1**:Example of rotors [1] ..... 3
**Figure 2**: Francis Turbine Cavitation Damage (A) [6] and (B) [5]. ..... 5
**Figure 3**: Turbine (A) Misalignment detection [6] and (B) Breakage of Wicket gate linkage [5]. ..... 6
**Figure 4**: Vibration Frequency Spectrum Characteristics of Rotor (A) before and (B) After fault [5] ..... 6
**Figure 5:** Electrorheological squeeze film damper[8] ..... 7
**Figure 6:** NER hydrostatic squeeze film damper geometry [12] ..... 8
**Figure 7:** Designed Electrorheological damper [15] ..... 9
**Figure 8:** Squeeze Film Damper configuration. (a) SFD with central feed groove.(b) SFD with end grooves and seals [18] ..... 10
**Figure 9:** Hydraustatic bearings with magnetic fluids [20] ..... 11
**Figure 10**: Principle of hydraustatic bearing [16]. ..... 12
**Figure 11**: First generation foil bearings with axially and circumferentially uniform elastic support elements: (a) leaf type foil bearing, (b) bump type foil bearing. [45] ..... 14
**Figure 12:** (a) schematic representatin of metal mesh foil bearings, (b) photograph of a metal mesh foil bearings [47]. ..... 14
**Figure 13**: Hydraustatic damper controlled by means of an electrorheological valve [59-60]16
**Figure 14:** Dispersions of one phase into a second one. Each phase can be in one of the three states of matter [65] ..... 18
**Figure 15**: Closed cell aluminum foams [72] ..... 18
**Figure 16**: Open cell nickel foam [72] ..... 19
**Figure 17:** Typical compressive stress–strain diagram exhibited by metallic foams(adapted from reference [76]. ..... 20
**Figure 18:** Typical tensile behaviour of metal foams '(adapted from ref [76]) ..... 20
**Figure 19**: Open-cell Al foams modeled with a tetrakaidecahedron unit cell consisted of square cross-sectioned ligaments with uniform thickness 2a and length L( adapted from reference [83]. ..... 22
**Figure 20:** Bently Nevada model RK 4 rotor kit. ..... 29
**Figure 21:** Vibration Calibrator VC 21D with clamping devices. ..... 30
**Figure 22:**Schematic illustration of the non-rotating test setup ..... 31
**Figure 23:** Wire mesh damper [96] ..... 31
**Figure 24:** Rotor Kit Assembly ..... 32

**Figure 25:** Assembly design of the rotor kit ..... 33
**Figure 26:(**a) The Recemat Open Cell Metal Foam (b) Type of Small pore aluminum foams and (c) Proposed Porous bearing Damper ..... 34
**Figure 27:** Illustration of metal foam isolator in vibrating system with corresponding input and output acceleration ..... 37
**Figure 28:** (a) Schematic diagram of a single degree of freedom spring mass oscillator system. (b) approximate transfer function for relative displacement y of mass [97]. ..... 37
**Figure 29:** Technical design of the modifications at the bearing adapter ..... 39
**Figure 30:** Proposed modification of the donuts damper ..... 40
**Figure 31:** Transmissibility vs Frequency of metal foam without rubber ..... 43
**Figure 32:** Isolation efficiency curve ..... 44
**Figure 33:**Rotating (x,y)and stationary (x,y)coordinates systems[95] ..... 47
**Figure 34:** Shaft finite element rotor degree of freedom[98] ..... 52
**Figure 35**:A typical ball bearing cross section [107] ..... 56
**Figure 36:** The simple three-element example to demonstrate matrix assembly[98] ..... 57
**Figure 37:** Half Power Bandwidth Method ..... 59
**Figure 38**: Organigramm of the vibration analysis of thet rotor ..... 62
**Figure 39**:Finite element model ..... 63
**Figure 40**: Campbell diagram at 4500rpm ..... 63
**Figure 41:** Mode shapes at 4500 rev-min ..... 64
**Figure 42:**Rotor response at disk location node 4 ..... 64
**Figure 43:**Whirl orbits for the foundation excitation without metal foam damper ..... 65
**Figure 44**:Variation of the lower positive critical speeds with bearing stiffness ..... 66
**Figure 45:** Variation of the first mode shape with bearing stiffness ..... 67
**Figure 46:** Variation of the second mode shape with bearing stiffness ..... 67
**Figure 47:** Variation of the third mode shape with bearing stiffness ..... 67
**Figure 48**: Campbell diagram ..... 68
**Figure 49**: Mode shape at 4500 rev-min with metal foam damper ..... 69
**Figure 50**: Rotor response at node 4 with metal foam damper ..... 69

**INDEX OF TABLES**

**Table 1:** Input and output frequency during calibrating metal foams and transmissibility..... 41
**Table 2:**Frequency vs isolation data of aluminum foam sample under the vibration calibrator ..... 44
**Table 3**:Properties of the metal foams damper sample..... 58
**Table 4:** Parameters of calculation: ..... 61
**Table 5:**Table of calculation parameter..... 68

## ABREVIATIONS AND SYMBOLS

| | | |
|---|---|---|
| $A_0$ | Heat transfer area of control volume | ($m_2$) |
| $A_L$ | Cross-sectional area of ligament | ($m_2$) |
| $A_L(s)$ | Cross-sectional area of ligament along solid ligaments | ($m_2$) |
| $c_p$ | Specific heat | $J \cdot kg^{-1} \cdot K^{-1}$ |
| $E$ | Real modulus of elasticity | ($N/mm^2$) |
| $E_c$ | Compression modulus | ($N/mm^2$) |
| $E_t$ | Tensile modulus | ($N/mm^2$) |
| $f_d$ | Driving frequency | (Hz) |
| $f_n$ | Natural frequency | (Hz) |
| G | Shear modulus | ($N/mm^2$) |
| $H_c$ | Height of control volume | (m) |
| $K_e$ | Effective thermal conductivity | ($Wm^{-1}K^{-1}$) |
| $K_s$ | Thermal conductivity of solid ligament | (W/m K) |
| $K_f$ | Thermal conductivity of saturating fluid | (W/m K) |
| $K_c$ | Thermal conductivity of a continuous phase | ($Wm^{-1}K^{-1}$) |
| K | Permeability | (-) |
| $L$ | Length of solid ligament | (m) |
| L | Length of panel | (mm) |
| M | Mass of the panel | (g) |
| $T_{\ell m}$ | Logarithmic mean temperature of the heat source | (-) |
| T | Transmissibility | (-) |

| | | |
|---|---|---|
| $a$ | Thickness of solid ligament | (m) |
| $\beta$ | Shape factor of a representative pore | (-) |
| Y | Poison's ratio | (-) |
| $\rho$ | Density of foam | ($kg/m^3$) |
| $\rho_s$ | Density of parent metal | ($kg/m^3$) |
| $\rho/\rho_s$ | Relative density of metal foam with respect to parent metal | ($kg/m^3$) |
| $\varepsilon_D$ | Densification strain | (-) |
| $\sigma_{pl}$ | Plateau stress | (MPa) |
| $e$ | Thickness ratio of node to solid ligament | (-) |
| $\varepsilon$ | Porosity | (%) |
| $\rho^*$ | Relative density | ($kg/m^3$) |
| $c_d$ | The drag coefficient | (-) |
| $\chi$ | flow tortuosity | ($m^3/s$) |
| $\omega$ | Rotor speed | (RPM) |
| $\xi$ | damping ratio | (-) |
| Ɒ | Damping factor | (-) |

# INTRODUCTION

Vibrations in rotating machinery are due to the destabilization forces, misalignment, looseness, unbalance, and resonance. They lead to excessive wear, create unwanted noise, decrease in life of the bearing system, and finally damage the machine components.

In rotor dynamics, the high response amplitudes of rotors should be minimized in order to avoid them in normal operation of the machine. The engineers used to add damping devices at bearing locations to decrease the vibration levels and dynamic loads.

Over the past few decades, the design of rotor dynamics showed a deep evolution because of the technological progress in such materials and devices. Noise and vibration control become important nowadays. Vibration control is important to prevent from resonance, large amplitude oscillations as well as the suppression of transient vibration.

A common design technic for reducing lateral rotor vibrations in air gas turbines is to implement squeeze film dampers (SFDs) with traditional ball bearings. The ball bearings and SFD become a means of controlling the vibrations of the rotors and the forces transmitted to the supports during the passage through critical speeds. If the damping is too large, the SFD acts as a rigid constraint to the rotor-bearing system with large forces transmitted to the supporting structure If damping is too light, the damper is ineffective and likely to permit large amplitudes of vibratory motion with likely sub synchronous motions.

Ball Element Bearing is an essential component in mechanical transmission to reduce friction between rotating parts. Nowadays, with the development of electrical motor in mechanical industry, ball element bearings may work at very high rotation speed. In addition to increasing the performance of these components, the provision of damping is a major concern.

The search for ever greater rotational speeds in turbomachines requires designers of shaft lines to find an ever-better match in the choice of the guiding and sealing components that compose them. Among the guide components, ball bearings are one of the most preferred solutions. However, if critical speeds must be crossed to reach the nominal speed, the ball bearings, which have very high stiffness but little or no damping, must be supplemented by damping devices.

The objective of this work is to study a new design of a ball bearing with a metal foam damper.

This new concept is designed for:

- ✓ reduce the rotor vibration amplitudes.
- ✓ minimize the transmitted forces into the supports.

- ✓ suppress the sound emissions during the passage through resonance.

A dynamic test is carried out on metal foam damper specimens made of aluminum foam in order to identify their dynamics characteristics such as the stiffness and damping.

The key modification take place in the bearing adapter of the Bently Nevada Rotor Kit, the housing covering the outer rings of the ball bearings will be modified in order to obtain a vibratory analysis with and without the use of a metal foam damper.

A numerical analysis by using the software Matlab® based on finite element method to study the free response of rototing machinel with and without the use of metal foam damper.

The thesis is divided into three chapters. It begins with a detailed introduction to the topic of research. In the first chapter, a literature review on rotordynamics will carried out. this section divided into two parts;

- ✓ First one is reviewing the main problem of vibrations in rotating machinery as well as the control of vibration in modern flexible rotors by means of squeeze film dampers, Electrorheological fluids and the Magnetorehological fluids dampers also the bearings and their effects on rotordynamics have been also cited.
- ✓ Second one represents the metal foams, their main properties and important research that used the potential of this new material as dampning sources in engineering application.

The second chapter describes the experimental set-up of vibration calibrator VC21D and gives the main features of the transmissibility and isolation efficiency of metal foam damper specimens.

Chapter 03 is about numerical simulation analysis with MATLAB® based on finite element method and the numerical model of a rotor. The software is set of scripts that consists of three aspects:

- ✓ Defining the model, forcing and operating conditions.
- ✓ Analysing the system.
- ✓ Interpretation of the model and results.

The free response of the rotor model is presented with and without the use of metal foam damper.

Finally, the main results are shown, the campbell diagram, the variation of the modes shapes with bearings stiffness and the response amplitude with the variation of the frequency.

.

# CHAPTER 01:LITERATURE REVIEW

## 1-1 INTRODUCTION

This chapter is a literarture review on the recent studies that contribute to reducing vibration in rotordynamics system. We are going to divide this chapter into two parts, the first one represent the studies that related with the classifications of rotors, main objectives of rotordynamics analysis and vibration in flexible rotor dynamics, its main reasons and the techniques that have made to minimize the unwanted effect of vibrations in rotating machinery such as squeeze film dampers as well as we mention how to control vibrations and minimize the forces transmissed during the passage through critical speed . The second one represents the metal foams, their types, their main properties and important research that used the potential of this new material as dampning sources in engineering application in order to suppress the vibrations.

## 1-2 ROTORDYNAMICS

rotor dynamic is concerned with the study of the stability of the movements of rotating machines. The analysis of the dynamics of rotors allows us to secure and improve the performance of these machines. When the rotational speed of the rotors increases, its vibration level often crosses a critical threshold which is called critical speed. This vibration is usually excited by an imbalance of the rotors, and if the amplitude of the vibration at these speeds becomes excessive, it can causes catastrophic failure to the whole system.

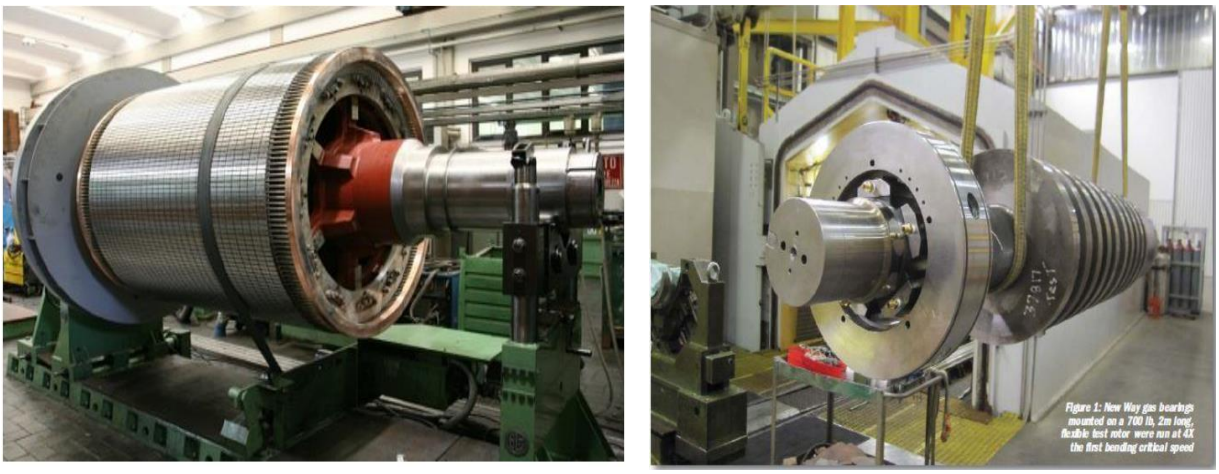


**Figure 1**:Example of rotors [1]

### 1-2-1 RIGID AND FLEXIBLE ROTOR DEFINITION

There are two historical definitions of rigid and flexible rotors.

A common industry standard, as specified in API 541 and other specifications, defines a rotor as rigid when it runs at a speed lower than its first critical speed. On the other hand, if

the rotor operates above its first critical speed, it is considered flexible [2].

The other definition of rotor flexibility is more scholarly and takes into account rotor deformations arising from unbalance and the necessary balancing techniques. When unbalance forces are not strong enough to cause the rotor to bend, it can be treated as a rigid body and balanced with rigid rotor balancing techniques.

Hartog [3] view is that any rotor that operates at a speed above half of its first critical speed shall be treated as flexible rotor. Since there is no change in vibration phase angle because the rotor has not passed the first critical, the current definitions of flexible and rigid rotors are not sufficient to describe all the practical problems presented in the industry. Even if the problem is simply a definition in a specification.

### 1-2-2 OBJECTIVES OF ROTORDYNAMICS ANALYSIS

In designing ,operating and troubleshooting of rotors, rotordynamics analysis can help to achieve the following objectives [4]:

- ✓ Predict critical speeds.
- ✓ Determine design modification to change the critical speed.
- ✓ Predict natural frequencies of torsional vibrations.
- ✓ Calculate balance correction masses and locations form measured vibration data.
- ✓ Predict amplitude of synchronous vibration caused by rotor imbalance.
- ✓ Predict threshold speeds and vibration frequencies for dynamic instability.
- ✓ Determine design modification to suppress dynamic instabilities.

### 1-2-3 CAUSES OF VIBRATION

Causes of vibration on rotating machinery equipment such as motors, turbines and rotors of the generators [5] have been illustrated in detail in this section as follows:

#### 1-2-3-1 MOTORS

The vibration in motors are classified as mechanical,aerodynamic and electromagnetic [5].

Mechanical causes of vibration are due to:

- ✓ Imbalance,
- ✓ Misalignements,
- ✓ Winding damage due to mechanical shock,
- ✓ Defective bearing,
- ✓ Looseness, and
- ✓ Soft foot impact or fretting etc.

Aerodynamic reasons of vibration in motors are due to:

- ✓ Discrete blade passing frequencies,
- ✓ Resonant Volume excitations with in motor,
- ✓ Ventilation fans and
- ✓ Broad band turbulence etc.

**1-2-3-2 TURBINES**

Vibration in hydraulic turbine [5] is due to extreme force fluctuations caused by cavitations. Vibration conditioning monitoring can be used to find the frequency at which resonance occurs in foundation and turbine supporting structure.

The essential reason for turbine erosive wear is cavitation, the damage of a francis hydro turbine due to cavitations has been shown in figure 02.

A B

**Figure 2**: Francis Turbine Cavitation Damage (A) [6] and (B) [5].

The main causes of vibration in turbine are :

- ✓ defect in bearings
- ✓ improper lubrication
- ✓ imbalance
- ✓ eccentricity
- ✓ misalignment

The picture, in which workers trying to detect the misalignment has been shown in Figure 3 (A). Misalignment from the line of shafts causes vibration in radial as well as in axial directions. These vibrations increase with rotational frequency of lower order harmonics [5].

It also leads to bearing failure and overheating [5].The shaft misalignment can be either angular or offset. If it is angular, the angle between the machine moved and the shaft center

line of a stationary machine is different in vertical and horizontal planes.

This angle is zero degrees for any stationary machine. Breakage of wicket gate linkage due to misalignment has been shown in figure 3 (B)

A B

**Figure 3**: Turbine (A) Misalignment detection [6] and (B) Breakage of Wicket gate linkage [5].

### 1-2-3-3 ROTORS

When a fault occurs, the rotor vibration increases with frequency. Due to rotor winding inter-turn fault, the air-gap distorts cause imbalanced magnetic pull on the rotor. This causes pulsating magnetic pull on the stator that ultimately results in stator vibrating [5].

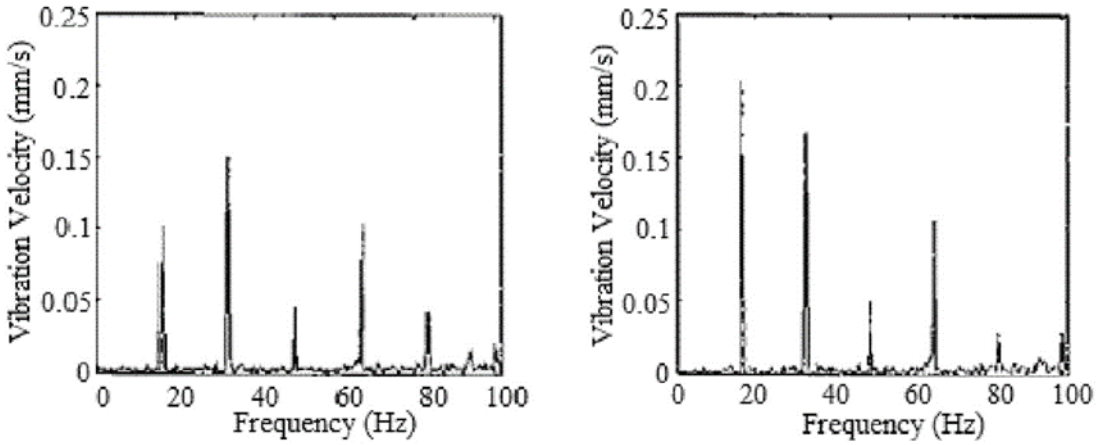


A B

**Figure 4**: Vibration Frequency Spectrum Characteristics of Rotor (A) before and (B) After fault [5]

## 1-2-4 CONTROL OF VIBRATION

Reduction of vibrations is still one of the key challenges in rotordynamics. To this end, one can think of three kinds of approaches: passive, active and semi active control means for the minimization of vibrations.

### 1-2-4-1 ACTIVE VIBRATION CONTROL

Important attempts in eurocopter's research activities on passive and active vibration

control in order to reduce the rotor induced vibration of a passenger friendly helicopter cabin [10].Jiancheng Fang et al [11] carried out a research on active vibration control method in order to minimize vibrations caused by rotor imbalance in an active magnetic bearings system. This method achieved the minimum vibration forces and torque within vibration displacement.Olivier Bonneau et al [12] studied the nonlinear dynamic beahaviour of flexible shaft supported at one end by ball bearings and at the other by an active squeeze film damper. They find that squeeze film damper dissipate a lot of energy near the passage through critical speed and there is decrease in the flexible rotor amplitude response.

In [12] the author proposed a new approach to control the vibration of the shaft supported bearing based on electrorheological squeeze film damper. They focus on adding to the SFD an ER fluids and apply an electric field between two electrodes.

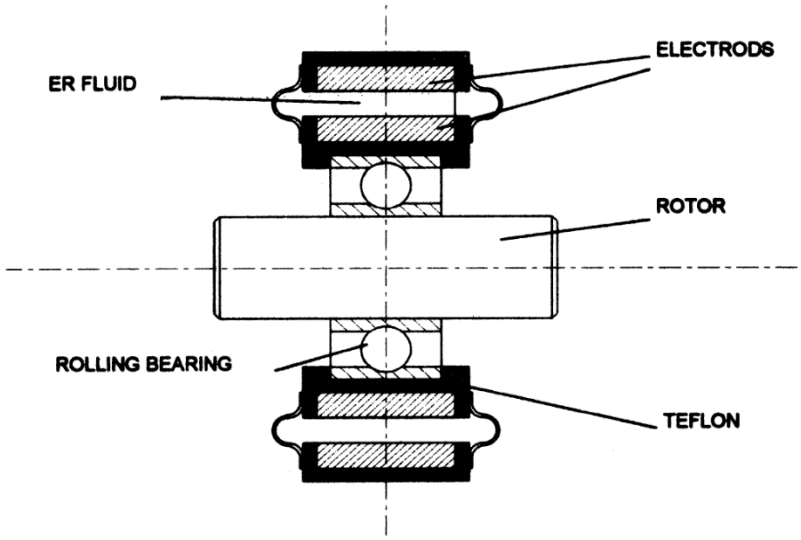


**Figure 5:** Electrorheological squeeze film damper[8]

Bouzidane.A et al [12-13] presented important study of the non linear dynamic behaviour of flexible shaft supported by smart hydrostatic squeeze film dampers. A negative electrorheological fluid feeds into the SFD. The Smart Hydrostatic SFD used to attenuate the transient response of the shaft, minimizing the transmitted forces to the foundation and lead to efficient active vibration control of modern flexible rotor.

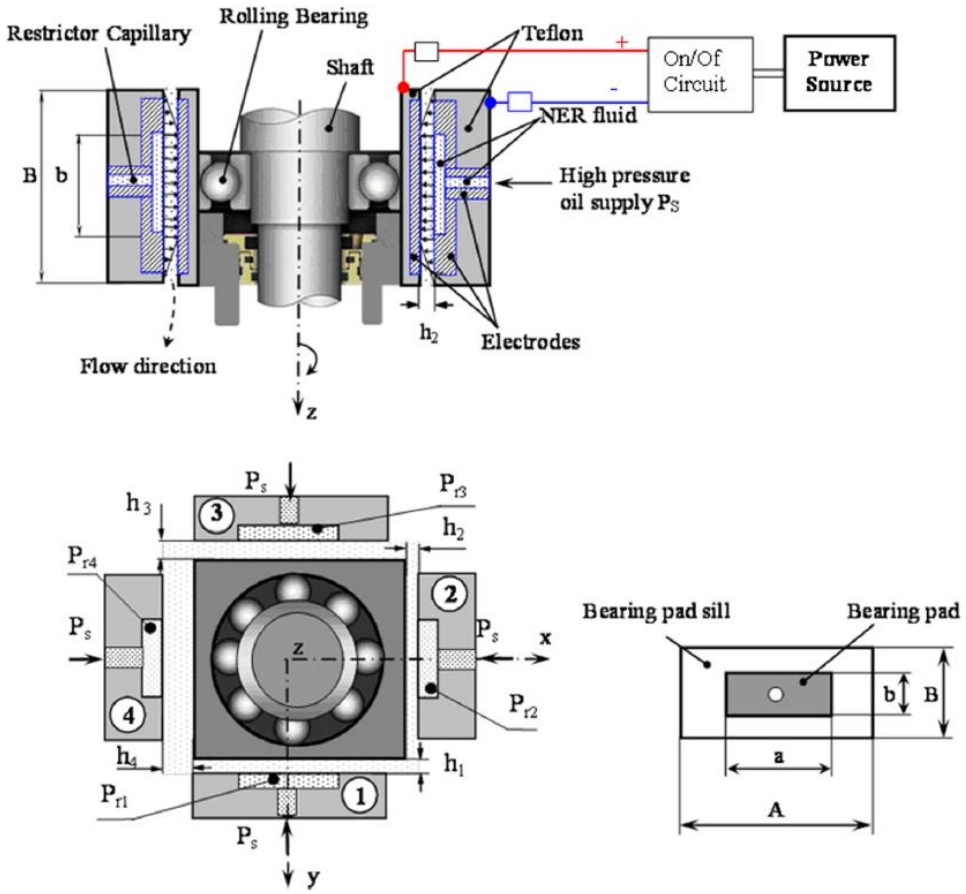


**Figure 6:** NER hydrostatic squeeze film damper geometry [12]

Figure 06 represents the developed negative electrorheological fluid hydrostatic journal bearing by Bouzidane .A et al [12] in order to study the effects of the Electrorheological fluid and rotational speed on the transient amplitude-speed response as well as the transmitted forces for a flexible shaft supported partly by an Electrorheological fluid hydrostatic squeeze film damper.

Olivier Bonneau et al [14] studied a new kind of active bearing for rotor vibration atteunuation. The variable bearing clearence permits for more energy to dissipated and lead to decreasing the dynamic amplitude of the unbalanced rotor in the critical speed range.

### 1-2-4-2 SEMI-ACTIVE VIBRATION CONTROL

To avoid the unwanted effect of vibrations in high speed flexible rotor. Artificial intelligent was used for this purpose to more vibration control, Seungchul et al [15] designed a new compact Electrorheological damper to atteunuate the rotor vibration using semi active vibration control approach, taking into account the stiffening effect of the point damper in flexible rotor applications.

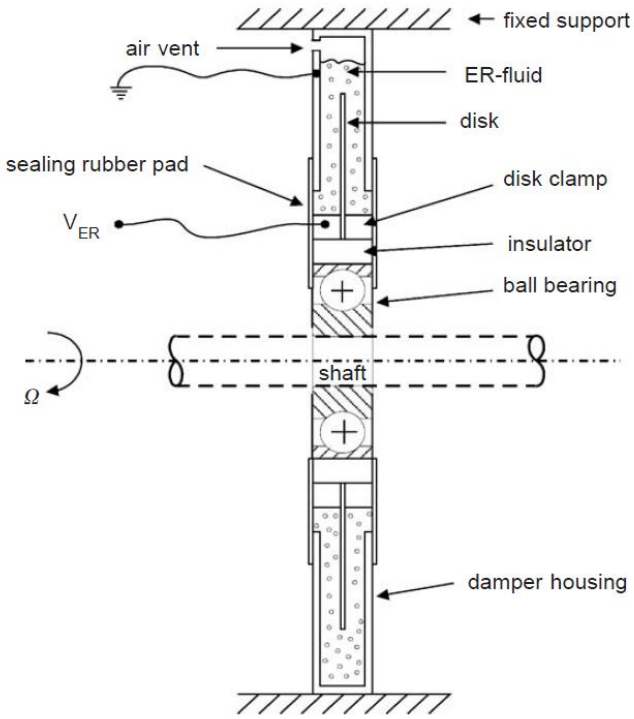


**Figure 7:** Designed Electrorheological damper [15]

Figure 7 represents the Electrorheological damper that contribute to atteunuate vibrations by [15].

### 1-2-4-3 PASSIVE VIBRATION CONTROL

Passive vibration insulation and dynamic vibration absorption, having the advantages of easy application, reliable operation and no energy consumption, are common technics used in shaft-bearing systems. However, for the control of low frequency vibration of multiple harmonics, neither of them can yield satisfying suppression. It is necessary to combine passive methods with active control to obtain satisfying attenuation of low-frequency vibrations [16]

## 1-2-5 BEARINGS AND THEIR EFFECT ON ROTORDYNAMICS

Bearings constitute one of the most critical components in turbo and rotating machinery today.Their influence on the rotordynamic performance, life, and reliability of the machine cannot be ignored. Many of the problems we face with machinery today can be attributed to the design and application of the bearings [17].

### 1-2-5-1 SQUEEZE FILM DAMPER

In rotor systems, a squeeze film damper is a lubricated component that provides viscous damping. It serves several functions, including structural isolation, reducing rotor response

amplitude to imbalance, and dampening rotordynamic instability.

High-speed turbomachinery requires squeeze film dampers (SFDs) due to their unique benefits. These include the dissipation of vibration energy and isolation of structural components, as well as the ability to improve dynamic stability in rotor-bearing systems that are inherently unstable. One primary application of SFDs is in aircraft jet engines, where they provide viscous damping to rolling element bearings with little or no damping. Another significant use is in high-performance compressor units, where SFDs are installed in series with tilting pad bearings. This configuration softens bearing support stiffness while also serving as a safety measure against rotordynamic instabilities [18].

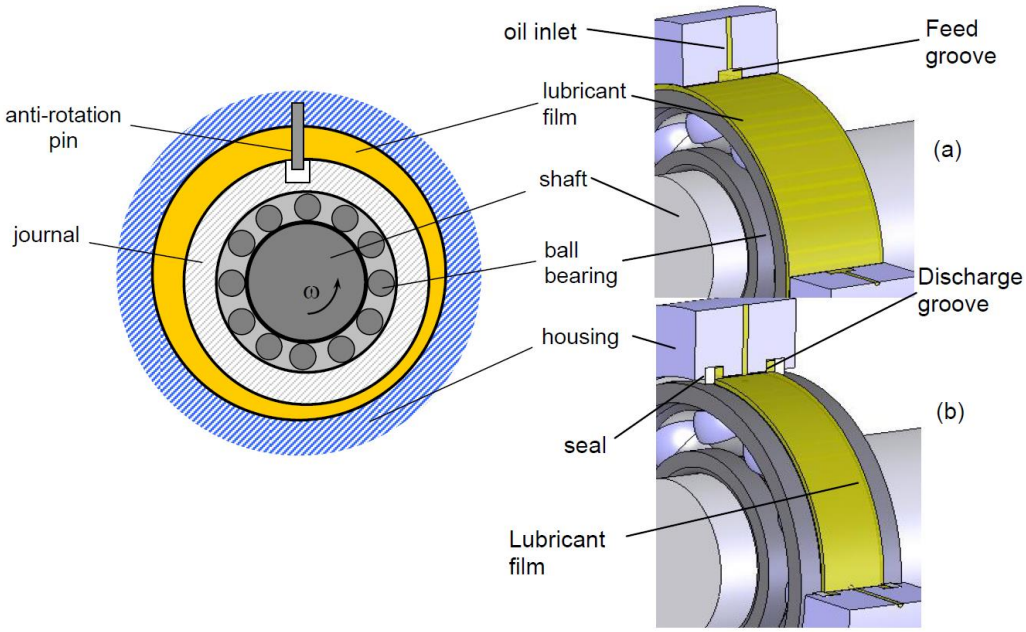


**Figure 8:** Squeeze Film Damper configuration. (a) SFD with central feed groove.(b) SFD with end grooves and seals [18]

Roberts.J.B et al [19] investigated experimentally the dynamic response of a flexible power transmission shaft by means of squeeze film damper. They found at high rotation speed that the SFD proved to be an effective device for suppressing dangerous vibrations with in the vicinity of critical speed.

### 1-2-5-2 HYDROSTATIC BEARING

In hydrostatic (also called externally pressurized) lubricated bearings the bearing surfaces are separated by a fluid film maintained by a pressure source outside the bearing. Therefore, these bearings are used when the requirements are extreme as in large telescopes and radar tracking units, where extremely heavy loads and extremely low speeds are used.

Hydrostatic bearings avoid low friction and extremely high load carrying capacity at low speed.

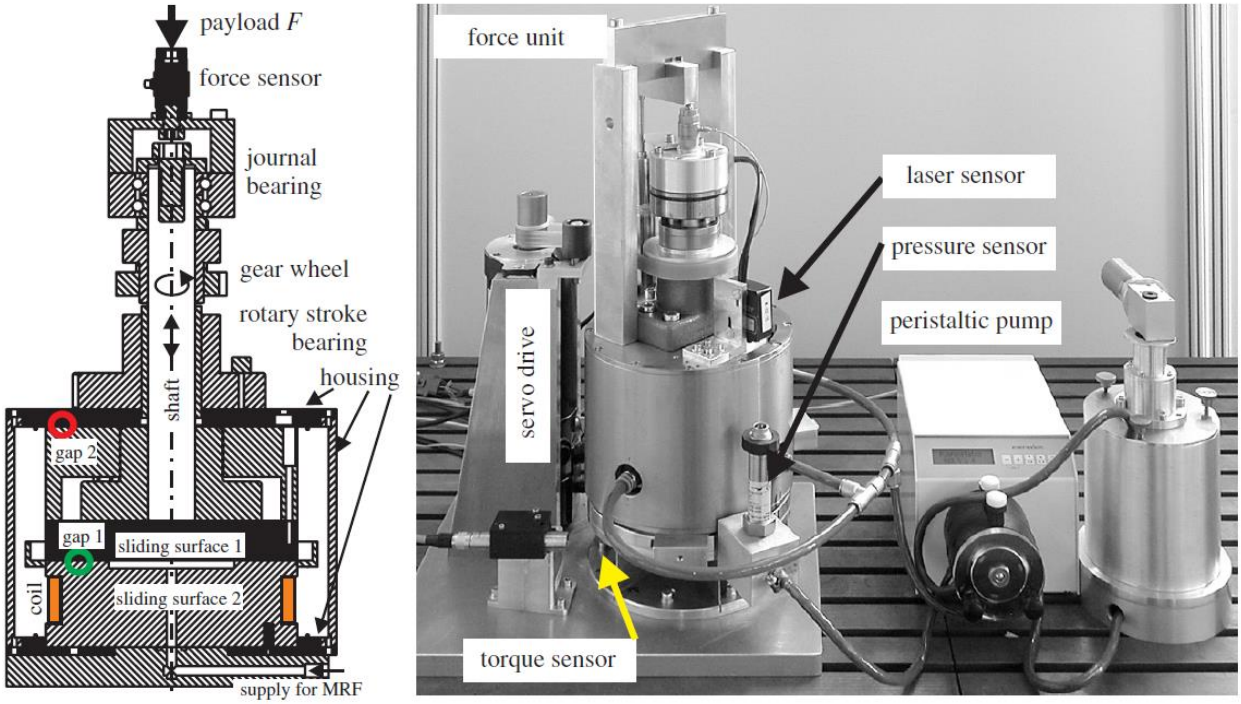


**Figure 9:** Hydraustatic bearings with magnetic fluids [20]

Hydrostatic bearings are an established technology in the field of machine tools. A conventional hydrostatic bearing consists of two sliding surfaces that are separated by a thin oil film. The oil is pressed with a constant flow rate $Q$ by an external pump through the evolving gap. In figure 10 this principle is shown.

If the oil flow rate and the load are staying constant, the gap h is constant. The bearing force depends only on the pressure in the pad pt and the effective pad area $A_{eff}$.[21]

$$F(Q) = p_t(Q).A_{eff} \tag{1}$$

The effective pad area is larger than the physical pad size because a part of the land contributes to the bearing force. Assuming a linear decrease of the pressure along the land, the mean value of the pressure inside the land is $\frac{1}{2}p_t$ . To calculate $p_t(Q)$ some calculations areneeded. For Newtonian fluids which are used in conventional devices is well known ($\kappa = viscosity$).

$$F(Q) = \frac{12\,.\,l_s\,.\,\kappa.\,Q}{b_t h^3}\,.A_{eff} \tag{2}$$

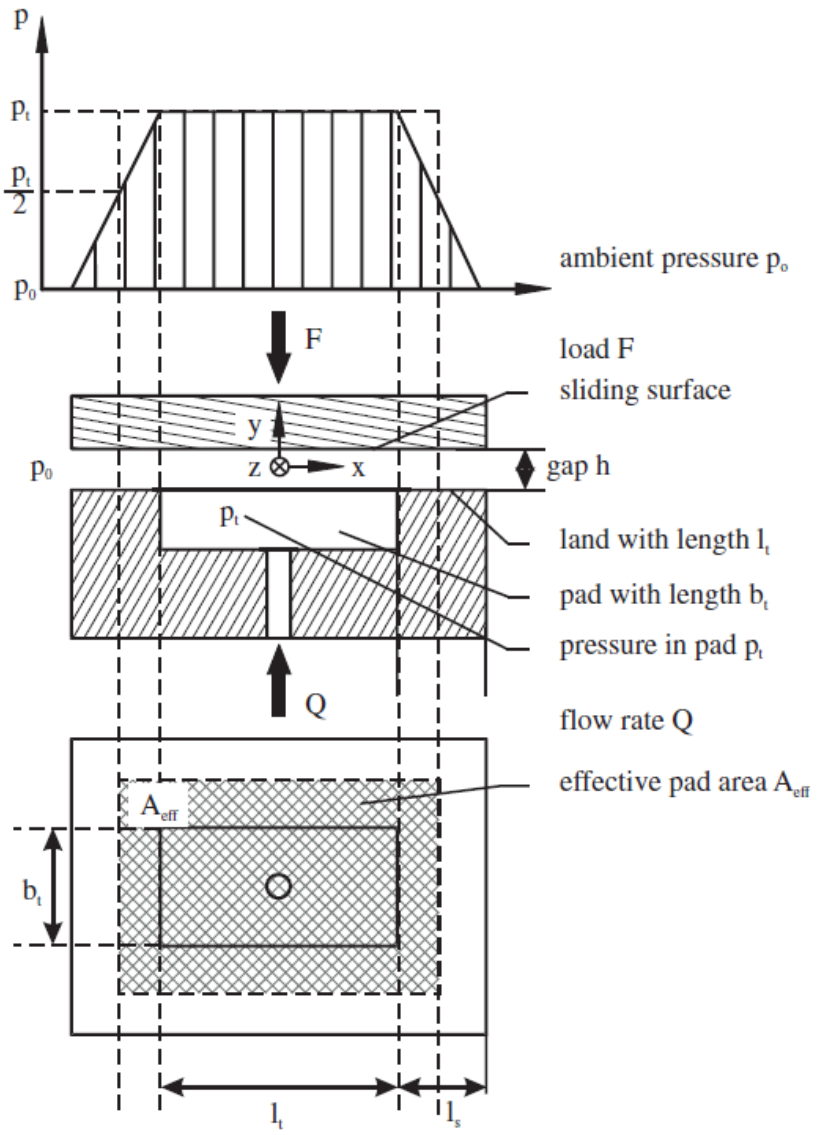


**Figure 10**: Principle of hydraustatic bearing [16].

### 1-2-5-3 HYDRODYNAMIC BEARINGS

A hydrodynamically lubricated bearing develops load-carrying capacity through the motion of two surfaces separated by a fluid film [22]. This type of bearing is commonly used to support radial loads and guide large, flexible rotors. Hydrodynamic bearings are specifically designed to operate under severe conditions, such as high loads and rotational frequencies. However, they do have some significant drawbacks [22].

- ✓ If the design speed is low, it may be not possible to generate sufficient hydrodynamic pressure.
- ✓ Fluid film lubrication may break down during starting, direction changing and stopping.
- ✓ In a journal bearing, the shaft runs eccentrically, and the bearing location varies with load, thus implying low stiffness.

### 1-2-5-4 WIRE MESH BEARING

The modern tendency towards oil free rotating machinery generates a new design of bearings with wire mesh damper. wire mesh not only provides comparative performances advantage over the SFD, but also retained most of its damping characteristics when tested at high temperature. This technology used in gas foil bearings [23] and contribute to attenuate vibration instabilities at high rotation speed.

To address the vibrations that occur in high-speed turbomachinery systems, it is crucial to install bearings. The purpose of these bearings is to mitigate the vibrations that the rotor will experience during its operation. Therefore, it is necessary to design a bearing system that has appropriate stiffness and damping characteristics, as well as a sufficient lifespan.

Efforts to address the problem described in this context led to the discovery of foil bearings in the 1950s [23-24], followed by the Wire Mesh Damper Bearings in the 1970s [25]. Foil bearings work by generating a self-acting and self-cooling air film between the flexible surface (top foil) attached to the inner radius of the rigid bearing surface and the journal. This feature affects the lubrication, pressurization, and supply system, resulting in a more lightweight, simplified, less expensive, and ultimately more desirable system [26]. Consequently, foil bearings are now used in various applications, such as air cycle machines [27-28], cryogenic applications [29-30], turbojet and turbofan engines [31-34], turbochargers [35], high-speed compressors [36], and even microsystems, including micro-power generator systems [37] and micro gas turbine engines [38].

Wire Mesh Dampers are characterized by their inherent high material loss factor and structural damping, which arise from the micro-slip that occurs at the junctions of the metal wire. These features make them well-suited for reducing synchronous and sub-synchronous instability caused by high cross-coupled stiffness [39-41].

Since 1980s, Wire Mesh Dampers were experienced in series with roller bearings, replacing squeeze film dampers (SFD) for aircraft engines [42]. Zarzour M. J. (1999) [43] showed that Wire Mesh Dampers equivalent viscous damping can match that of oil-lubricated SFDs under various conditions, such as balanced rotor, unbalanced rotor, heated metal mesh and, surprisingly, in oil-lubricated environment, indicating that WMDs do not only provide damping through dry friction, but also through material hysteresis.

Okayasu et al. [44] also demonstrated the benefits of Wire Mesh Dampers in suppressing synchronous and sub-synchronous rotor oscillations. They achieved this by utilizing ring-shaped Wire Mesh Dampers to support the liquid hydrogen pump bearings in the LE-7 rocket engines.

The turbopump's operating speed was 46,139 rpm, which is above its third critical speed. When such rotating speeds were reached, vibrations were as high as 80 and 150 µm at the first and third critical speeds respectively, rendering the system unreliable. After the addition of Wire Mesh Dampers, the turbopump passed through the first and second critical speed with low response amplitude.

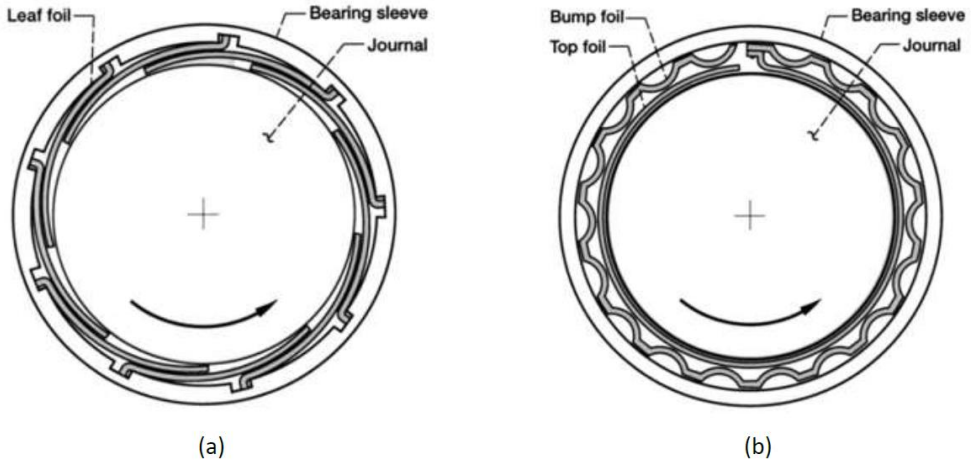


**Figure 11**: First generation foil bearings with axially and circumferentially uniform elastic support elements: (a) leaf type foil bearing, (b) bump type foil bearing. [45]

In a study conducted by Al-Khateeb (2002) [46], Wire Mesh Dampers were examined as an alternative to Squeeze Film Dampers, which are known to have limitations in terms of their performance at high temperatures and small displacement. The research showed that Wire Mesh Dampers can effectively reduce vibration levels and overcome the limitations of Squeeze Film Dampers, while also being more affordable and readily available.

In conclusion, Al-Khateeb's study proposed an improved formulation of older models to accurately predict the stiffness and damping of Wire Mesh Dampers. Furthermore, the study provided design guidelines for using Wire Mesh Dampers in turbomachinery applications.

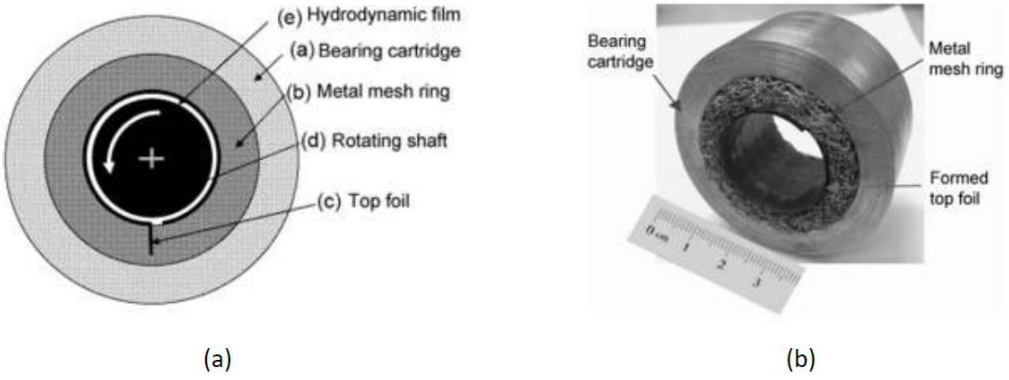


**Figure 12:** (a) schematic representatin of metal mesh foil bearings, (b) photograph of a metal mesh foil bearings [47].

Considering the latest technological tendencies in turbochargers, the engineers need to continuously adjust their bearing system design in order to achieve further downsizing of the turbocharger and better fuel efficiency, all while lowering its gas emissions [48-49].

### 1-2-6 INTELIGENT MATERIALS IN VIBRATION CONTROL

To achieve high standards in rotordynamics such precision,efficacity, functionality, durability and adaptability smart or intelligent materials systems are used to better control of vibrations. These materials exhibit non-negligible deformation or material property change with the application of thermal fields, electrical fields, or magnetic fields.

These materials include Electrorheological (ER) fluids, Magnetorheological (MR) fluids.

Smart fluid is defined as fluid in which the flow can be controlled through the application of an electric or magnetic field. Electrorheological (ER) and Magnetorheological (MR) materials belong to the family of controllable fluids.

#### 1-2-6-1 ELECTRORHOLOGICAL FLUIDS DAMPER

The ER effect was first discovered by Winslow in the late 1940s. However, more active research studies on the ER and MR fluids and their applications began in the mid-1980s [50].

Many researchers studied the dynamic behaviour of rotor by means of electrorhological fluids in order to control the vibration.

Nikolajsen.J.L et al [51] developed and tested an electroviscous damper for vibration attenuation in a flexible rotor system.this electrorheological damper achieved its higher performances when applying electric field and highly contribute to quenching high levels of unbalanced exited vibrations as well as the vibration control.

Morishita et al [52] successfully controlled the squeeze film damper by electrorheological fluids damper. they found that vibrations amplitude of a flexible rotor in a wide range of rotating speed has been remarkably reduced as well as the ER squeeze film damper is capable of supplying a continuously variable damping force, and thus provides an optimum damping for each mode.

These materials have been proposed as smart lubricants. The existing ER fluids are best described by the bingham model. John.A Tichy [53] studied theoretically the behaviour of SFD operating with an ER fluids in simple rotordynamic system. They illustrate an aptimization of the eccentricity and transmissibility by varying the ER properties.

Guozhi et al [54] investigated theoretically and experimentally the effect of ER fluids damper for controlling the rotordynamics systems as well as to suppress the resonance and the

sudden unbalance response.

Lim et al [55] investigated the design and application of an electrorheological fluid damper to semiactive vibration control of high-speed rotor systems. Peng and Ke-Qin[56] investigated the hydrodynamic characteristics of electrorheological fluid flows in journal bearing based on computational fluid dynamics techniques using the Bingham plastic model to describe the behaviour of the ER fluid.

Sun and Thomas [57] proposed an electrorheological dynamic torsional absorber in order to control the torsional vibrations of a rotor system. They found that the ER dynamic absorber exhibits very good performances where the smart absorber allows a 150% reduction in the vibration amplitude

A.Abed et al. [58] presented numerical analyses of a three-pad hydrostatic damper with electrorheological valve restrictors. Figure. 16 presents a diagram of a hybrid bearing with three identical hydrostatic pads. Each pad is powered by a negative electrorheological fluid using an electrorheological valve. Numerical analyses proved that the viscosity of a smart fluid can be controlled by an electric field, which in turn creates a possibility of controlling the static and dynamic characteristics. As a result, rotor vibrations can be controlled.

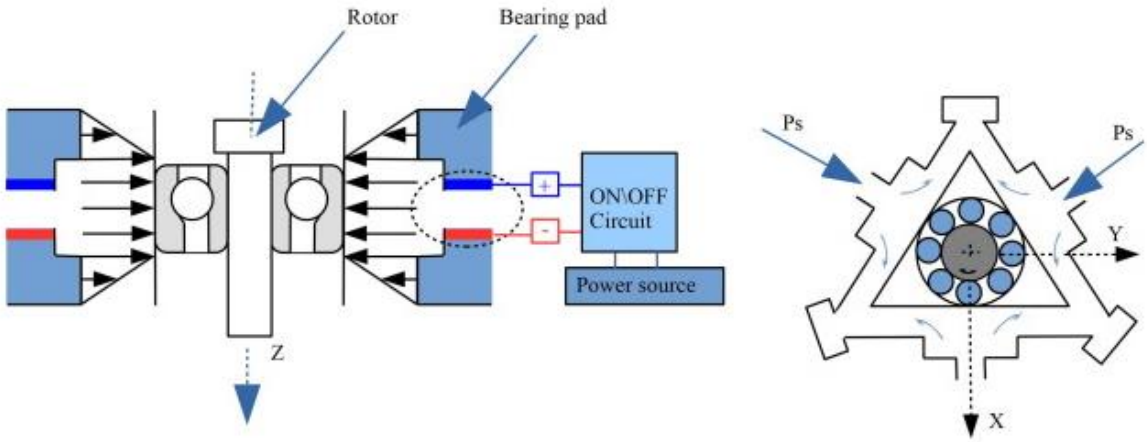


**Figure 13**: Hydraustatic damper controlled by means of an electrorheological valve [59-60]

### 1-2-6-2 MAGNETORHOLOGICAL FLUIDS DAMPER

The problem of vibration in rotordynamics is commonly faced with passive squeeze fluid film or elastomeric dampers. In the last decade there has been increasing attention directed toward the use of magnetorheological fluids.

Forte.P et al [61] investigated for the first time the magnetorheological squeeze film damper for vibration control of rotordynamics. The MR damper contribute for reducing the rotor vibration amplitudes in the range of 1000 to 5000 rpm. MR fluids can rapidely change

from liquid state to quasi-solid state under the action of an external magnetic field, and change process is continuos controllable and reversible. Jun Wang et al [62] studied the effect mechanism of MR damper to a rotordynamic system. The MR dampers is introduced to a simple Jeffcott rotor. They found that the MR damper has obvious suppression on the vibration of rotordynamics system at the critical speed.

The advantages of MR fluids is a yield strength of up to 50-100 kPa, which is one order of magnitude higher than ER fluids, insensitivity to contaminants, using 12–24 V low voltage, relatively broad working temperature range (typically -40 to 150 °C). Since the early 1990s there has been a resurgence of interest in MR fluids. In recent years, MR fluids devices have been applied commercially to engineering fields, such as automobiles, exercise equipment and polishing machines.

Changsheng Zhu [63]published a paper about the use of a Disk-type MR fluids damper in vibration control of flexible rotordynamics. He found that this system is very effective for atteunuating vibrations at the passage through critical speed.

By using MR fluids in place of luricating oil in a traditional squeeze film damper one can build a variable damping SFD, thereby controlling the vibration of the rotor by controlling the magnetics field. Wang J et al [64] studied the dynamics performances of an MR fluid SFD flexible rotor system for vibration control. They found encouraging results on the reduction of critical speed and response amplitudes by using MR fluids damper.

## 1-3 METAL FOAMS

### 1-3-1 DEFINITION OF METAL FOAMS

Metal foams materials, due to their unique structural shapes and gas dispersion in solids (see Figure 17), combine unique physical qualities such as low density, sound and vibration attenuation [65]. The collected knowledge enables the production of a wide range of porous metals and alloys, including aluminum [66], titanium [67], iron [68], copper [69], lead [70], magnesium [71], and many more. The primary criteria to consider when applying the material for the relevant application are the apparent (base) metal, the porosity morphology (such as open or closed -cell, size and shape), and the relative density.

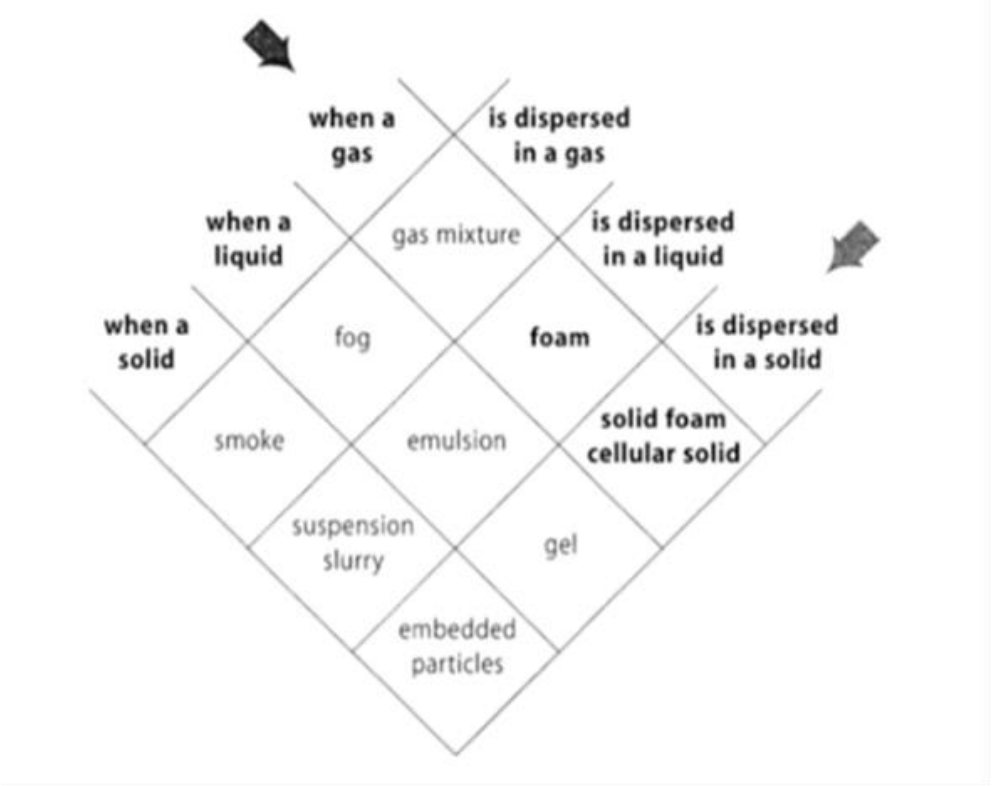


**Figure 14:** Dispersions of one phase into a second one. Each phase can be in one of the three states of matter [65]

### 1-3-2 TYPE OF METAL FOAMS

Metal foams typically retain some physical properties of their base materials, we have two types of metal foams according to the literature.

#### 1-3-2-1 CLOSED CELL METAL FOAMS

The closed cell metal foams group (see figure 15) is appropriate for structural applications, such as energy absorbers or load bearing components, where light solutions are often built on stiffness/weight ratios that are as high as possible.

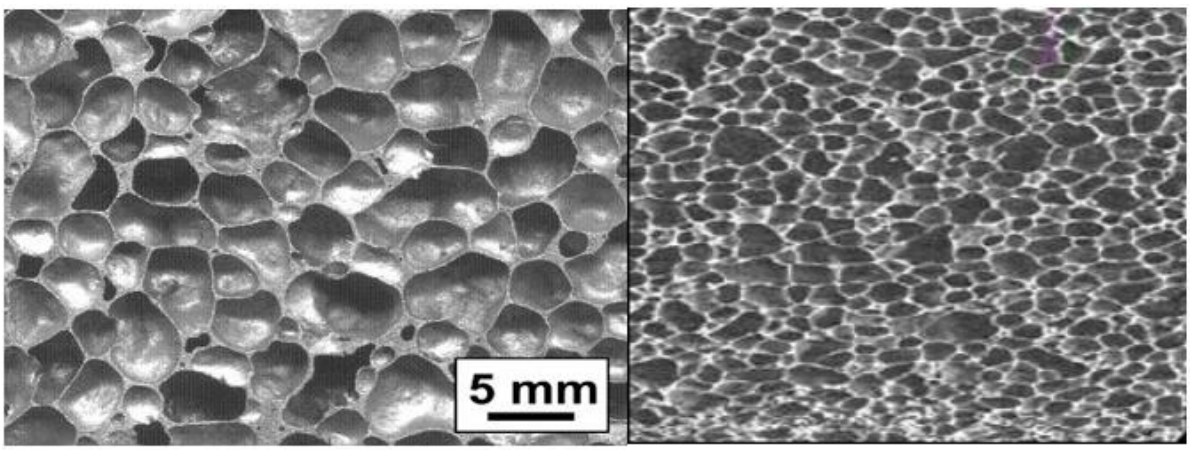


**Figure 15**: Closed cell aluminum foams [72]

### 1-3-2-2 OPEN CELL METAL FOAMS

The open metal foams group (see figure 16) is mostly used in functional applications such as heat exchangers, filters, silencers, and catalyst supports, where a liquid or gas must pass through the foam's degree of porosity.

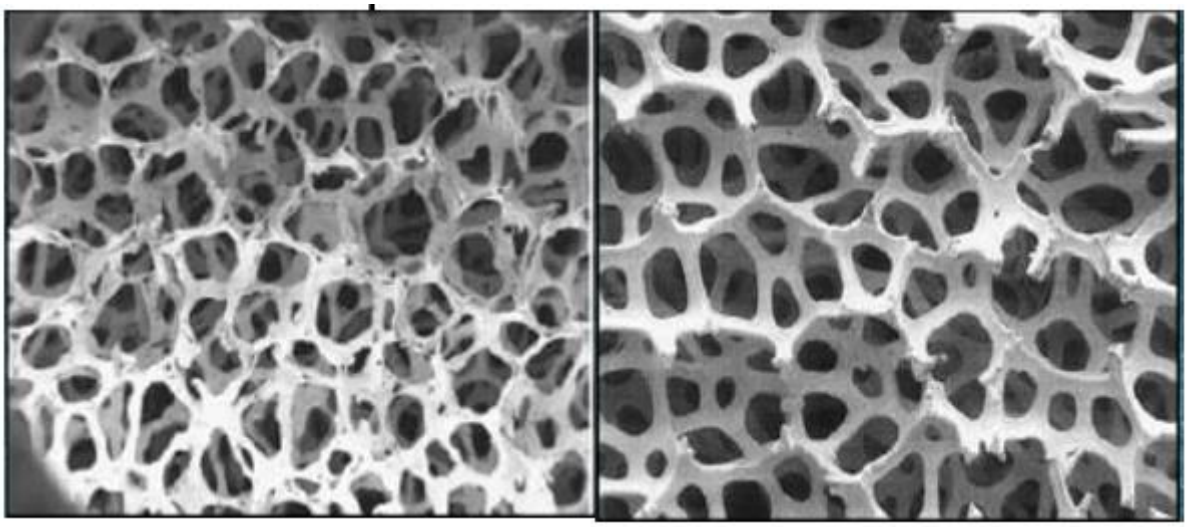

**Figure 16**: Open cell nickel foam [72]

## 1-3-3 PROPERTIES OF METAL FOAMS

### 1-3-3-1 MECHANICAL PROPERTIES

#### COMPRESSION PROPERTIES

Metal foam characteristics vary depending on whether it is open-cell or closed-cell foam. A metal foam's compression property is critical, especially for energy-absorbing applications. Figure 17 depicts the stress–strain curves for metal foams under compression loading (open-cell and closed-cell). Metal foam compressive stress–strain curves normally have three states: linear elastic deformation, plateau, and densification zone [73-75].

Therefore, the modulus of elasticity obtained during initial loading is less than the real modulus of elasticity E. The slope of the unloading curve gives the real Young's Modulus. Modulus of elasticity (E), for open-cell (Eq.3) and closed-cell(Eq.4) foams, modulus of rigidity (G) (Eq.5) and poison's ratio ($\upsilon \approx 0.3$) are related to relative density for open- and closed-cell structure as follows [80].

$$E \approx (0.1 - 4)E_s^*(\rho/\rho_s)^n \quad (3)$$

The value of "n" varies between 1.8 and 2.2. To note that the tensile modulus $E_t$ of metal foam and compression modulus $E_c$ differ from each other. The tensile modulus is

greater than the compression modulus by ~10%.

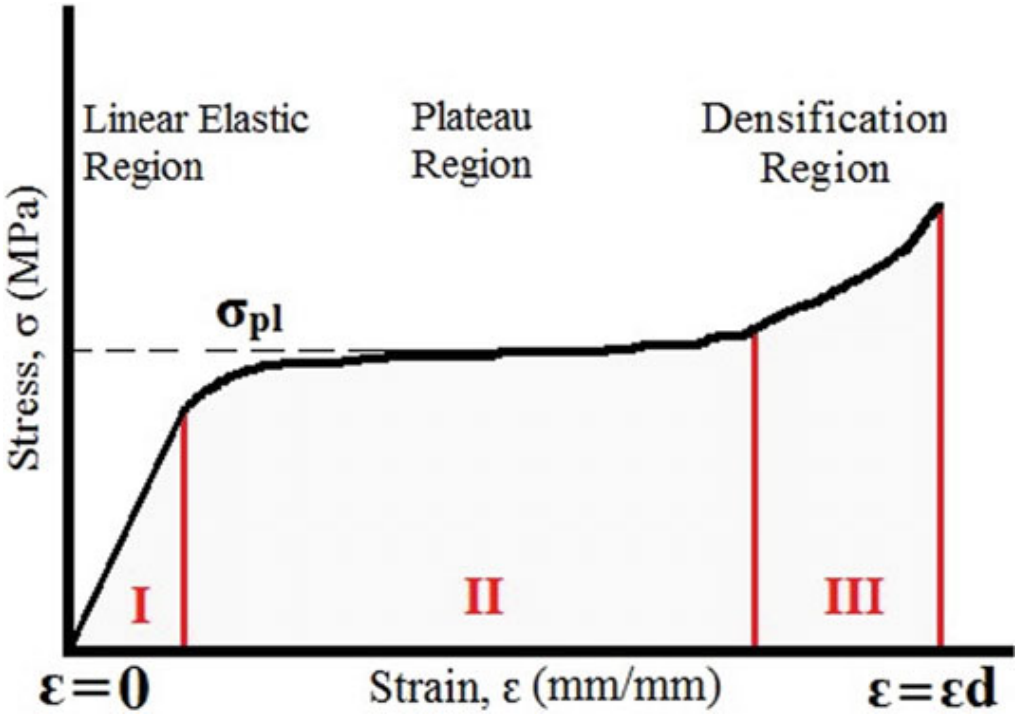


**Figure 17:** Typical compressive stress–strain diagram exhibited by metallic foams(adapted from reference [76].

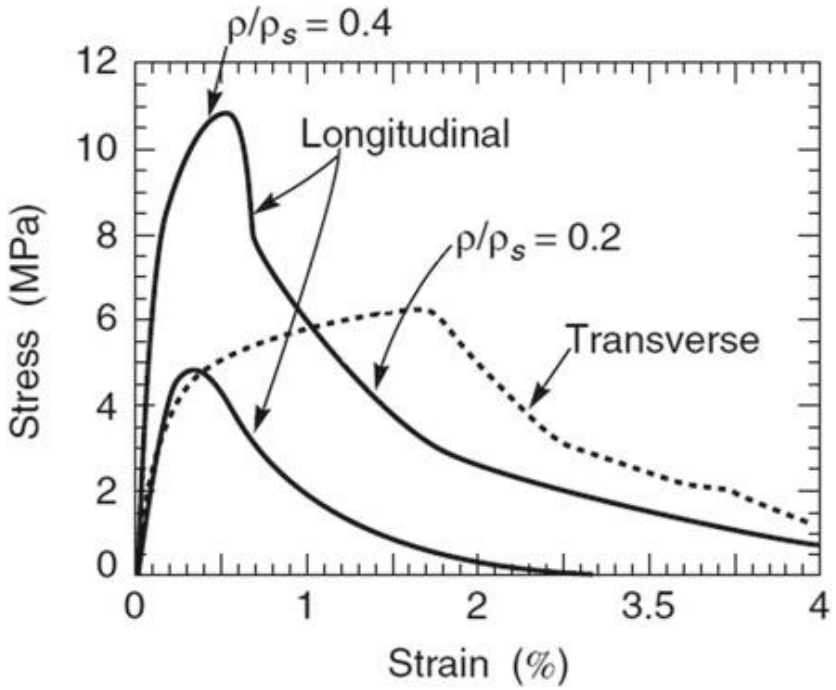


**Figure 18:** Typical tensile behaviour of metal foams '(adapted from ref [76])

$$E \approx (0.1-1)E_s^*[0.5(\rho/\rho_s)^n + 0.3(\rho/\rho_s)] \quad (4)$$

$$G \approx (3/8) \times E \quad (5)$$

In the case of an open-cell foam, The compressive stress rises extremely quickly as the strain rises until a certain stress point is achieved, which is the plateau stress. With further loading, the stress remains constant and strain keeps increasing until the point of densification strain ($\varepsilon_D$) [77]. Up to the point of densification strain, the density of metal foam continuously increases and pores collapses at $\varepsilon_D$.Hereafter, from this point, strain increases rapidly due to semi-dense form[80].

The plateau stress σp1 and the densification strain $\varepsilon_D$ are related to relative density as follows:

$$\sigma_{pl} \approx (0.25\ to\ 0.35)^{*}\sigma^{*}_{y,s}(\rho/\rho_s)^n,\ \varepsilon_D \approx (1-\alpha^{*}_{I}(\rho/\rho_s)) \quad (6)$$

For the currently available metal foams, the value of "n" varies between 1.5 and 2.0 and "$\alpha_1$" between 1.4 and 2.0. Experiments have revealed that formetal foams, the strain rate does not have considerable effect on the value of plateau stress[77-81].

### 1-3-1-2 THERMAL AND PHYSICAL PROPERTIES

Metal foams have identical melting point, specific heat and coefficient of expansion as their parent metals. For high-temperature applications, the effect of thermal radiation on k needs to be taken into account as radiation works on the fourth power of absolute temperature difference [82], [76].

### ANALYTICAL EXPRESSION ASSUMING ONE-DIMENSIONAL HEAT CONDUCTION

A simplified analytical modeling of a tetrakaidecahedron unit cell fully saturated in a fluid phase as illustrated in figure 19. let $k_e$ denote its effective thermal conductivity and let $k_s$and $k_f$ denote the thermal conductivity of the solid ligament material and the saturated fluid phase, Due to symmetry, we only consider one-sixteenth out of a single tetrakaidecahedron cell as a control volume (CV), namely, a cuboid with the dimension of $\sqrt{2}L$ (length)× $\sqrt{2}L$ (width)×$\sqrt{2L}/2$ (height); see figure 21 [83].

This CV contains two entire ligaments each with length L and thickness 2a as well as a partialligament having L in length and a in thickness.

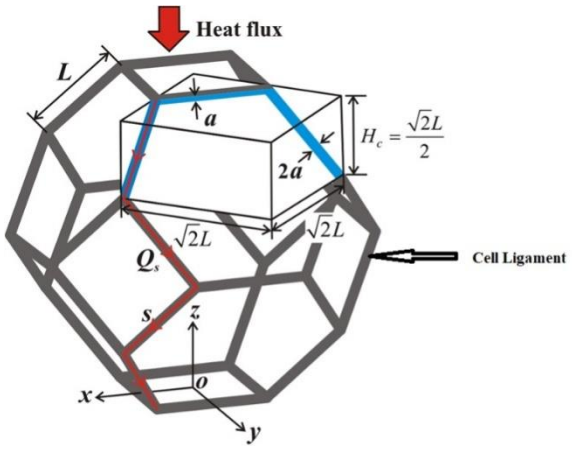


**Figure 19**: Open-cell Al foams modeled with a tetrakaidecahedron unit cell consisted of square cross-sectioned ligaments with uniform thickness 2a and length L( adapted from reference [83].

Following Fourier's law of heat conduction,the total amount of heat transferred through the CV may be expressed as:

$$Q_t = K_e A_0 \frac{\Delta T}{H_c} \tag{7}$$

where $A_0$ is the heat transfer area of the CV, $H_c$ is the thickness of the CV, and ΔT is thetemperature difference across the CV along the z-axis.

By Fourier's law, theheat conducted along the ligaments may be expressed as:

$$Q_s = -K_s A_L(s) \frac{dT}{ds} \tag{8}$$

where s is the axis along the ligaments which is strongly dependent on the topology of theporous medium of interest, and $A_L(s)$ representing the cross-sectional area of each ligamentis a function of ds independent of dT.

Accordingly, the relative density of open-cell foams having such tetrakaidecahedron unitcells with cuboid nodes may be obtained as

$$\rho^* = 1 - \varepsilon = \left[\frac{6(1-e) + 3\alpha e}{4\sqrt{2}}\right] \times \frac{A_L}{L^2} \tag{9}$$

**EFFECTIVE THERMAL CONDUCTIVITY**

The thermo-physical characteristics of the porous media are frequently used to characterize transport phenomena. Among many other qualities, effective thermal

conductivity influences heat transmission in porous media, particularly for use in thermal management systems.

The final expression of thermal effective conductivity in open cell metal foam is expressed as[83-84]:

$$\frac{K_e}{K_s} = \frac{(1-\varepsilon)}{(1-e+\frac{3e}{2\alpha})\left[3(1-e)+\frac{3}{2}\alpha e\right]} + \frac{K_f}{K_s}\varepsilon \tag{10}$$

an effective thermal conductivity model derived from the Laplace heatconduction equation with the circularity (sphericity) concept for a shape factor specially for closed cell metal foams are presented as [85]:

$$\frac{K_e}{K_c} = (1-\varepsilon)^{3\beta/2} \tag{11}$$

where kc denotes the thermal conductivity of a continuous phase and ε represents the totalvolume fraction of pores (porosity) and Ke represent the effective thermal conductivity of closed cell foams (honeycomb foams) [85].

**PERMEABILITY**

Permeability K and inertial coefficient $C_E$obtained as [86]:

$$\mathrm{K} = \frac{\varepsilon\left[1-\varepsilon)^{1/3}\right]}{108[1-\varepsilon)^{1/3}-(1-\varepsilon)]}{d_p}^2 \tag{12}$$

$$C_E = 0.095\frac{c_d}{12}\sqrt{\frac{\varepsilon}{3(\chi-1)}\left(1.18\sqrt{\frac{1-\varepsilon}{3\pi}}\frac{1}{G}\right)^{-1}} \tag{13}$$

In the above-mentioned models for determining thermophysicalproperties, the subscripts e, f, s separately demonstrated the (effective)thermal conductivity of the Aluminum or copper composite Phase Change Materials, interstitial medium andskeleton; e and α denoted the dimensionless thickness and cross-sectionalarea of a ligament (e = 0.3, α = 1.5); $c_d$ was the drag coefficient(cd = 1.56 )[87]; χ and G represented the tortuosity and shape functionfor metal foam, with expressed by[80]:

$$\chi = \frac{\varepsilon}{1-(1-\varepsilon^{1/3})} \tag{14}$$

$$G = 1 - e^{-(1-\varepsilon)/0.04} \tag{15}$$

**HEAT FLUXES**

The cellular metal is envisaged as a system that transfers heat from a hot surface into a fluid. Thermal performance is characterized by an effective heat transfer coefficient, Hc, which is related to the heat flux, per unit area, Q, from the hot surface in the standard manner which is formulated as [80] :

$$Q = LH_c\Delta T_{\ell m} \tag{16}$$

where L = length of foamed metal. $T_{\ell m}$= logarithmic mean temperature, which is linked to the temperature of the given heat source Ts , as well as fluid temperatures ($T_f$ ) at inlet and outlet, i.e., $T_{in}$ and $T_{out}$ , respectively, by [76]:

$$\Delta T_{\imath m} = \frac{T_{out} - T_{\ell m}}{\ell n[(T_s - T_{in})/(T_s - T_{out})]} \tag{17}$$

Generally, Ts and $T_{in}$ are quantified by the usage of fluid. As a matter of fact, $T_{out}$ is essential to find Q. Based on the primary assessment calculation, one may show $\Delta T_{\ell m}$as

$$\Delta T_{\ell m} \approx\ T_s - T_{in} \tag{18}$$

Experiments regarding fluid flow and its measurement can be summed up as follows [72]:

$$T_f = T_s - (T_s - T_{in})e^{(-\frac{x}{\ell})} \tag{19}$$

where $\ell$signifies the length, to be covered by the fluid, which is dependent upon fluid pump, characteristics of the metal foam and that of the used substrate. When thermal resistance is absent, the length is expressed by Eq. 20 , as follows:

$$\ell = \frac{\rho_a c_p b v_f}{2\eta_f K_{eff}\sqrt{Bi_{eff}}}\left[1 + \frac{\check{\rho}}{1.5\eta_f}\tan h\frac{2b_f}{d_f}\sqrt{Bi_{eff}}\right]^{-1} \quad (20)$$

In which, $\eta_f = 1 - 0.22(\rho/\rho_s)$ and $c_p$ is the specific heat transmitting capacity of the fluid. The exit temperature, thus can be established by finding $\ell$ , then adjusting x = L and setting temperature as $T_f \equiv T_{out}$ . Predictable variations in heat flux, dispelled through foamed metal (in $W/m^2$) are manipulated by means of the derived formulations.Generally, it is accomplished by plotting of dimensionless factorswhile considering cooling fluid as air. Properties of air include Reynolds number = 5000, Nusselt number =1, Pradtl number =0.7, foam thickness=0.2 and thermal conductivity = 0.011 ($\alpha_a$ = thermal diffusivity of cooling f luid). The parameters have been defined in . One can conclude that there is a considerable increment in heat dissipation, which then can be attained by enhancing the relative density, $\rho/\rho_s$ or by reducing the cell edge diameter d. Finally, a boundary condition is accomplished, which is administrated by means of the specific heat capacity of a given fluid [76];[88].

### 1-3-4 DAMPING IN METAL FOAMS

Aluminum foams are used as filling materials in several applications that take advantages from one or more characteristics of the material. If the machine tool field is taken into account, the vibrational behavior of the structure is of great importance.with the aim to obtain the best vibrational behavior for the selected application, the dynamic materials properties should be known.

The determination of damping of aluminum foam has been analyzed in few studies with quite different results.

Experimental modal analysis method of open pore aluminum foams was used to verify the effect of the pores density on damping properties. In this study, L. DAHIL et al [89] present an experimental result for different density pores of 03 samples D1, D2 and D3, which are respectively 0.951-gr/cm3, 0.931 gr/cm3, 0.896 gr/cm3. A compression test with deformation velocity of 01mm/min was applied to these samples which are manufactured from aluminum foams produced by vacuum casting system and Na Cl dissolution process. In Vibration analysis, the obtained results, by using Fast Fourier Transform analyzer, show that the damping ratio increases as the number of pores increases.

J.F. Ramirez et al [90] investigated the elasto-plastic deformation behavior of open cell aluminum foams and to verify experimentally, a numerical modeling and simulation of uniaxial compression tests applied to the specimens by using Abaqus 6.12-3 based on 3D computer tomography images to establish the mechanical behavior. The obtained

compression test results show that the plateau stress at a certain strain point increase with the increasing of the relative density and the decreasing the pore size.

Recent technological breakthrough generates an enormous demand for novel material, such as porous hybrid materials. Shunjie Yin et al [911] present a study to characterize the dynamic and damping properties of aluminum foam and elastomer composite to use in vibration damping and isolation. The silicon and RTV rubber are used to fill the open cell aluminum foam to fabricate the hybrid material which is modeled as single degree of freedom spring-damper system in order to measure the dynamic stiffness and damping coefficient under a sinusoidal compressive force. A dynamic compression test was applied to the specimens of (1-inch square cylinder and 1.35-inch-tall). The obtained results show that the addition of the rubber inside the aluminum foams ligaments has a significant increase of 31.7% and 15.4% average both in damping loss factor and dynamic stiffness respectively.

Massimo Golettie et al [92] reviewed the available experimental procedures applied for metal porous materials and determine the damping parameters and their applicability into metallic foams to improve finite element method modeling. They tested the aluminum foam beam specimens under two experimental setups (a PCB 2075E modal shaker and instrumented hammer) with constraint-imposed vibration. They compared the dynamic measurement results with the obtained by FE models to validate the chosen procedure.

Beshoy Markos et al [93] investigated the effect of different geometry parameters of metal foams such as porosity, pore size and ligaments geometry for its thermal energy dissipation applications, where both thermal convection and fluid flow were examined. An experimentally study was performed on a circulation type wind tunnel and an anemometer to measuring the velocity of air flowing through four different open cell metallic foam samples at different wind tunnel speeds ranging from 0 to 7.5 m/s in order to optimize metal foam geometry to achieve a fluid flow which maximize heat transfer for a given condition. It was found that any increase in porosity and pore size decreases the velocity loss in metal foam. And their major finding was that the cross-section shape of the foam ligaments can have a significant effect on flow through the foam.

Emanuele Lamanna et al [94] investigated the syntactic foam core sandwich composite for vibration responses. They tested the sandwich core which is made of aluminum alloy filled with alumina hollow sphere particles and contained a carbonic fabric layer in order to identify its dynamics mechanical properties. Experimental tests were performed using an Kjaer impact hammer type 8204 to excite core sandwich specimens. The dynamic modulus, storage modulus, loss modulus and damping ratio were calculated from the test results and used to validate the predictions of a theoretical model. It was found that the results obtained

on storage modulus are important because the damping parameter is relatively small, and these results can provide an indication about the level of the elastic modulus of such composites.

Recently in MAY 2017, Lenko Stanev et al [95] reviewed the manufacturing of Hight porosity open-cell metallic materials by using powder sintering and different space holder techniques. They have critically reviewed the effect of space holder particles like NaCl, magnesium, carbamide, saccharose, acrowax preform, ammonium acid carbonate, potassium carbonate, starch, polymethyl methacrylate and ice. They exactly focused on the Al, Cu, Ti and NiTi foam fabrication techniques. Their review precisely highlights the controlling parameters in the powder metallurgy method and the properties of different space holder materials. it is concluded that space holder process is an effective way for production of higher porous metal materials with an open-cell structure which can offer better absorption efficiency and possess Excellent energy absorption capacity.

## 1-4 CONCLUSION

With the increasing applications of metal foams in different engineering sectors, Metal foams have become multifunctional materials in almost every engineering design, but the orientation of using metal foams in rotor systems is novel for application in this field of rotating machinery research.

Here in the use of metal foam in the rotating machinery field, is an original work inspired by the experimental evaluation of wire mesh for design as a bearing damper in turbomachinery applications such as in vibration isolators, bearing dampers, and wire mesh dampers.

Overell , this chapter has provided an overview of the importance of rotor dynamics and the various factors that contribute to vibrations in rotating machinery. The use of traditional damping devices such as squeeze film dampers, electrorheological fluids, and magnetorehological fluids was discussed, as well as the role of ball bearings in rotordynamics. Additionally, the potential of metal foams as damping sources in engineering applications was explored. The literature review conducted in this chapter serves as a foundation for the subsequent chapters of this thesis, which will focus on the experimental and numerical analysis of a new design of a ball bearing with a metal foam damper.

# CHAPTER 02: EXPERIMENTAL STUDY

## 2-1 INTRODUCTION

This chapter describe the experimental procedure of making metal foam as dampening source in the bearing adabter of the bently Nevada RK4 rotor kit. After selection and supply according to literature data one type of metal foam. The chosen aluminum foam has a good damping characterestics , excellent sound absorption and contribute in the vibration isolation.

The main objective of this chapter is to make modification in the bearing adapter that include the ball bearings, the metal foam disk placed between the outer ring of the ball bearings and the housing covering the outer ring of the ball bearings. To achieve this aim, first a specimen made of aluminum foam sheet was tested under the vibration calibrator VC21 D in order to know their dynamic behaviour. Here, we identify the transmissibility and isolation efficiency.

The Bently Nevada RK-4 rotor kit, representing the dynamic test rig , consists of two ball bearings, a shaft, and a disk. The new approach is to channel the vibration to where it can be absorbed and dissipated safely. A prototype of an aluminum foam damper will be studied under the vibration calibrator for vibration characteristics.

## 2-2 EXPERIMENTAL STUDY

The metal foam damper specimen is tested under vibrations, by using the vibration calibrator VC21D, it can be easy to study the dynamic behaviour of the metal foam damper. The transmissibility and isolation can be determined through this non rotating equipment. Than the structural damping of the metal foam damper is calculated analytically by using a method called the Half Power Bandwidth Method (see chapter 03). At This point we have the damping and the stiffness of the metal foam damper. Now it can be easy to implement this properties in our rotor test rig.

The steps below illustrate the process of calculation the damping properties of the metal foam damper during this experiment:

a- Obtain the metal foams sample material
b- Cutting the metal foam sample
c- Determine the dimensions,porosity,and density of the foam damper.
d- Preparing the equipment vibration calibrator VC21D.
e- Configure the metal foam sample in the VC21D.
f- Measurement of the transmissibility and the isolation
g- determine the dynamic properties such as the damping,stiffness and loss factor of the metal foam damper.

h- Using the obtained properties for vibration analysis of lateral motion of Jeffcott rotor using MATLAB® and compre the results by using or without using metal foam damper in the bearing adapter.

i- Illustrating the results.

### 2-2-1 ROTOR KIT DESCRIPTION

The physical rotor kit system, developed by Bently Nevada, allows different rotor dynamic experiments to be run in a laboratory setting with great modularity. By changing the characteristics of the system, different vibration phenomena typically found in large rotating machinery can be duplicated on this smaller scale model. The main components of the RK 4 model are labeled in figure 20. The experiments and analysis described in this thesis were performed using the provided ball bearings, rotor mass wheels, and steel shaft. For other types of analysis, the rotor kit is also able to accommodate a fluid film bearing, shaft rubbing or hitting conditions, and perturbation options.

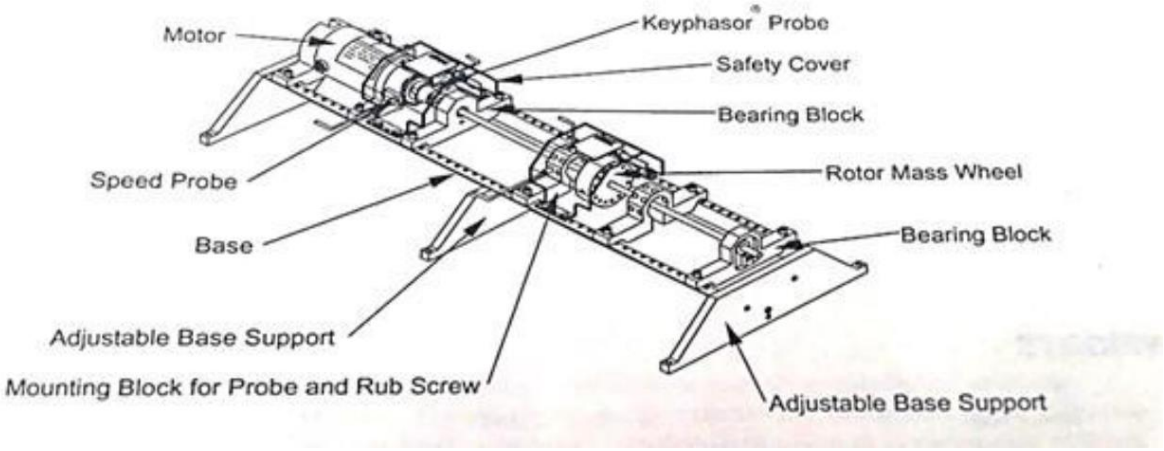


**Figure 20:** Bently Nevada model RK 4 rotor kit.

### 2-2-2 EXPERIMENTAL SET-UP

In this experiment, we are interested in studying the aluminum foam under the vibration calibrator VC21D. The vibrations through the selected sample will be investigated under different input amplitudes. The vibration calibrator is a very useful tool that allows us to dynamically characterize the foam without causing any damage to the sample during vibration measurements. A simple method of vibration analysis is proposed.


**Figure 21:** Vibration Calibrator VC 21D with clamping devices.

Here, we should start by investigating the behaviour of the metal foam damper under certain ranges of vibrations in order to know the vibration management in this novel engineering design.

The reason from putting the metal foam damper between the proximity probes of the vibration calibrator VC21D is to determine the damping properties of the selected sample of aluminum foam under frequency regime of 12.85 to 1285Hz.

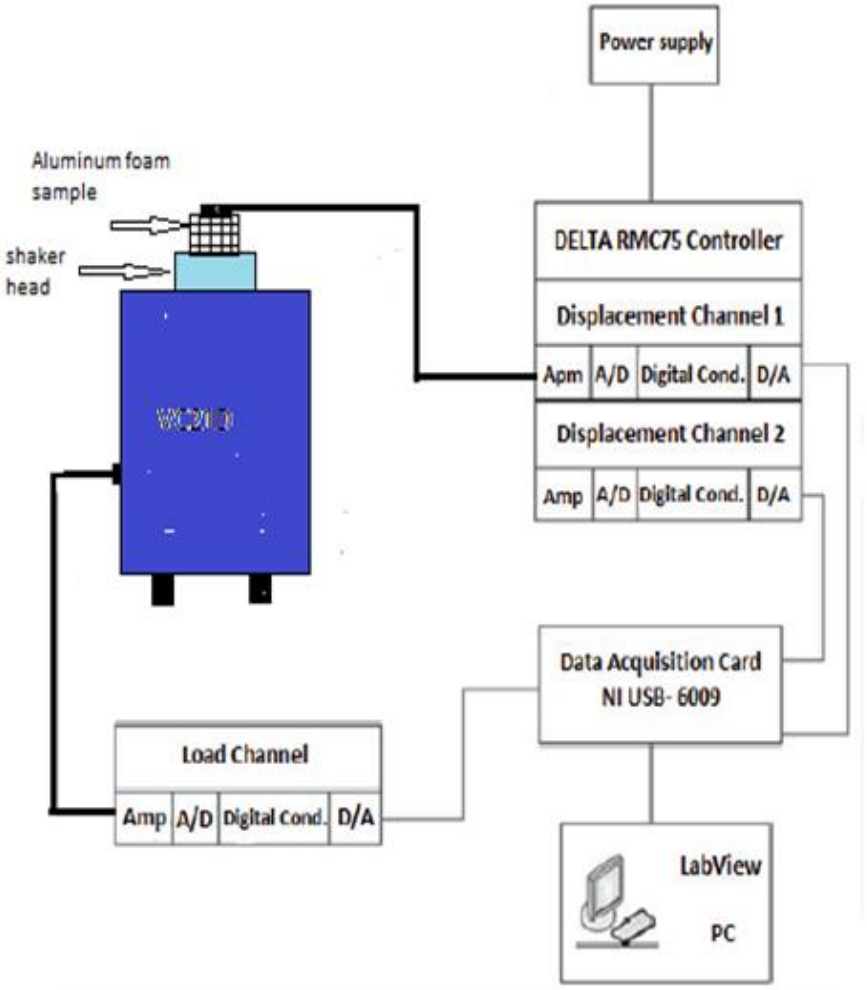


**Figure 22:**Schematic illustration of the non-rotating test setup


**Figure 23:** Wire mesh damper [96]

The main intent of this experimental part is to evaluate the metal foams as an alternative approach to minimize the vibrations caused by the forces produced during the rotating of ball bearings, and also giving appropriate solution of the problems related with the Squeeze Film Damper.

To channel the vibration energy to where it can be absorbed and dissipated safely in a flexible shaft supported by two journal bearings with metal foam damper, it is important to know the sources of vibrations. Vibration in rotating machines is due to destabilization forces,misalignement and looseness. The only solution is to try to reduce and minimize always the sources.

The purpose of this contribution of metal foams into rotor dynamics it is consists of making some modification to the bearings adapter part in order to integrate it with the metal foam disc (donuts). as you can see from figure 25 this modification will be between the outer ring of the Misumi bearing and the cage. then the metal foam specimens should be cut as donuts with precise dimensions. these parameters should be taken into consideration: The outer diameter of the bearing adapter, the inner diameter, the radial thickness of the donuts and the axial thickness.

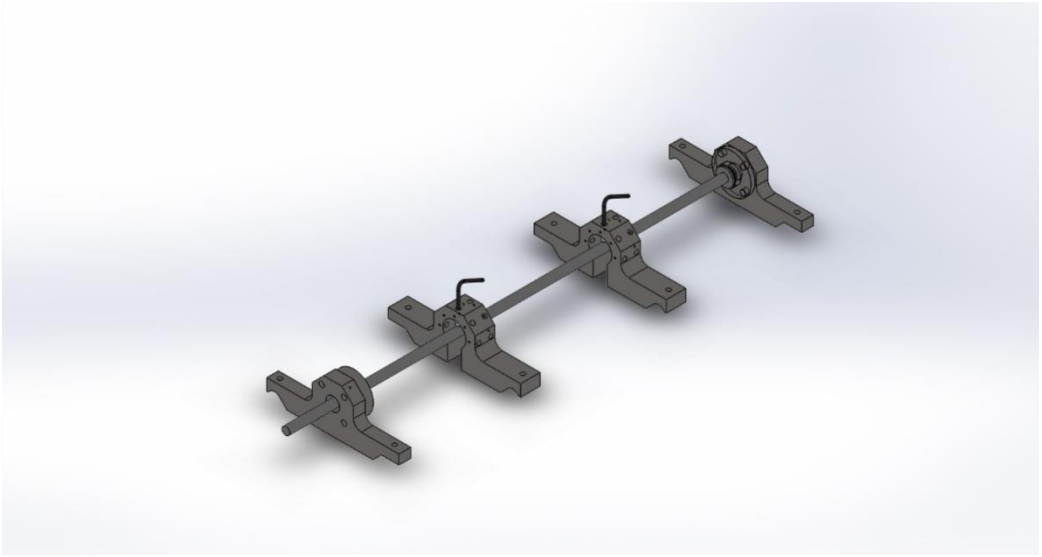

**Figure 24:** Rotor Kit Assembly

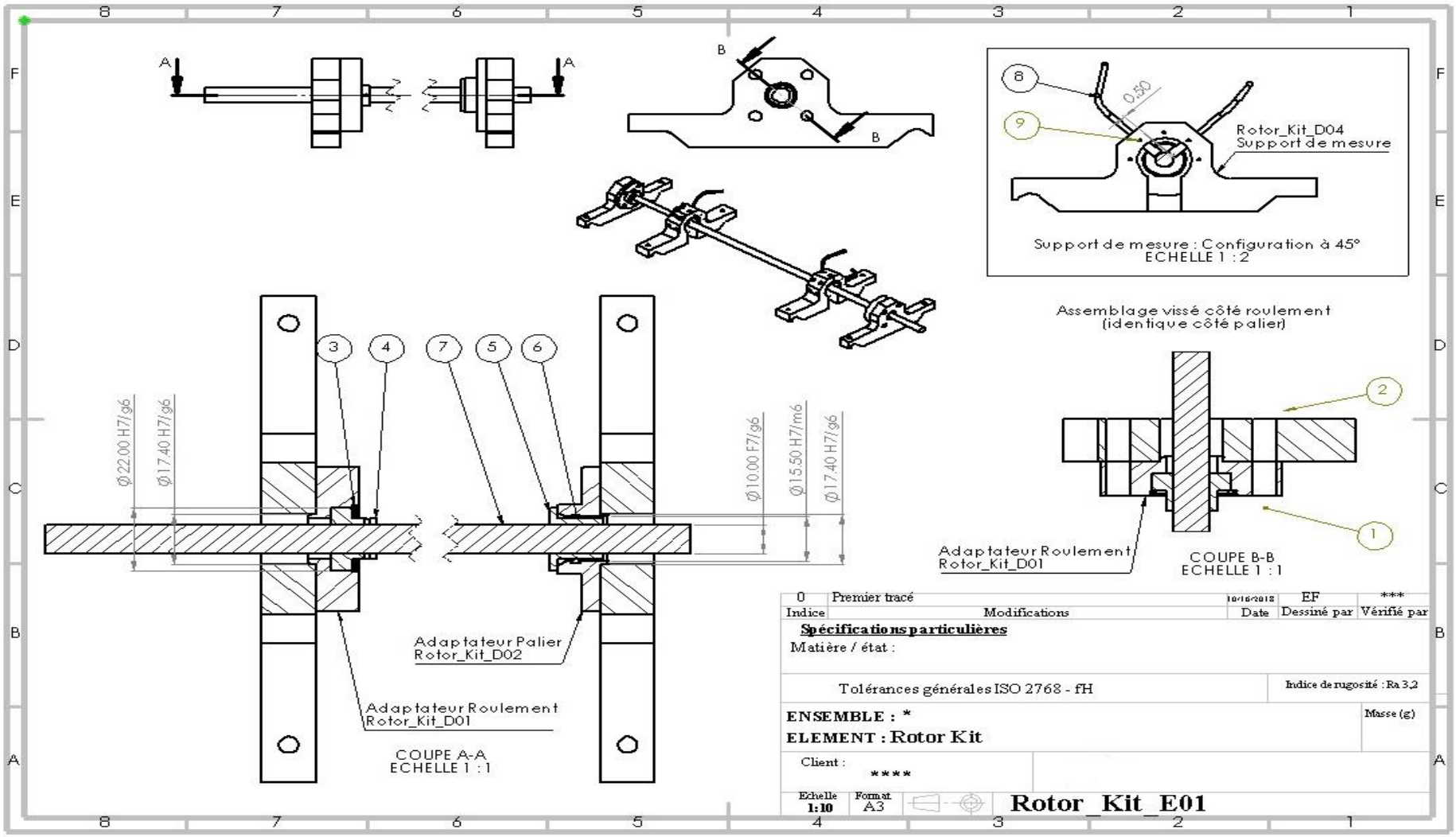


**Figure 25:** Assembly design of the rotor kit

There are two set of vibrations management : isolation and damping. The first one is the prevention of vibrations from entering a rotor system. The latter is the absorption of the vibration energy that is entering the system and dissipating it by changing the kinetic energy of vibration into a different form of energy.

Before we are going to study the analysis of the shaft supported by two ball bearings with metal foam damper, Non-rotating dynamic tests were conducted on different aluminum foam donuts elements to analyze the effect of axial thickness, radial thickness, axial compression, radial interference, and displacement amplitude. The results from these tests were used to update the design guidelines for metal foam donut as a bearing damper.

The metal foam donut specimen may have to be an excellent solution to attenuate vibrations resulting from the rotating element of the rotor and therefore the instabilities. The Recemat open-cell aluminum foams include an attractive damping property with high acoustic attenuating capacity and may be an answer to our problem associated with the minimization of vibrations during the passage from the low speed to the high speed of the flexible rotor supported by two journal bearing with metal foam damper.

a b c

**Figure 26:(**a) The Recemat Open Cell Metal Foam (b) Type of Small pore aluminum foams and (c) Proposed Porous bearing Damper

The figure 26 present the Recemat metal foam specimen and the proposed porous metal foam disc damper replaced the conventional SFD. The proposed porous metal foam damper present energy plastic dissipation role. Here the cause of this dissipation of energy is the plasticity of a part of the system. High external loads generate significant internal stresses. If these exceed a threshold the system is irreversibly altered (plasticity of the materials for example) but retains its integrity.

This device for absorbing energy by plastic deformation of metal materials (see figures 26 a and 26 b) is used, for example, in the aeronautical sector to absorb slight shocks and is present at the front of the cockpit of the aircraft. The same principle is used in the automotive sector for absorbing shocks at low speeds: metal profiles in the shape of tubes with rectangular cross sections attaching the front and rear automobile bumpers to the body of the vehicle are deformed by buckling in the event of an impact, and those absorb kinetic energy at low speeds. (of the order of 10 kilometers per hour).

The aluminum foam that has been utilized in this new research towards application in simple rotor dynamic system is inspired by the authors, it's manufactured by The RECEMAT BV company from Netherland. the initial aluminum foam sheet dimension of 900*600*10mm. The aluminum foam samples is about 38*34mm$^2$ and 10 mm thickness

The porous metal foam disc damper should be replaced in modified adapter bearing element. This modification dedicated to the use of ball bearing in sample Jeffcott rotor system with shaft and disc rather than the Misummi bearing TBB6900ZZ. The modified bearing adapter show in next figure

The purpose from this experiment is to study the transmissibility of vibration through porous metallic medium without any elastomer materials added to the pore cell of aluminum foams.

The vibration calibrator will be used for that purpose. The metal aluminum foam will be calibrated between the two clamps of the device and then tested the sample sheet investigated under different input frequencies and amplitudes.

Recent technological breakthrough generates an enormous demand for novel material, such as porous metal or hybrid materials. Experimental modal analysis method of open pore aluminum foams was used to verify the effect of the pores density on damping properties. L. DAHIL et al [97] present an experimental result for different density pores of 03 samples D1, D2 and D3, which are respectively 0.951-gr/cm3, 0.931 gr/cm3, 0.896 gr/cm3. A compression test with deformation velocity of 01mm/min was applied to these samples which are manufactured from aluminum foams produced by vacuum casting system and Na Cl dissolution process.

Lenko Stanev et al [103] reviewed the manufacturing of Hight porosity open-cell metallic materials by using powder sintering and different space holder techniques. They have critically reviewed the effect of space holder particles like NaCl, magnesium, carbamide, saccharose, acrowax preform, ammonium acid car-bonate, potassium carbonate, starch, polymethyl methacrylate and ice. They exactly focused on the Al, Cu, Ti and NiTi foam fabrication techniques. Their review precisely highlights the controlling parameters in the

powder metallurgy method and the properties of different space holder materials. it is concluded that space holder process is an effective way for production of higher porous metal materials with an open-cell structure which can offer better absorption efficiency and possess Excellent energy absorption capacity.

Transmissibility of vibration through metallic porous media is not yet known by most researchers worldwide. Many researchers have concentrated their efforts in recent decades on production characterization processes and the use of metallic foams.Metal foams have generally been classified as new and emerging materials since 2000. The relative density and porosity remain the important factors in metallic foams before going towards any application process. Here, testing vibration by using static and dynamics systems will be a new axe of research in the future in materials.

The static vibration calibrator is a very useful system to understand the behaviour of metallic foam under small vibration amplitude responses. The dynamic experiment test on VC 21D is getting good results for the isolation efficiency that changes different new aspects in the next decade.

In the experimental part, attention is focused on the transmissibility of the aluminum foam sample under the vibration calibrator VC 21D. In order to understand what isolation and damping are and how to apply them by using the vibration calibrator VC21 D, first of all, we must understand the transmissibility through the foam sample. Transmissibility is a measurement used in the classification of materials for vibration management characteristics. It is the ratio of the vibrational force being measured in a system to the vibrational force entering a system that is presented in the law below [89]:Which $A_0$ is the Amplitude of the Vibrational Response and Ai is the Amplitude of the Vibrational input.

$$T = \left|\frac{A_0}{A_i}\right| = \sqrt{\frac{1 + \left(2\xi \frac{f_d}{f_n}\right)^2}{\left[1 - \left(\frac{f_d}{f_n}\right)^2\right]^2 + \left[2\xi \frac{f_d}{f_n}\right]^2}} \quad (21)$$

Transmissibility is more easily defined as the percent of vibrational energy that is being transmitted through a structure here (metal foam sample structure element).

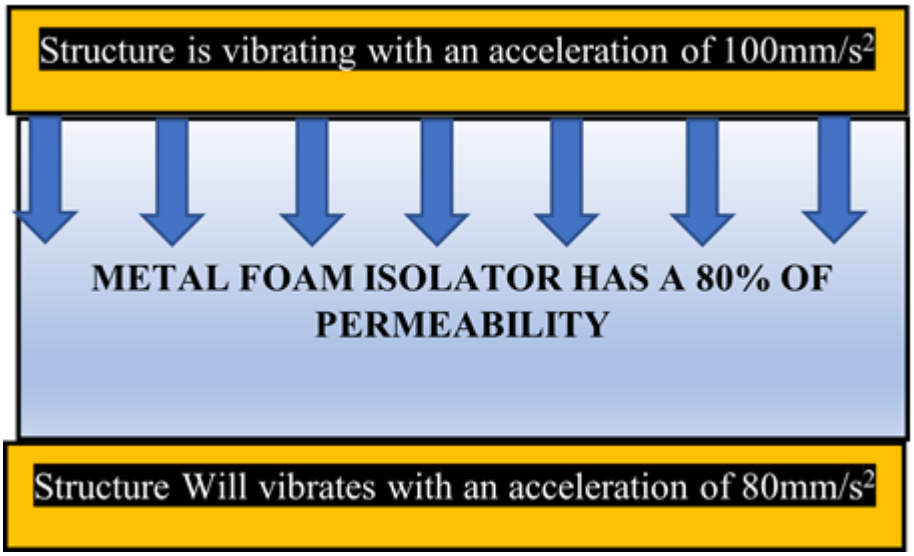


**Figure 27:** Illustration of metal foam isolator in vibrating system with corresponding input and output acceleration.

The vibration characteristics of materials are typically represented by a graph of transmissibility vs. frequency. The vibration exciter of the VC21D has a tapped M5 hole with a 7 mm depth for the attachment of the metal foam specimens under test. The supplied stud bolts and stud adapters or a clamping magnet can be used for mounting. The vibration signal becomes stable after attaching to the sample under test.

Metal foam exhibits higher damping characteristics than its parent metals. Consider a single degree of freedom spring mass system as shown in figure 28. The mass is fastened to the base with the support of a spring and viscous damper. The oscillates at a single frequency and has an amplitude of X. The displacement of the base will accordingly be expressed as $X=Xe^{iwt}$. Therefore, the relative displacement of the supported mass is expressed by $Y=Ye^{iwt}$.

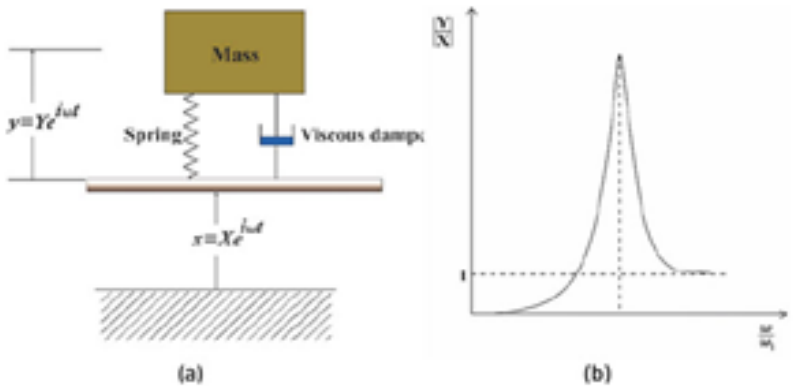


**Figure 28:** (a) Schematic diagram of a single degree of freedom spring mass oscillator system. (b) approximate transfer function for relative displacement y of mass [97].

The transfer function (F (w)) is presented by Eq [89]:

$$F_{(\omega)} = \frac{Y}{X} = \frac{(\omega/\omega 1)^2}{1 - \left(\frac{\omega}{\omega 2}\right)^2 + i\eta(\frac{\omega}{\omega 1})} \quad (22)$$

### 2-2-2-1 PROPOSED MODIFICATION AT BEARING ADAPTER

The core modification is take place at the bearing adapter of the bently Nevada rotor kit. The bearing adapter element of the modified rotor kit support the ball bearings during their high-speed rotating. as one of the benefits of metal foams is to provide more damping than the apparent metal, The metal foam donuts could have the capacity to become as solution as porous squeeze film damper to minimize the vibrations of rotor kit during the passage of the critical speed means the resonance.

The metal foam donut specimen may have to be an excellent solution to attenuate vibrations resulting from the rotating element of the rotor and therefore the instabilities. The Recemat open-cell aluminum foams include an attractive damping property with high acoustic attenuating capacity and may be an answer to our problem associated with the minimization of vibrations during the passage from the low speed to the high speed of the simple Jeffcott rotor system.

The engineering technical design of the proposed modification at the bearing adapter will be presented below in figure 30.

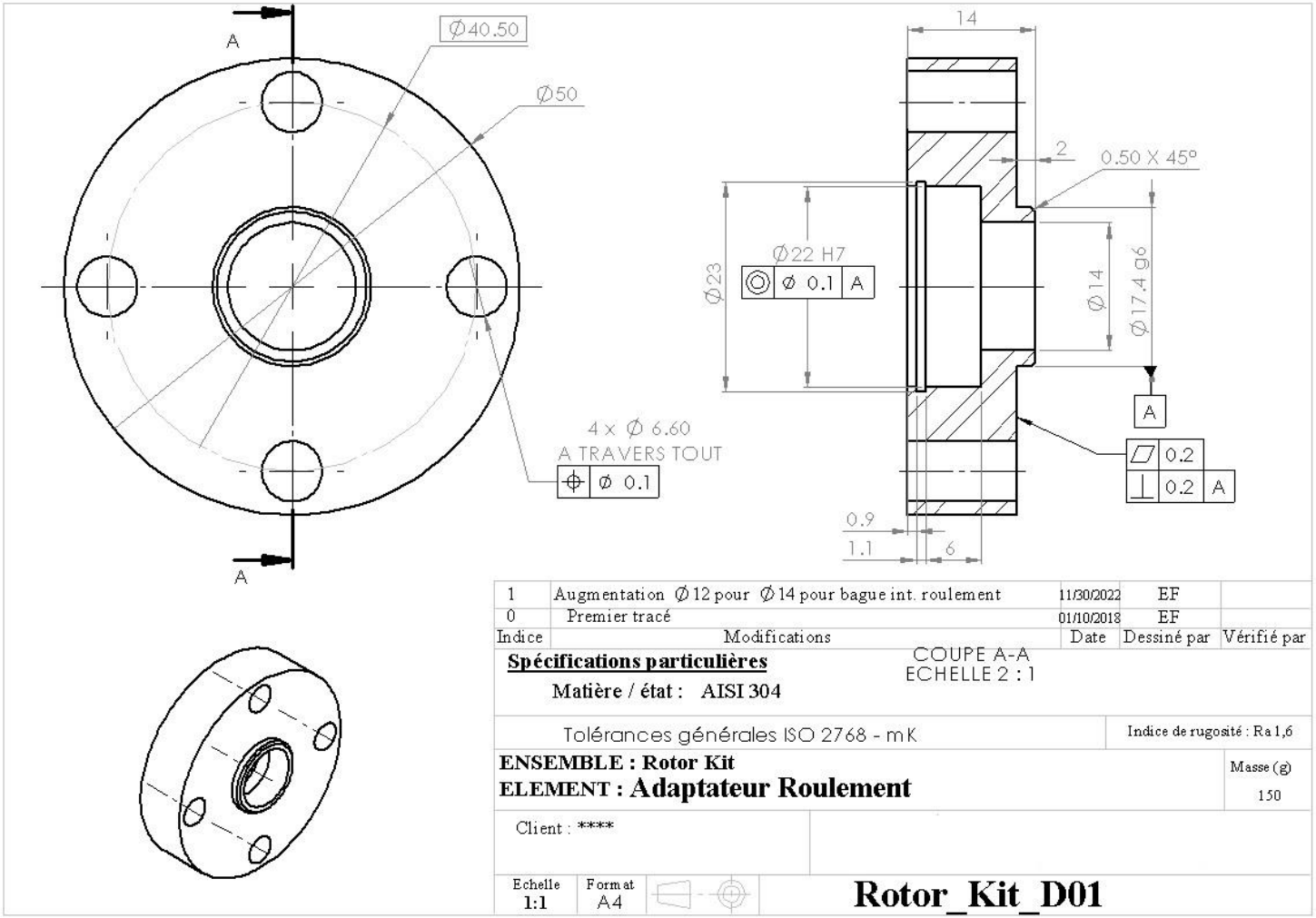


**Figure 29:** Technical design of the modifications at the bearing adapter

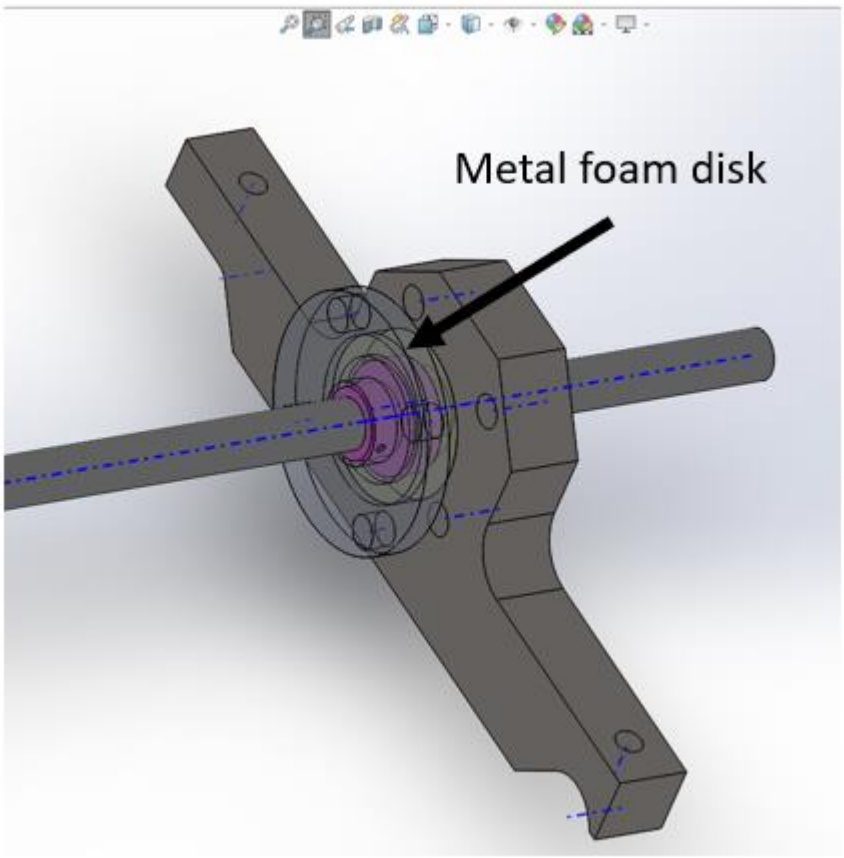


**Figure 30:** Proposed modification of the donuts damper

The metal foam damper will be used as a donut between the outer ring of the ball bearing and the housing covering the outer race of the ball bearing (see figure 30). This new approach offers more damping at the bearing location because metal foam has an important damping characterstics.

### 2-2-3 TRANSMISSIBILITY RESULTS

To measure the transmissibility of the metal foam damper, a vibration calibrator (VC21D) was used. The metal foam specimens were mounted onto the calibrator and the calibrator was set to vibrate at a specific frequency and amplitude. The vibration transmitted through the metal foam specimens was then measured using an accelerometer.

The transmissibility of the metal foam damper was calculated as the ratio of the transmitted vibration amplitude to the input vibration amplitude. To ensure accuracy, each specimen was tested multiple times and the average transmissibility was calculated.

Overall, the metal foam specimens were carefully prepared and the transmissibility of the metal foam damper was accurately measured using a vibration calibrator. These measurements provide important data on the effectiveness of the metal foam damper in reducing vibration in the rotor system.

The vibration characteristics of metal foam are typically represented by a graph of transmissibility versus frequency . As you can see from figure 31, a typical plot of a material's transmissibility curve. From the graph, we notice that this aluminum foam has a very important damping coefficient. The circled region represents the value of the damping efficiency against the insolation below 0. The natural frequency zone could be beneficial for attenuating the high value of resonance of the vibration amplitude passing through the foam specimen. The remaining part minus 1 shows the permeability, or the porosity, of this aluminum foam. Using this curve, engineers can extract useful information about the material's properties with regard to vibration, including natural frequency, damping ratio, and isolation.

The peak on the curve at around 40 Hz is representative of the material's natural frequency. Using this peak and some math, engineers calculate the amount of damping in a material. When the curve crosses the Y-axis into negative values (at approximately 80 Hz on the plot above), the material begins to isolate vibrations. As frequencies increase, the amount of energy transmitted from vibration is reduced, which means isolation performance increases.

The input value of amplitude is between 00 Hz and 1285 Hz, produced by the vibration calibrator. For any results, the metal foam specimen should be calibrated and clamped between two sensors.

The table below presents the value of transmissibility through the metal foam sample and the input and output values of amplitude are shown.

**Table 1:** Input and output frequency during calibrating metal foams and transmissibility

| Frequency (Hz) | Input amplitude ($m/s^2$) | Output amplitude (g) | Transmissibility (dB) |
|---|---|---|---|
| 15.82 | 2 | 0.20 | 0.06 |
| 40 | 2 | 0.21 | 0.11 |
| 40 | 5 | 0.50 | 0.02 |
| 80 | 5 | 0.50 | 0.03 |
| 80 | 10 | 1.02 | 0.07 |
| 159.2 | 20 | 1.02 | -2.59 |

| | | | |
|---|---|---|---|
| 159.2 | 20 | 1.34 | -1.73 |
| 320 | 20 | 1.44 | -1.41 |
| 640 | 20 | 1.52 | -1.18 |
| 1280 | 20 | 0.92 | -3.38 |
| 1280 | 10 | 0.47 | -3.32 |

Frequency is plotted on the X-axis in Hertz (HZ) and transmissibility is plotted on the Y-axis in decibels. The equation for coverting the ratio into decibels is below [80]:

$$dB = 20\ LOG\ (\ A_0/A_i) \quad (23)$$

The vibration characteristics of metal foam are typically represented by a graph of transmissibility versus frequency . As you can see from figure 31, a typical plot of a material's transmissibility curve.

The specimen's aluminum foam under test behavior passes through three essential steps: elastic behavior, followed by plastic deformation, and finally, the collapsed period. The vibration calibrator helps us to characterize the metal foam sample nondestructively.

All these three major steps affect the transmissibility efficiency of the test sample from 15.82 Hz to 1285 Hz.

From the graph (see picture 36), we notice that this aluminum foam has a very important damping coefficient. The region higher than zero represents the value of the damping efficiency against the insolation below 0. The natural frequency zone could be beneficial for attenuating the high value of resonance of the vibration amplitude passing through the foam specimen. The remaining part minus 0 shows the permeability or porosity of this aluminum foam. Using this curve, engineers can extract useful information about the material's properties regarding vibration, including natural frequency, damping ratio, and isolation.

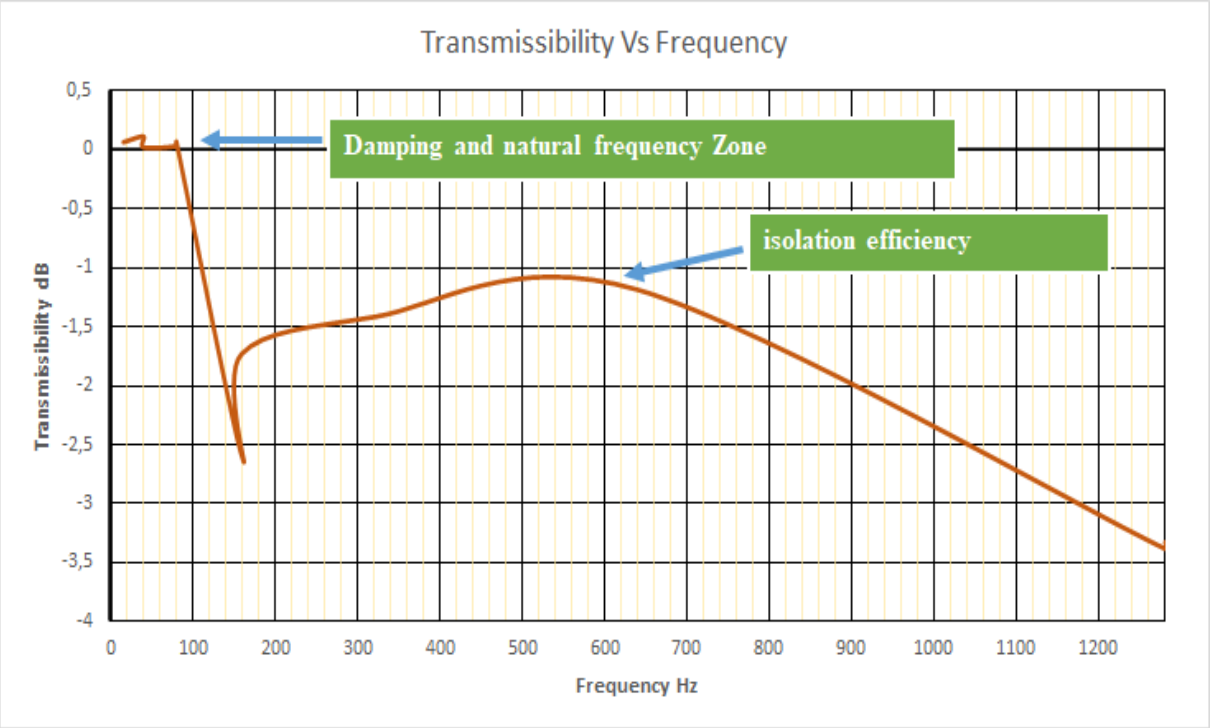


**Figure 31:** Transmissibility vs Frequency of metal foam without rubber

The peak on the curve at around 32 Hz is representative of the material's natural frequency. Using this peak and some math, engineers calculate the amount of damping in a material.

When the curve crosses the Y-axis into negative values ( at approximately 80 Hz on the plot above ), the material begins to isolate vibrations. As frequencies increase, the amount of energy transmitted from vibration is reduced, which means isolation performance increases.

### 2-2-4 ISOLATION RESULTS

Firstly, we define isolation as the prevention of vibration from entering a system; we also define transmissibility as the percentage of vibration energy that is being transmitted through a structure.

The static vibration measurements with the vibration calibrator are a very useful system to understand the behaviour of metallic foam under small vibration amplitude responses.

The dynamic experiment test on VC 21D is getting good results for the isolation efficiency that changes different new aspects in the next decade.

Mathematically [89], these two terms are simply related.

$$\%\, isolation \;=\; 100 - \%\, transmissibility \tag{24}$$

The purpose of this experiment is to study the isolation of vibrations through porous metallic media without any elastomer materials added to the pore cell of aluminum foam. The vibration calibrator will be used for that purpose.

The aluminum foam will be calibrated between the two clamps of the device and then tested with the sample sheet investigated under different input frequencies and amplitudes. The result shows that the damping coefficient is always less than 0.80 of aluminum foam of 84% porosity.

The table below depicts the value of the isolation of the aluminum foams at different amplitude values.

**Table 2:**Frequency vs isolation data of aluminum foam sample under the vibration calibrator

| Frequency | transmissibility | isolation |
|---|---|---|
| 15.82 | 0.06 | 0.94 |
| 40 | 0.11 | 0.89 |
| 40 | 0.02 | 0.98 |
| 80 | 0.03 | 0.97 |
| 80 | 0.06 | 0.93 |
| 159.2 | -2.56 | 3.58 |
| 159.2 | -1.73 | 2.73 |
| 320 | -1.41 | 2.41 |
| 640 | -1.19 | 2.19 |
| 1280 | -3.38 | 4.38 |
| 1280 | -3.32 | 4.32 |

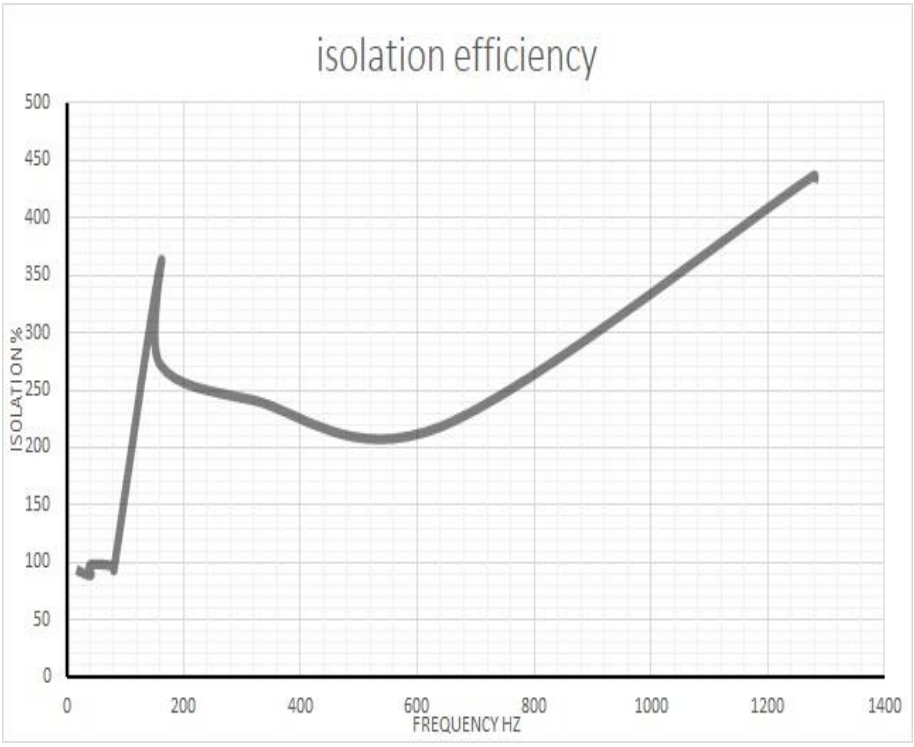


**Figure 32:** Isolation efficiency curve

## 2-3 CONCLUSION

The results of the transmissibility analysis are shown in Figure 38. It can be observed that the transmissibility decreases as the frequency increases for all metal foam specimens. The maximum transmissibility reduction is achieved for the specimen with the highest porosity. This indicates that the metal foam specimens have a significant effect in reducing the vibration transmitted through the rotor system.

The effect of transmissibility on this study is that it provides a measure of the damping and isolation properties of the metal foam damper. By measuring the transmissibility, it is possible to determine how much of the input vibration is being transmitted through the damper and how much is being absorbed or dissipated. This information can then be used to calculate the damping and stiffness of the damper using the Half Power Bandwidth Method, which is a commonly used analytical method for determining the dynamic properties of a system.

Transmissibility plays an important role in understanding the behavior of the metal foam damper and its effectiveness in reducing vibration response and transmitted forces in the ball bearing system.

The vibration calibrator VC21D was used in this experiments to measure the transmissibility and the isolation efficiency of the metal foam damper. The metal foam damper sample was integrated in the vibration calibrator as donuts to study their vibration behaviour in simple vibration manner.

The bently Nevada rotor kit is very important test rig for our study, the prepared sample will be placed in the bearing adapter exactly in the housing covering the outer ring of the ball bearings in order to obtain vibratory analysis with or without the use of metal foam damper.

The foam damper sample shows good vibrations characteristics. The isolation versus frequency curve present valuable results which is with the increase of frequency the isolation of vibration from the foam damper increases and could be good solution for vibration minimization in simple rotor supported by two ball bearings with metal foam damper.

# CHAPTER 03: NUMERICAL ANALYSIS

## 3-1 INTRODUCTION

This chapter present numerical study of simple rotor system made of two ball bearings, a shaft and a disc. We focus mainly on studying the effect of metal foam damper on the vibrational behaviour of flexible rotor.

The lateral motion of flexible shaft supported by two ball bearings with metal foam damper is presented. At a basic level the finite element program consists of three aspects:Defining the model, forcing and operating conditions;Analyzing the system and generating the results; and Graphical means for interpreting the model and results.

Free response of a rotor is studied with and without application of metal foam damper. The dynamic coefficients of the metal foam damper are determined, the damping and stiffness are calculated by using a method called half power bandwidth method. The addition of metal foam damper to the overall model has a good impact on the rotor response results.

## 3-2FINITE ELEMENT MODELING OF A FLEXIBLE SHAFT SUPPORTED BY TWO BALL BEARINGS

### 3-2-1 ROTATING COORDINATE SYSTEM

In rotating systems, many instabilities arise because of the effects of the rotation. Therefore, we must be able to transform between the response in the rotating and stationary frames of reference. The transformations are developed by looking at displacements and forces in the x and y directions; however, rotations and moments about the Ox and Oy axes use the same transformations. Coordinates in the rotating frame are denoted by a tilde; therefore, $u$ and $v$ are the displacements in the x and y directions in the stationary frame, and $\bar{u}$ and $\bar{v}$ are the displacements in the $\bar{x}$ and $\bar{y}$ directions in the rotating frame. Once per revolution, these axis sets coincide. With reference to Figure 33, we can express the displacement in the rotating frame in terms of the displacement in the stationary frame as [98].

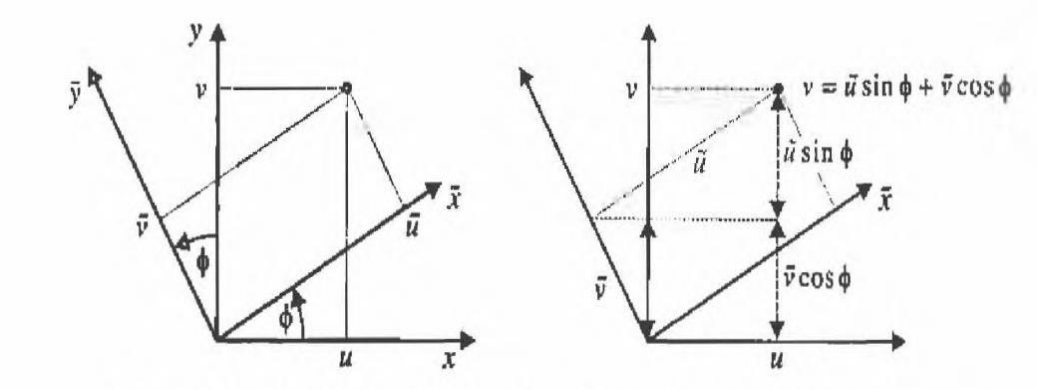


**Figure 33:**Rotating (x,y)and stationary (x,y)coordinates systems[95]

$$u = \bar{u}cos\phi - \bar{v}\sin\phi$$
$$v = \bar{u}sin\phi + \bar{v}\cos\phi \quad (25)$$

where $\phi$ is the angle between the two frames.Only the derivation for $v$ is illustrated in Figure 53; the derivation for $u$ is similar

Equation (25) may be written in matrix terms as:[98]

$$\begin{Bmatrix} u \\ v \end{Bmatrix} = \begin{bmatrix} \cos\phi & -\sin\phi \\ \sin\phi & \cos\phi \end{bmatrix} \begin{Bmatrix} \bar{u} \\ \bar{v} \end{Bmatrix} = \mathrm{T} \begin{Bmatrix} \bar{u} \\ \bar{v} \end{Bmatrix} \quad (26)$$

The 2x2 matrix is called the transformation matrix and is denoted by **T**. This matrix is orthogonal; hence,

$$\mathrm{T}\mathrm{T}^{\mathrm{T}} = I \text{ and , thus } \mathrm{T}^{-1} = \mathrm{T}^{\mathrm{T}} \quad (27)$$

where ***I*** is the identity matrix. The displacements in the rotating frame may be obtained from Equation (26) as:[98]

$$\begin{Bmatrix} \bar{u} \\ \bar{v} \end{Bmatrix} = \mathrm{T}^{-1} \begin{Bmatrix} u \\ v \end{Bmatrix} = \mathrm{T}^{T} \begin{Bmatrix} u \\ v \end{Bmatrix} = \begin{bmatrix} \cos\phi & \sin\phi \\ -\sin\phi & \cos\phi \end{bmatrix} \begin{Bmatrix} u \\ v \end{Bmatrix} \quad (28)$$

Thus, the transformation from the stationary to the rotating frame is given by $T^T$.

Suppose that the moving coordinate frame rotates relative to the stationary frame with a constant angular velocity Ω Then, $\phi = \Omega t$ and:

$$\mathrm{T} = \begin{bmatrix} \cos\Omega t & -\sin\Omega t \\ \sin\Omega t & \cos\Omega t \end{bmatrix} \quad (29)$$

Differentiating Equation (26) with respect to time, with **T** defined by Equation (29), gives:

$$\begin{Bmatrix}\dot{u}\\ \dot{v}\end{Bmatrix} = \mathrm{T}\begin{Bmatrix}\dot{\bar{u}}\\ \dot{\bar{v}}\end{Bmatrix} + \dot{\mathrm{T}}\begin{Bmatrix}\bar{u}\\ \bar{v}\end{Bmatrix} \tag{30}$$

Where

$$\dot{\mathrm{T}} = \Omega\begin{bmatrix}-\sin\Omega t & -\cos\Omega t\\ \cos\Omega t & -\sin\Omega t\end{bmatrix} \tag{31}$$

differentiating Equation (30) gives

$$\begin{Bmatrix}\ddot{u}\\ \ddot{v}\end{Bmatrix} = \mathrm{T}\left(\begin{Bmatrix}\ddot{\bar{u}}\\ \ddot{\bar{v}}\end{Bmatrix} - \Omega^2\begin{Bmatrix}\bar{u}\\ \bar{v}\end{Bmatrix}\right) + 2\dot{\mathrm{T}}\begin{Bmatrix}\dot{\bar{u}}\\ \dot{\bar{v}}\end{Bmatrix} \tag{32}$$

Similarly, differentiating Equation (28), with **T** defined by Equation (29), gives

$$\begin{Bmatrix}\dot{\bar{u}}\\ \dot{\bar{v}}\end{Bmatrix} = \mathrm{T}^T\begin{Bmatrix}\dot{u}\\ \dot{v}\end{Bmatrix} + \dot{\mathrm{T}}^T\begin{Bmatrix}u\\ v\end{Bmatrix} \tag{33}$$

Differentiating again gives:

$$\begin{Bmatrix}\ddot{\bar{u}}\\ \ddot{\bar{v}}\end{Bmatrix} = \mathrm{T}^T\left(\begin{Bmatrix}\ddot{u}\\ \ddot{v}\end{Bmatrix} - \Omega^2\begin{Bmatrix}u\\ v\end{Bmatrix}\right) + 2\dot{\mathrm{T}}^T\begin{Bmatrix}\dot{u}\\ \dot{v}\end{Bmatrix} \tag{34}$$

Having developed the transformation matrices, we can now convert between the stationary and rotating frames as required.

Each node now has four degrees of freedom because the rotations, as well as the displacements, must be included [99].

$$\begin{Bmatrix}u\\ v\\ \theta\\ \psi\end{Bmatrix} = T_2\begin{Bmatrix}u\\ v\\ \theta\\ \psi\end{Bmatrix} \tag{35}$$

Where

$$T_2 = \begin{bmatrix}T & 0\\ 0 & T\end{bmatrix} = \begin{bmatrix}cos\Omega t & -sin\Omega t & 0 & 0\\ sin\Omega t & cos\Omega t & 0 & 0\\ 0 & 0 & cos\Omega t & -sin\Omega t\\ 0 & 0 & sin\Omega t & cos\Omega t\end{bmatrix} \tag{36}$$

For a single node, the degrees of freedom are denoted by the vector$q_n = [\,u\ v\ \theta\ \psi]^T$and similarly by $q_n$ in rotating coordinates, these coordinates are transformed using $T_2$. Shaft elements have eight degree of freedomdenoted by the vector $q_\ell = \begin{Bmatrix}q_{n1}\\ q_{n2}\end{Bmatrix}$, where $n_1$ and $n_2$ are

the two nodes at each end of the shaft element. The degree of freedom for the shaft element must be transformed by:

$$T_4 = \begin{bmatrix} T & 0 & 0 & 0 \\ 0 & T & 0 & 0 \\ 0 & 0 & T & 0 \\ 0 & 0 & 0 & T \end{bmatrix} \tag{37}$$

With the coordinates and transformations defined, we may now consider the elements of the model.

### 3-2-2 DISK ELEMENTS MODEL

In this section we develop the properties of a rigid disk from an energy viewpoint.

The diametral inertia of the disk is assumed to be different in the $\bar{x}$ and $\bar{y}$ directions denoted by$I_{d\bar{x}}$and $I_{d\bar{y}}$ and the axes fixed in the disk are assumed to coincide with the principal axes of inertia.

The kinetic energy due to the translation of the disk is:[98]

$$T_{disk} = \frac{1}{2}m(\dot{u}^2 + \dot{v}^2) + \frac{1}{2}I_{d\bar{x}}\omega_x^2 + \frac{1}{2}I_{d\bar{y}}\omega_y^2 + \frac{1}{2}I_p\omega_z^2 \tag{38}$$

where $\omega_x$,$\omega_y$ and $w_z$ are the instantaneous angular velocities about the Ox, Oy, and Oz axes fixed in the disk.

The equations of motion must be developed in the stationary frame and transformed to the rotating frame.

The kinetic energy due to the rotation of the disk is more difficult to calculate because the inertia properties are not identical in all directions. Here, we assumethat the disk is symmetric so that the inertia properties may be calculated using the polar moment of inertia, $I_p$, about the shaft and the diametral moment of inertia, $I_d$ about any axis perpendicular to the shaft line. The kinetic energy due to the rotational motion of the disk is then:

$$\frac{1}{2}I_d\left(\omega_x^2 + \omega_y^2\right) + \frac{1}{2}I_p\omega_z^2 \tag{39}$$

Consider the angular velocity of the disk measured in a frame of reference that rotates with the disk. Making use of transformation matrices, this angular velocity is:[98]

$$\begin{Bmatrix}\omega_x\\ \omega_y\\ \omega_z\end{Bmatrix}=\begin{Bmatrix}0\\0\\\Omega\end{Bmatrix}+\begin{bmatrix}\cos\phi & \sin\phi & 0\\ -\sin\phi & \cos\phi & 0\\ 0 & 0 & 1\end{bmatrix}\begin{Bmatrix}\dot{\theta}\\0\\0\end{Bmatrix}$$
$$+\begin{bmatrix}\cos\phi & \sin\phi & 0\\ -\sin\phi & \cos\phi & 0\\ 0 & 0 & 1\end{bmatrix}\begin{bmatrix}1 & 0 & 0\\ 0 & \cos\theta & \sin\theta\\ 0 & -\sin\theta & \cos\theta\end{bmatrix}\begin{Bmatrix}0\\\dot{\psi}\\0\end{Bmatrix} \quad (40)$$

Although Equation (40) appears complicated, the origin of each term is easy to describe. The instantaneous angular velocity about the zaxis is $\Omega=\dot{\phi}$, where Ω is the disk rotational speed (assumed constant). Because the rotation $\phi$ is applied last, this angular velocity is given directly in axes fixed in the disk (given as the first term on the right side of Equation (40)).

The instantaneous angular velocity about the x axis is $\dot{\theta}$, but this must be rotated about the zaxis by the angle $\phi$.

This is the second term on the right side of Equation (40), where the angular velocity is clearly in the local xaxis position of the vector. The matrix is the standard form of a rotation about the zaxis because the transformation does not affect the z direction.

The last term transforms the instantaneous angular velocity about the yaxis $\dot{\psi}$ first by a rotation $\theta$ about the local x axis and then by a rotation $\phi$ about the z-axis. Multiplying out Equation (40) produces:[98]

$$\begin{Bmatrix}\omega_x\\ \omega_y\\ \omega_z\end{Bmatrix}=\begin{Bmatrix}\dot{\theta}cos\phi+\dot{\psi}\sin\phi\,cos\theta\\ -\dot{\theta}\sin\phi+\dot{\psi}cos\phi\cos\theta\\ \Omega-\dot{\psi}\sin\theta\end{Bmatrix} \quad (41)$$

The total kinetic energy is then:

$$T_d=\frac{1}{2}m_d(\dot{u}^2+\dot{v}^2)+\frac{1}{2}I_d\left(\omega_x^2+\omega_y^2\right)+\frac{1}{2}I_p\omega_z^2$$
$$=\frac{1}{2}m_d(\dot{u}^2+\dot{v}^2)$$
$$+\frac{1}{2}I_d\left(\dot{\theta}^2+\dot{\psi}^2cos^2\theta\right)+\frac{1}{2}I_p(\Omega^2$$
$$-2\Omega\dot{\psi}\sin\theta+\dot{\psi}^2sin^2\theta \quad (42)$$

Assuming the rotations $\theta$ and $\psi$ are small, we can neglect terms higher than second order and their derivatives. Thus,

$$T_d=\frac{1}{2}m_d(\dot{u}^2+\dot{v}^2)+\frac{1}{2}I_d\left(\dot{\theta}^2+\dot{\psi}^2\right)+\frac{1}{2}I_p(\Omega^2-2\Omega\psi\dot{\theta}) \quad (43)$$

The last term arises from the gyroscopic effects of the disk. The reason that $\dot{\psi}$ appears but not $\dot{\theta}$ is because of the order in which the rotations are applied.

The element matrices are obtained by applying Lagrange's equations to Equation (43). If the local coordinates are arranged in the vector $[u, v, \theta, \psi]^T$, then the inertia terms from Lagrange's equations are:[98]

$$\begin{Bmatrix} \frac{d}{dt}\left(\frac{\partial T_d}{\partial \dot{u}}\right) - \frac{\partial T_d}{\partial u} \\ \vdots \\ \vdots \\ \frac{d}{dt}\left(\frac{\partial T_d}{\partial \dot{\psi}}\right) - \frac{\partial T_d}{\partial \psi} \end{Bmatrix} = \begin{bmatrix} m_d & 0 & 0 & 0 \\ 0 & m_d & 0 & 0 \\ 0 & 0 & I_d & 0 \\ 0 & 0 & 0 & I_d \end{bmatrix} \begin{Bmatrix} \ddot{u} \\ \ddot{v} \\ \ddot{\theta} \\ \ddot{\psi} \end{Bmatrix} + \Omega \begin{bmatrix} 0 & 0 & 0 & 0 \\ 0 & 0 & 0 & 0 \\ 0 & 0 & 0 & I_p \\ 0 & 0 & -I_p & 0 \end{bmatrix} \begin{Bmatrix} \dot{u} \\ \dot{v} \\ \dot{\theta} \\ \dot{\psi} \end{Bmatrix} \tag{44}$$

Thus, we have the element mass matrix for the disk:

$$M_\ell = \begin{bmatrix} m_d & 0 & 0 & 0 \\ 0 & m_d & 0 & 0 \\ 0 & 0 & I_d & 0 \\ 0 & 0 & 0 & I_d \end{bmatrix} \tag{45}$$

and the element gyroscopic matrix for the disk

$$G_\ell = \begin{bmatrix} 0 & 0 & 0 & 0 \\ 0 & 0 & 0 & 0 \\ 0 & 0 & 0 & I_p \\ 0 & 0 & -I_p & 0 \end{bmatrix} \tag{46}$$

### 3-2-3 SHAFT MODEL

The shaft contributes both mass and stiffness to the overall rotor model.

The Euler-Bernoulli beam theory will be considered for the elastic shaft since the modeled shaft is long and slender. Other theories, like the Timoshenko beam theory is proper for shorter beams and larger cross-sections and includes the influence cause by shear loads on the shaft. This affects its total stiffness.

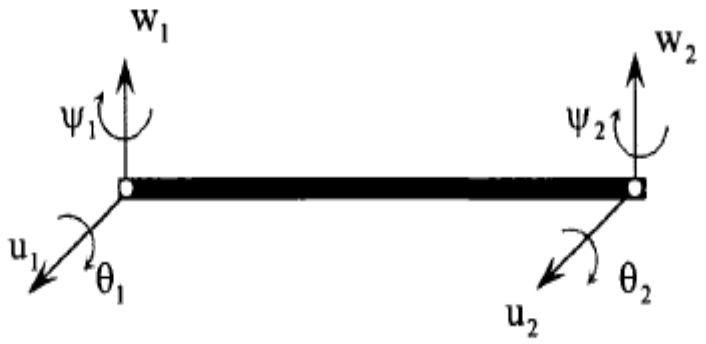


**Figure 34:** Shaft finite element rotor degree of freedom[98]

The nodal displacement vector for the shaft element can be written as:

$$\delta = [u_1, w_1, \theta_1, \psi_1, u_2, w_2, \theta_2, \psi_2]^T \tag{47}$$

Based on the local coordinate vector, the assumption is made that the two bending planes do not couple, therefore, the element matrices for the two planes are merely inserted into the correct location in the 8*8 shaft element matrices.

The stiffness matrix for the shaft elements does not need to be transformed because the asymmetry is fixed in the rotating frame. However, the stiffness matrices of a circular shaft must be extended to include the asymmetry.[98]

Assume that the principal axes of stiffness symmetry are in the $\bar{x}$ and $\bar{y}$ directions. This means that a force in the $\bar{x}$ direction does not produce a displacement in the $\bar{y}$direction and vice versa.

Thus, the stiffness matrix for a Euler-Bernoulli beam element is

$$\boldsymbol{K_\ell} = \boldsymbol{K_{\ell\bar{x}}} + \boldsymbol{K_{\ell\bar{y}}} \tag{48}$$

Where:

$$K_{\ell x} = \frac{EI_{\ell x}}{{l_\ell}^3}\begin{bmatrix} 12 & 0 & 0 & 6l_\ell & -12 & 0 & 0 & 6l_\ell \\ 0 & 0 & 0 & 0 & 0 & 0 & 0 & 0 \\ 0 & 0 & 0 & 0 & 0 & 0 & 0 & 0 \\ 6l_\ell & 0 & 0 & {4l_\ell}^2 & -6l_\ell & 0 & 0 & {2l_\ell}^2 \\ -12 & 0 & 0 & -6l_\ell & 12 & 0 & 0 & -6l_\ell \\ 0 & 0 & 0 & 0 & 0 & 0 & 0 & 0 \\ 0 & 0 & 0 & 0 & 0 & 0 & 0 & 0 \\ 6l_\ell & 0 & 0 & {2l_\ell}^2 & -6l_\ell & 0 & 0 & {4l_\ell}^2 \end{bmatrix} \tag{49}$$

$$K_{\ell y} = \frac{EI_{\ell y}}{{l_\ell}^3}\begin{bmatrix} 0 & 0 & 0 & 0 & 0 & 0 & 0 & 0 \\ 0 & 12 & -6l_\ell & 0 & 0 & -12 & -6l_\ell & 0 \\ 0 & -6l_\ell & 4{l_\ell}^2 & 0 & 0 & 6l_\ell & 2{l_\ell}^2 & 0 \\ 0 & 0 & 0 & 0 & 0 & 0 & 0 & 0 \\ 0 & 0 & 0 & 0 & 0 & 0 & 0 & 0 \\ 0 & 12 & 6l_\ell & 0 & 0 & 12 & 6l_\ell & 0 \\ 0 & -6l_\ell & 2{l_\ell}^2 & 0 & 0 & 6l_\ell & 4{l_\ell}^2 & 0 \\ 0 & 0 & 0 & 0 & 0 & 0 & 0 & 0 \end{bmatrix} \tag{50}$$

To obtain the mass matrices for the shaft elements, an approach similar to that used to obtain the inertia terms due to a disk must be used. However, for most shafts, the asymmetry in the diametral inertia is small and the shaft mass is assumed to be symmetric.

Consider first a Euler-Bernoulli beam element, In this case, the mass matrix depends only on the product of density and cross-sectional area of the rotor. The transformation between the stationary and rotating frames is given by Equation (35) for each node.

Thus, the equation of motion for the element is: [98]

$$M_\ell \ddot{q}_\ell + \Omega(M_{1\ell} + G_\ell)\dot{q}_\ell + \Omega^2(-M_\ell + \mathrm{G}_{1\ell})q_\ell = Q_\ell \tag{51}$$

Where$q_\ell$ is the usual vector of linear and rotational displacements at the two nodes and $Q_\ell$ is the applied force.

The matrix $M_{1\ell}$, is skewsymmetric and easily computed from the transformation and the element-mass matrix as:

$$M_{1\ell} = \frac{\rho_\ell A_\ell \ell_\ell}{210}\begin{bmatrix} 0 & -156 & 22\ell_\ell & 0 & 0 & -54 & -13\ell_\ell & 0 \\ 156 & 0 & 0 & 22\ell_\ell & 54 & 0 & 0 & -13\ell_\ell \\ -22\ell_\ell & 0 & 0 & -4\ell_\ell^2 & -13\ell_\ell & 0 & 0 & 3\ell_\ell^2 \\ 0 & -22\ell_\ell & 4\ell_\ell^2 & 0 & 0 & -13\ell_\ell & -3\ell_\ell^2 & 0 \\ 0 & -54 & 13\ell_\ell & 0 & 0 & -156 & -22\ell_\ell & 0 \\ 54 & 0 & 0 & 13\ell_\ell & 156 & 0 & 0 & -22\ell_\ell \\ 13\ell_\ell & 0 & 0 & 3\ell_\ell^2 & 22\ell_\ell & 0 & 0 & -4\ell_\ell^2 \\ 0 & 13\ell_\ell & -3\ell_\ell^2 & 0 & 0 & 22\ell_\ell & 4\ell_\ell^2 & 0 \end{bmatrix} \tag{52}$$

And $\mathbf{G_{1\ell}}$ is:

$$G_{1\ell} = \frac{2\rho_\ell I_\ell}{15\ell_\ell}\begin{bmatrix} 36 & 0 & 0 & 3\ell_\ell & -36 & 0 & 0 & 3\ell_\ell \\ 0 & 36 & -3\ell_\ell & 0 & 0 & -36 & -3\ell_\ell & 0 \\ 0 & -3\ell_\ell & 4\ell_\ell^2 & 0 & 0 & 3\ell_\ell & -\ell_\ell^2 & 0 \\ 3\ell_\ell & 0 & 0 & 4\ell_\ell^2 & -3\ell_\ell & 0 & 0 & -\ell_\ell^2 \\ -36 & 0 & 0 & -3\ell_\ell & 36 & 0 & 0 & -3\ell_\ell \\ 0 & -36 & 3\ell_\ell & 0 & 0 & 36 & 3\ell_\ell & 0 \\ 0 & -3\ell_\ell & -\ell_\ell^2 & 0 & 0 & 3\ell_\ell & 4\ell_\ell^2 & 0 \\ 3\ell_\ell & 0 & 0 & -\ell_\ell^2 & -3\ell_\ell & 0 & 0 & 4\ell_\ell^2 \end{bmatrix} \tag{53}$$

The rotary inertia effects are incorporated based on the average inertia properties of the

shaft section in the two directions. Although not strictly correct, the errors introduced are minor because most of the mass is usually in the disks. If we neglect shear deformations, the effect of rotary inertia is to add the following matrix to $\mathbf{M}_{\ell}$:[98]

$$M_{r\ell} = \frac{\rho_\ell I_\ell}{30\ell_\ell}\begin{bmatrix} 36 & 0 & 0 & 3\ell_\ell & -36 & 0 & 0 & 3\ell_\ell \\ 0 & 36 & -3\ell_\ell & 0 & 0 & -36 & -3\ell_\ell & 0 \\ 0 & -3\ell_\ell & 4\ell_\ell^2 & 0 & 0 & 3\ell_\ell & -\ell_\ell^2 & 0 \\ 3\ell_\ell & 0 & 0 & 4\ell_\ell^2 & -3\ell_\ell & 0 & 0 & -\ell_\ell^2 \\ -36 & 0 & 0 & -3\ell_\ell & 36 & 0 & 0 & -3\ell_\ell \\ 0 & -36 & 3\ell_\ell & 0 & 0 & 36 & 3\ell_\ell & 0 \\ 0 & -3\ell_\ell & -\ell_\ell^2 & 0 & 0 & 3\ell_\ell & 4\ell_\ell^2 & 0 \\ 3\ell_\ell & 0 & 0 & -\ell_\ell^2 & -3\ell_\ell & 0 & 0 & 4\ell_\ell^2 \end{bmatrix} \tag{54}$$

And the following matrix to $M_{1\ell}$ :

$$M_{r1\ell} = \frac{\rho_\ell I_\ell}{15\ell_\ell}\begin{bmatrix} 0 & -36 & 3\ell_\ell & 0 & 0 & 36 & 3\ell_\ell & 0 \\ 36 & 0 & 0 & 3\ell_\ell & -36 & 0 & 0 & 3\ell_\ell \\ 0 & 0 & 0 & -4\ell_\ell^2 & 3\ell_\ell & 0 & 0 & \ell_\ell^2 \\ 3\ell_\ell & -3\ell_\ell & 4\ell_\ell^2 & 0 & 0 & 3\ell_\ell & -\ell_\ell^2 & 0 \\ -36 & 36 & -3\ell_\ell & 0 & 0 & -36 & -3\ell_\ell & 0 \\ 0 & 0 & 0 & -3\ell_\ell & 36 & 0 & 0 & -3\ell_\ell \\ 0 & 0 & 0 & \ell_\ell^2 & 3\ell_\ell & 0 & 0 & -4\ell_\ell^2 \\ 3\ell_\ell & -3\ell_\ell & -\ell_\ell^2 & 0 & 0 & 3\ell_\ell & 4\ell_\ell^2 & 0 \end{bmatrix} \tag{55}$$

Hence, we have the model for the rotating parts of the machine; it remains to derive models for the bearings

### 3-2-4 BEARINGS MODEL

To simplify dynamic analysis, one widely used approach is to assume that the bearing has a linear load deflection relationship. This assumption is reasonably valid provided that the dynamic displacement are small and the degree of error inherent in this approach may be illustrated graphically or formally by the use of a Taylor series. Thus, the relationship between the forces acting on the shaft due to the bearing and the resultant velocities and displacement of the shaft may be approximated by:[98]

$$\begin{Bmatrix} f_x \\ f_y \end{Bmatrix} = -\begin{bmatrix} k_{uu} & k_{uv} \\ k_{vu} & k_{vv} \end{bmatrix}\begin{Bmatrix} u \\ v \end{Bmatrix} - \begin{bmatrix} C_{uu} & C_{uv} \\ C_{vu} & C_{vv} \end{bmatrix}\begin{Bmatrix} \dot{u} \\ \dot{v} \end{Bmatrix} \tag{56}$$

Where $f_x$and $f_y$are the dynamic forces in the x and y directions, and $u$ and $v$ are the

dynamic displacements of the shaft journal relative to the bearing housing in the x and y directions. Inertia terms also may be included in equations 56 if they are significant [98].

In vector notation, with $Q_s = \begin{Bmatrix} f_x \\ f_y \end{Bmatrix}$ and $q = \begin{Bmatrix} u \\ v \end{Bmatrix}$

$$Q_s = -K(\Omega)q - C(\Omega)\dot{q} \tag{57}$$

If the housing is fixed, q is the absolute dynamic displacement of the shaft journal. If the housing can displace due to lack of rigidity in the bearing supports, then

$$q = q_s - q_f \tag{58}$$

Where $q_s$are the coordinates at the shaft and $q_f$are the coordinate at the foundation or housing.thus,

$$Q_s = -K(\Omega)(q_s - q_f) - C(\Omega)(\dot{q_s} - \dot{q_f}) \tag{59}$$

The force on the foundation due to the bearing is:

$$Q_f = -Q_s \tag{60}$$

Thus, combining these two equations, we have

$$\begin{Bmatrix} Q_s \\ Q_f \end{Bmatrix} = -\begin{bmatrix} K(\Omega) & -K(\Omega) \\ -K(\Omega) & K(\Omega) \end{bmatrix}\begin{Bmatrix} q_s \\ q_f \end{Bmatrix} - \begin{bmatrix} C(\Omega) & -C(\Omega) \\ -C(\Omega) & C(\Omega) \end{bmatrix}\begin{Bmatrix} \dot{q_s} \\ \dot{q_f} \end{Bmatrix} \tag{61}$$

We now discuss the specific type of rouling elements bearings.

We now consider the stiffness of a rolling-element bearing. It has been shown [98,100-101] that the deflection $\delta$ (in meters) of a single steel ball or roller being compressed between two flat plates by a force $f$ (in Newtons) is given by [98]:

$$\delta = 4.36 \times 10^{-8} d^{-8} f^{2/3} (for\ a\ ball\ of\ diameter\ d\ in\ meters) \tag{62}$$

And

$$\delta = 3.06 \times 10^{-10} l^{-0.8} f^{0.9} (for\ a\ roller\ of\ length\ l\ in\ meters) \tag{63}$$

These approximations are sufficient for rolling-element bearings in which the rolling-

element radius is small compared to the radii of the inner and outer races.

The vertical stiffness of a ball bearing, $df/dy$, is then approximated [98] by

$$k_{vv} = k_b n_b^{2/3} d^{1/3} f_s^{1/3} cos^{5/3}\alpha \tag{64}$$

where $n_b$is the number of steel balls of diameter $d$ in the race, $\alpha$ is the contact angle (Figure 35), $f_s$ is the vertical static load acting on the bearing, and the constant is $k_b = 13 \times 10^6 N^{2/3} m^{-4/3}$. Similarly, for rolling-element bearings

$$k_{vv} = k_r n_r^{0.9} l^{0.8} f_s^{0.1} cos^{1.9}\alpha \tag{65}$$

where $n_r$ is the number of steel rolling elements of length $l$ in the race, $f_s$ is the static load due to gravity acting on the bearing in the vertical direction, $\alpha$ is again the contact angle, and the constant is $k_r = 1.0 \times 10^9 N^{0.9} m^{-1.8}$.

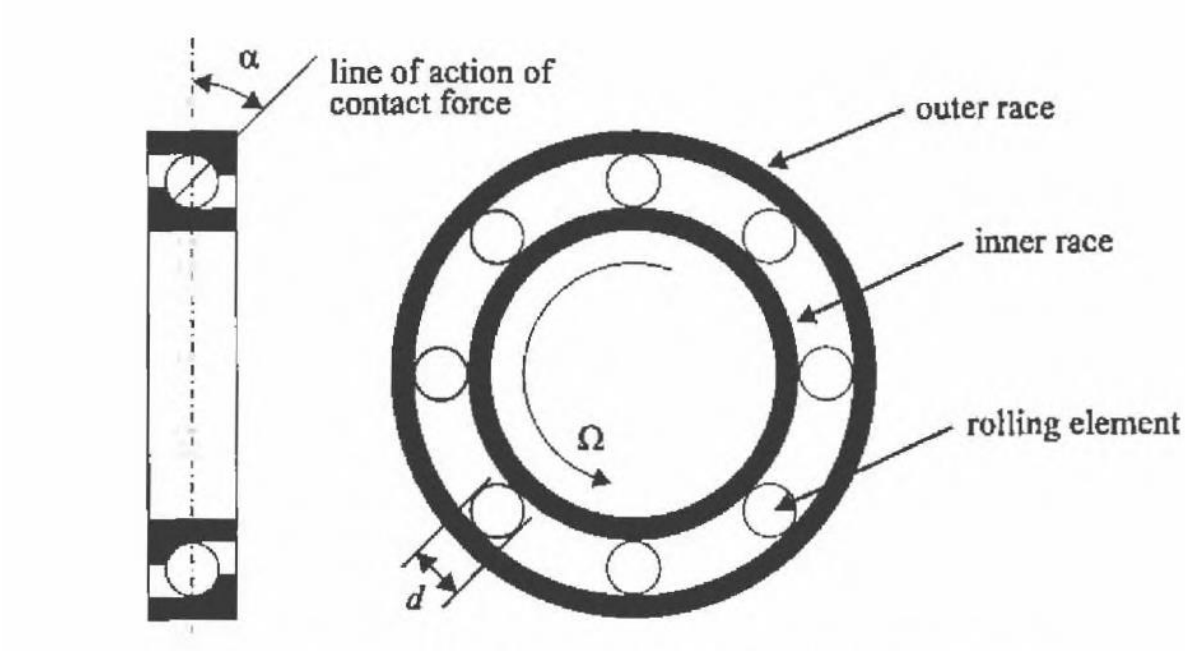


**Figure 35**:A typical ball bearing cross section [107]

Assuming the load is vertical, the ratio of the horizontal stiffness, $k_{uu}$, to the vertical stiffness,$k_{vv}$ , can be calculated.Kramer (1993)[97] gives the following data for ball and rolling-element bearings:

Ball bearing:$k_{uu}/k_{vv} = 0.46,0.64,0.73\ for\ 8,12,16\ balls, respectively.$

Roller bearing: $k_{uu}/k_{vv} = 0.49,0.66,0.74 \ \ for \ 8,12,16 \ rollers, respectively.$

This ratio is independent of the static load,$f_s$. Damping is low in rollingelement bearings and the damping coefficient c is typically in the range of $(0.25\sim2.5) \times 10^{-5} s \times k$, where k is a typical bearing stiffness.

### 3-2-5 ASSEMBLY OF THE FULL EQUATIONS OF MOTION

Combining all of the element matrices gives equations of motion of the form:[98]

$$[M_0]\ddot{q} + [C_0 + \Omega(G_0 + M_1)]\dot{q} + [K_0 + \Omega C_1 + \Omega^2(G_1 + M_2)]q = Q \tag{66}$$

Where $q$ represents the assembled generalized coordinate vector in the rotating frame and $Q$ is the generalized force, also in the rotating frame. The matrices $M_0, C_0, G_1, K_0$, and $M_2$ are symmetric and the matrices $M_1, C_1$ and $G_0$ are skew-symetric. $K_0$ represents the combined stiffness of the shaft and the foundation, expressed in rotating coordinates.

Consider the example shown in Figure 36, with three elements, four nodes, a disk at the second node, and short rigid bearings at each end

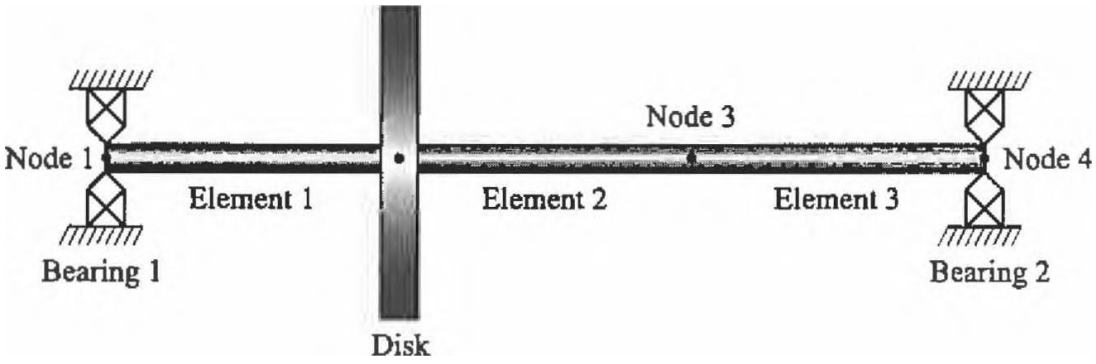


**Figure 36:** The simple three-element example to demonstrate matrix assembly[98]

The matrices for the shaft are assembled and then the constraints are applied. Before applying the support constraints, the shaft model has the following 16 degrees of freedom

$$q = [u_1, w_1, \theta_1, \psi_1, u_2, w_2, \theta_2, \psi_2, u_3, w_3, \theta_3, \psi_3, u_4, w_4, \theta_4, \psi_4]^T \tag{67}$$

The shaft-element matrices are 8 x 8 and the full-system matrices are 16 x 16. The first element corresponds to global degrees of freedom 1 to 8, the second element to degrees of freedom 5 to 12, and the third element to degrees of freedom 9 to 16.

$$M = \frac{\rho_\ell A l_\ell}{420}\begin{bmatrix} 156 & 0 & -221 & 54 & 0 & 0 & 131 & 0 & 0 & 0 & 0 & 0 & 0 & 0 & 0 & 0 \\ 0 & 156 & 221 & 0 & 0 & 54 & -131 & 0 & 0 & 0 & 0 & 0 & 0 & 0 & 0 & 0 \\ 0 & 221 & 41^2 & 0 & 0 & 131 & -31^2 & 0 & 0 & 0 & 0 & 0 & 0 & 0 & 0 & 0 \\ -221 & 0 & 0 & 41^2 & -131 & 0 & 0 & -31^2 & 0 & 0 & 0 & 0 & 0 & 0 & 0 & 0 \\ 54 & 0 & 0 & -131 & 312 & 0 & 0 & 0 & 54 & 0 & 0 & 131 & 0 & 0 & 0 & 0 \\ 0 & 54 & 131 & 0 & 0 & 312 & 0 & 0 & 0 & 54 & -131 & 0 & 0 & 0 & 0 & 0 \\ 0 & -131 & -31^2 & 0 & 0 & 0 & 81^2 & -131 & 0 & 0 & -31^2 & 0 & 0 & 0 & 0 & 0 \\ 131 & 0 & 0 & -31^2 & 0 & 0 & 0 & 81^2 & -131 & 0 & 0 & -31^2 & 0 & 0 & 0 & 0 \\ 0 & 0 & 0 & 0 & 54 & 0 & 0 & -131 & 312 & 0 & 0 & 0 & 54 & 0 & 0 & 131 \\ 0 & 0 & 0 & 0 & 0 & 54 & 131 & 0 & 0 & 312 & 0 & 0 & 0 & 54 & -131 & 0 \\ 0 & 0 & 0 & 0 & 0 & -131 & -31^2 & 0 & 0 & 0 & 81^2 & 0 & 0 & 131 & -31^2 & 0 \\ 0 & 0 & 0 & 0 & 131 & 0 & 0 & -31^2 & 0 & 0 & 0 & 81^2 & -131 & 0 & 0 & -31^2 \\ 0 & 0 & 0 & 0 & 0 & 0 & 0 & 0 & 54 & 0 & 0 & -131 & 156 & 0 & 0 & 221 \\ 0 & 0 & 0 & 0 & 0 & 0 & 0 & 0 & 0 & 54 & 131 & 0 & 0 & 156 & -221 & 0 \\ 0 & 0 & 0 & 0 & 0 & 0 & 0 & 0 & 0 & -131 & -31^2 & 0 & 0 & -221 & 41^2 & 0 \\ 0 & 0 & 0 & 0 & 0 & 0 & 0 & 0 & 131 & 0 & 0 & -31^2 & 221 & 0 & 0 & 41^2 \end{bmatrix}$$

$$M = \frac{\rho I}{301}\begin{bmatrix} 12 & 0 & -61 & -12 & 0 & 0 & -61 & 0 & 0 & 0 & 0 & 0 & 0 & 0 & 0 & 0 \\ 0 & 12 & 61 & 0 & 0 & -12 & 61 & 0 & 0 & 0 & 0 & 0 & 0 & 0 & 0 & 0 \\ 0 & 61 & 41^2 & 0 & 0 & -61 & 21^2 & 0 & 0 & 0 & 0 & 0 & 0 & 0 & 0 & 0 \\ -61 & 0 & 0 & 41^2 & 61 & 0 & 0 & 21^2 & 0 & 0 & 0 & 0 & 0 & 0 & 0 & 0 \\ -12 & 0 & 0 & 61 & 24 & 0 & 0 & 0 & -12 & 0 & 0 & -6 & 0 & 0 & 0 & 0 \\ 0 & -12 & -61 & 0 & 0 & 24 & 0 & 0 & 0 & -12 & 61 & 0 & 0 & 0 & 0 & 0 \\ 0 & 61 & 21^2 & 0 & 0 & 0 & 81^2 & 61 & 0 & 0 & 21^2 & 0 & 0 & 0 & 0 & 0 \\ -61 & 0 & 0 & 21^2 & 0 & 0 & 0 & 81^2 & 61 & 0 & 0 & 21^2 & 0 & 0 & 0 & 0 \\ 0 & 0 & 0 & 0 & -12 & 0 & 0 & 61 & 24 & 0 & 0 & 0 & -12 & 0 & 0 & -61 \\ 0 & 0 & 0 & 0 & 0 & -12 & -61 & 0 & 0 & 24 & 0 & 0 & 0 & -12 & 61 & 0 \\ 0 & 0 & 0 & 0 & 0 & 61 & 21^2 & 0 & 0 & 0 & 81^2 & 0 & 0 & -61 & 21^2 & 0 \\ 0 & 0 & 0 & 0 & -61 & 0 & 0 & 21^2 & 0 & 0 & 0 & 81^2 & 61 & 0 & 0 & 21^2 \\ 0 & 0 & 0 & 0 & 0 & 0 & 0 & 0 & -12 & 0 & 0 & 61 & 12 & 0 & 0 & 61 \\ 0 & 0 & 0 & 0 & 0 & 0 & 0 & 0 & 0 & -12 & 61 & 0 & 0 & 12 & -61 & 0 \\ 0 & 0 & 0 & 0 & 0 & 0 & 0 & 0 & 0 & 61 & 21^2 & 0 & 0 & -61 & 41^2 & 0 \\ 0 & 0 & 0 & 0 & 0 & 0 & 0 & 0 & -61 & 0 & 0 & 21^2 & 61 & 0 & 0 & 41^2 \end{bmatrix}$$

### 3-2-6 CALCULATION OF THE STIFFNESS K AND THE VDAMPING C OF THE FOAM DAMPER

The properties of the metal foams damper sample are:

**Table 3**:Properties of the metal foams damper sample

| **Properties** | **Value** |
|---|---|
| Porosity | 84% |
| E | 12.7mm |
| PPI | 08 |
| Mass | 0.083kg |
| Density | $3.32\times 10^{-3}$kg.m$^{-5}$ |

Damping can be calculated using the transmissibility curve using a method called the Half Power Bandwidth Method.

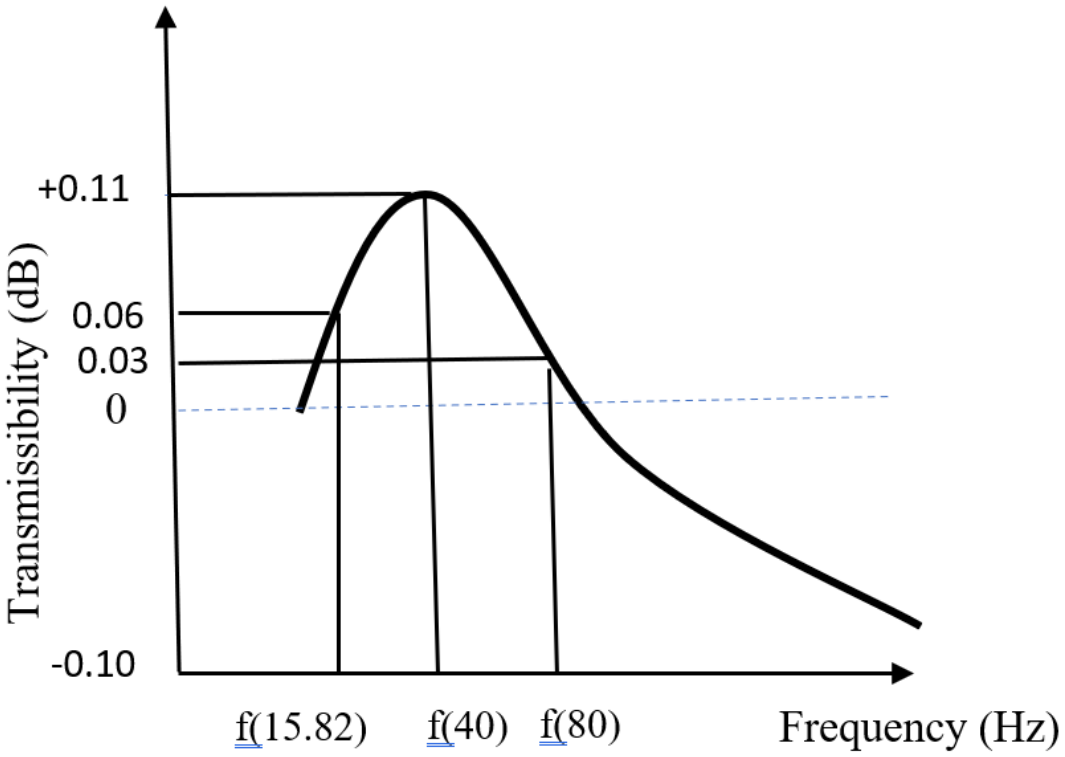


**Figure 37:** Half Power Bandwidth Method

$$\Delta f = 2f_n \tag{68}$$

$$f_n = \frac{\Delta f}{2}$$

NA: the natural frequency of the foam damper is: $f_0 = 12.09\ Hz$

$$\omega_n = 2\pi f_n \tag{69}$$

We know that :

$$\omega_0 = \sqrt{\frac{K}{M}} = 2\pi f_0 \tag{70}$$

So the stiffness of the foam damper is :

$$K_{FD} = M.(2\pi f_n)^2 \tag{71}$$

NA: $K_{FD} = 5.2427 \times 10^3$N/m

NA: $\omega_0 = \sqrt{\frac{K}{M}} = \sqrt{\frac{5.2427\times10^3}{0.083}} = 76\ rad.s^{-1}$

### 3-2-6-1 DAMPING COEFFICIENT $\xi$

The damping coefficient is calculated by:

$$\xi = \frac{1}{2\sqrt{T^2 - 1}} \tag{72}$$

Where T is the transmissibility

NA: $\xi = \frac{1}{2\sqrt{1.0257^2 - 1}}$

$\xi = 2.1314$

Now we can calculate the damping $C_{FD}$ of the foam damper by:

$$C_{FD} = 2 \times \xi \times \sqrt{(K_{FD} \times M)} \tag{73}$$

$C_{FD} = 2 \times 2.1314 \times \sqrt{(0.479 \times 10^3 \times 0.083)}$

NA: $C_{FD} = 91.4257 \text{Nm}^{-1}\text{s}^{-1}$

### 3-2-6-2 CALCULATION OF EQUIVALENT STIFFNESS AND DAMPING COEFFICIENTS

The stiffness of foams damper $K_{FD} = 5.2427 \times 10^3$ N/m is known, and the damping of the foam damper is $C_{FD} = 91.4257$ $\text{Nm}^{-1}\text{s}^{-1}$.

We assume that the stiffness and damping of the foam damper in the x and y direction is identical.

$$K_{FD} = K_{FDX} = K_{FDY} \tag{74}$$
$$C_{FD} = C_{FDX} = C_{FDY}$$

Where $K_{FDX}$ and $K_{FDY}$ are the stifness of the foam damper in the x and y direction, and $C_{FDX}\ and\ C_{FDY}$ are the damping of the foam damper in the x and y axis.

The equivalent dynamic coefficients relating to the bearings and the metal foam damper are determined according to the work of Hydrostatic journal bearing [102], then the equivalent dynamic coefficients are:

$$\frac{1}{K_{eqx}} = \frac{1}{K_{xx\ bearing}} + \frac{1}{K_{FDX}}\ \ and\ C_{eqx} = C_{xx\ bearing} + C_{FDX}$$
$$\frac{1}{K_{eqy}} = \frac{1}{K_{yy\ bearing}} + \frac{1}{K_{FDY}}\ \ and\ C_{eqy} = C_{yy\ bearing} + C_{FDY} \tag{75}$$

Where $K_{eqx}$ and $K_{eqy}$ are the equivalent stiffness coefficient according to the x and y axis. And $C_{eqx}$ and $C_{eqy}$ are the equivalent damping according to the x and y axis.

Now we calculate the value of Kxx and Kyy of the bearing. The bently Nevada rotor kit has a misumi TB6900zz ball bearing of diameter d=0.020m has 8 balls and $\alpha$ consider 0.

NA: $K_{xx} = 13 \times 10^9 \times 8^{2/3} 0.020^{1/3} \times cos\alpha^{5/3}$

$$K_{xxbearing} = 15.2 \times 10^9 N/m$$

NA: $K_{yybearing} = 2.9 \times 10^8 N/m$

The value of the diagonal damping of the ball bearing $C_{xx}$ and $C_{yy}$ is the same and equal to $C_{xx} = C_{yy} = 0\ N\ m^{-1}s^{-1}$

The numerical application of equation (8) gives:

$$\frac{1}{K_{eqx}} = \frac{1}{15.2 \times 10^9} + \frac{1}{5.2427 \times 10^3}$$

$$K_{eqx} = 5.2 \times 10^3 N/m$$

$$\frac{1}{K_{eqy}} = \frac{1}{2.9 \times 10^8} + \frac{1}{5.2427 \times 10^3}$$

$$K_{eqy} = 5.2 \times 10^3 N/m$$

NA : $C_{eqx} = 0 + 91.4257$

$$C_{eqx} = 91.4257\ Nm^{-1}s^{-1}$$

## 3-3FREE LATERAL RESPONSE OF A FLEXIBLE SHAFT SUPPORTED BY TWO BALL BEARINGS WITHOUT METAL FOAM DAMPER

### 3-3-1 MODELLING EXAMPLE

**Table 4:** Parameters of calculation:

| | |
|---|---|
| Young's modulus | $2.11\times10^9$N/mm$^2$ |
| Poisons' ratio | 0.3 |
| Density | 7810 Kg/m$^3$ |
| G | $81.2 \times10^9$ N/mm$^2$ |
| Bearing stiffness | $15.9*10^9$ N/m |
| Equivalent Bearing damping | 0Ns/m |

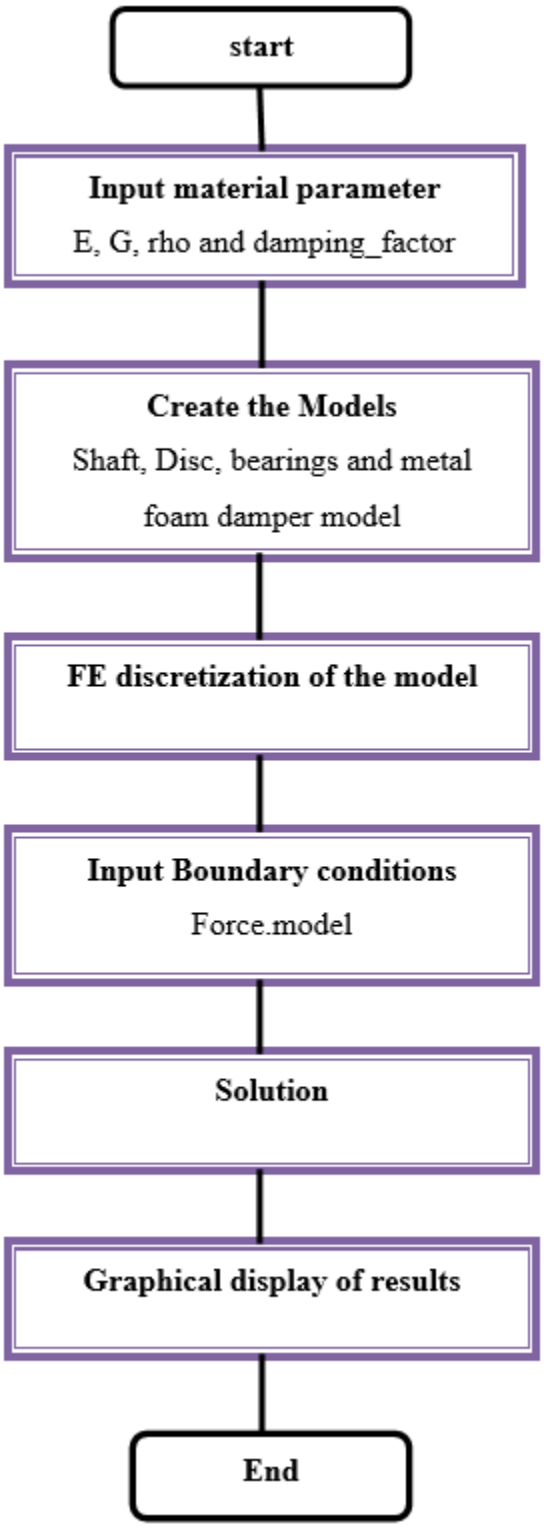


**Figure 38**: Organigramm of the vibration analysis of thet rotor

Now we have a simple rotor system, the finite element model is represented in figure 39:

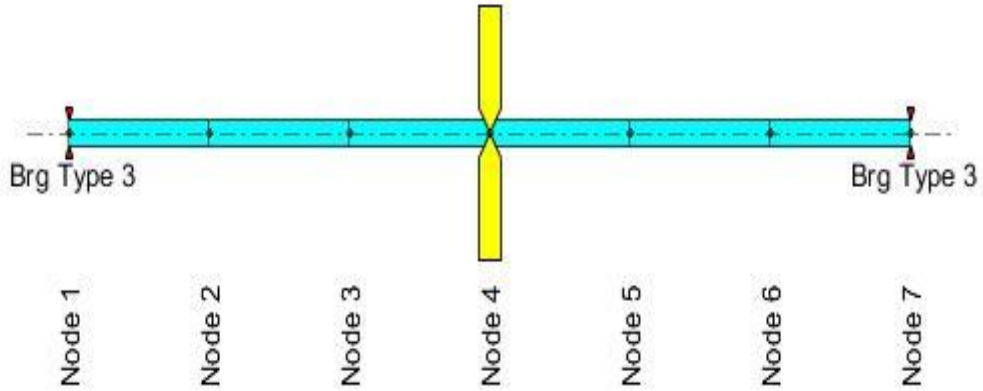


**Figure 39**:Finite element model

The Campbell diagram of the rotor :

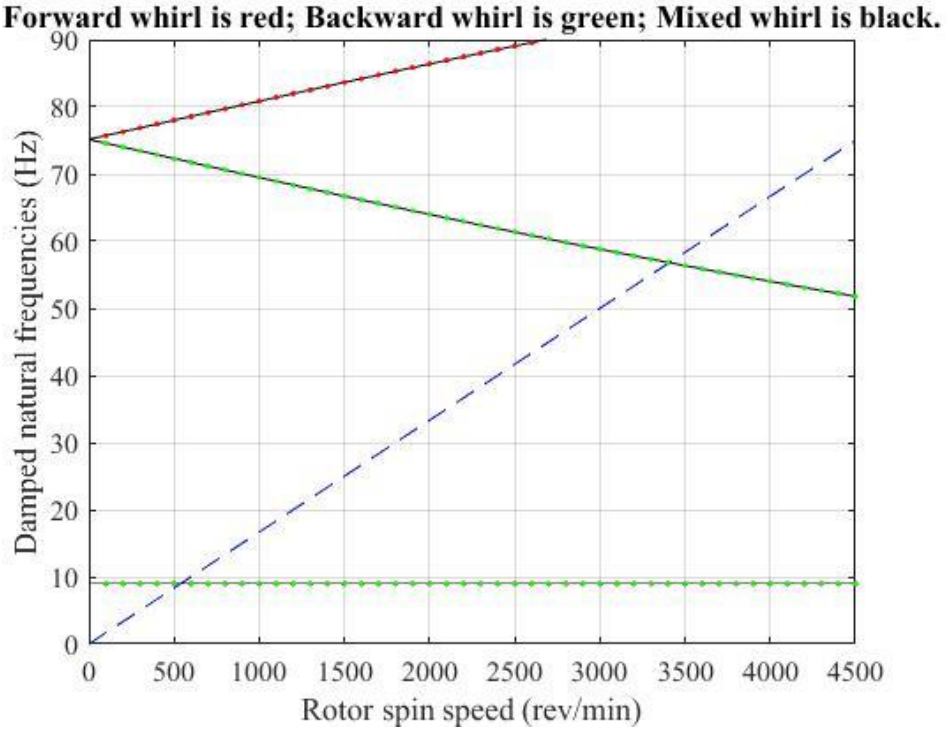


**Figure 40**: Campbell diagram at 4500rpm

The mode shapes and those for the isotropic bearings are shown below in figure 41. Here the mode shapes involve the deformation of the shaft at deferent natural frequency. For example at 8.960 Hz we have one mode shape, at 54.0088 and 96.4865Hz we have two mode shape for the shaft.

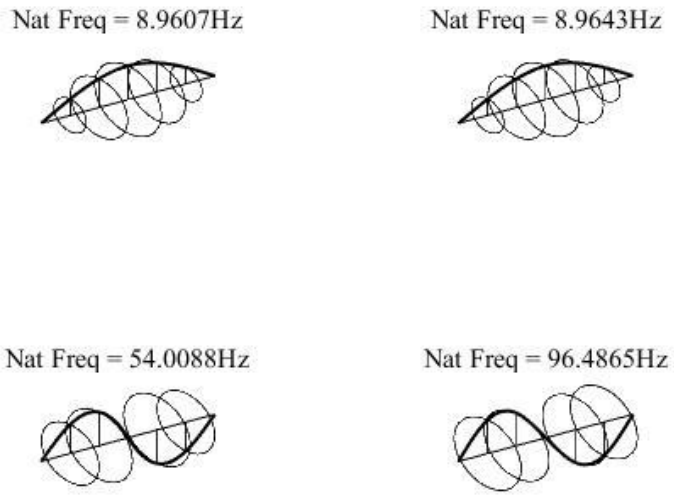


**Figure 41:** Mode shapes at 4500 rev-min

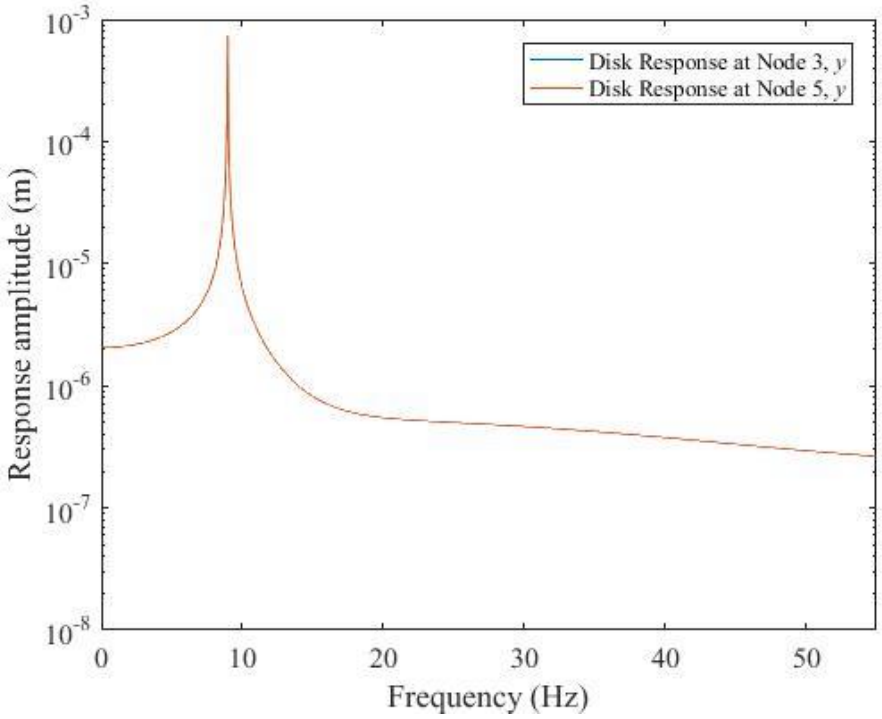


**Figure 42:**Rotor response at disk location node 4

Figure 42 shows the variation of the response amplitude with the frequency, we can notice that at certain frequency for example around 10Hz the response amplitude is maximum and reached a value of $10^{-3}$.

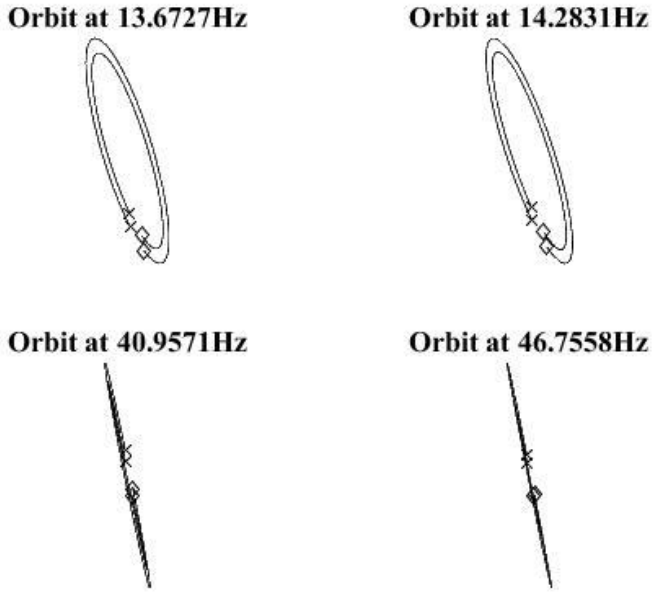


**Figure 43:**Whirl orbits for the foundation excitation without metal foam damper

## 3-4 FREE LATERAL RESPONSE OF A FLEXIBLE SHAFT SUPPORTED BY TWO BALL BEARINGS WITH METAL FOAM DAMPER

### 3-4-1 RUNNING THROUGH CRITICAL SPEED

The metal foam damper is used as a donut between the outer ring of the ball bearing and the housing covering the outer race of the ball bearing . This new approach offers more damping at the bearing location because metal foam has an important damping ratio. The stiffness of the ball bearing may change. In the matlab program, the stiffness of the bearing is calculated by adding to it the stiffness of the metal foam donut.

Frequently, in the design of machines, some of the parameters that directly affect the rotordynamics of the machine are not accurately known. In particular, bearing-support stiffness is one such parameter.

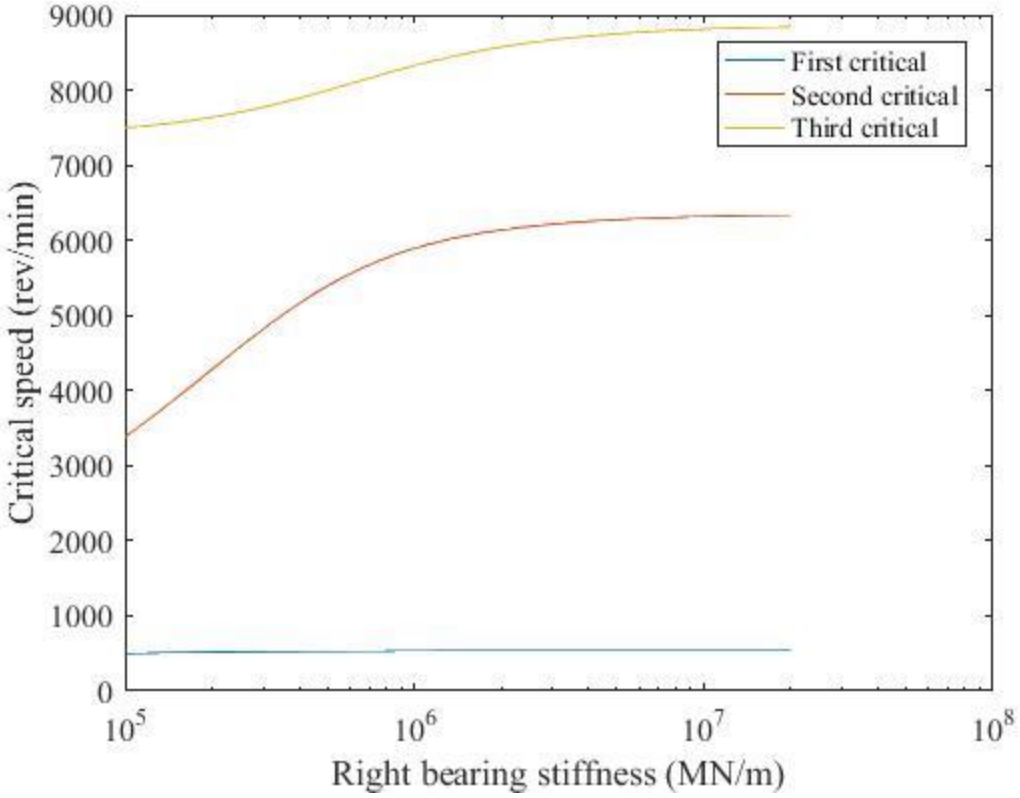


**Figure 44**:Variation of the lower positive critical speeds with bearing stiffness

Maps of critical speed and mode shapes enable an engineer to obtain rapidly an impression of how the uncertainty in one of the parameters affects the behavior of the machine. The most relevant concern is that the parameter cannot assume a value that causes one of the machine critical speeds to occur at an undesirable part of the running range of speeds.

In the Matlab program, the stiffness of the metal foam damper will be added to the stiffness of the bearing in order to achieve our goal (vibrational analysis of the shaft with the use of a metal foam damper).

The Young modulus of the foam damper is also integrated with the young modulus of the ball bearing.

The damping ratio and the density are added as input parameters to the matlab program.

The results shown in the next few pages are related to the use of metal foam dampers in the bearing, also known as donuts.

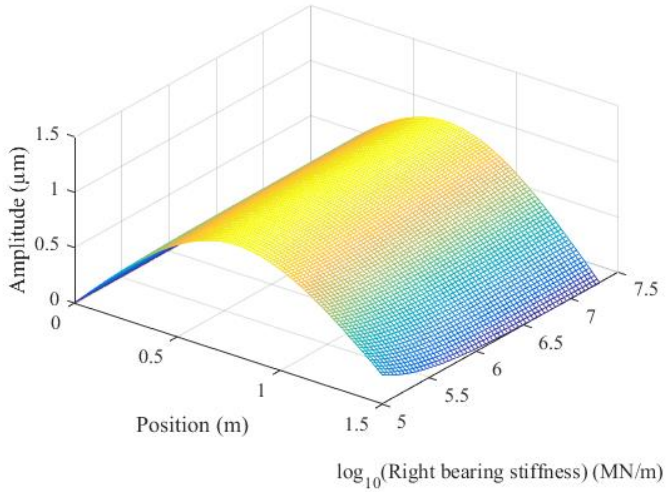


**Figure 45:** Variation of the first mode shape with bearing stiffness

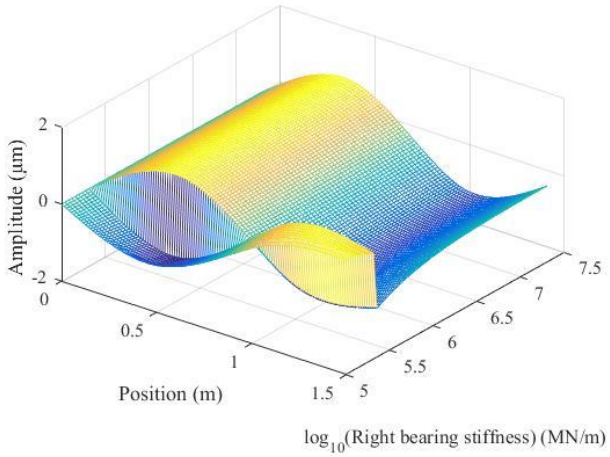


**Figure 46:** Variation of the second mode shape with bearing stiffness

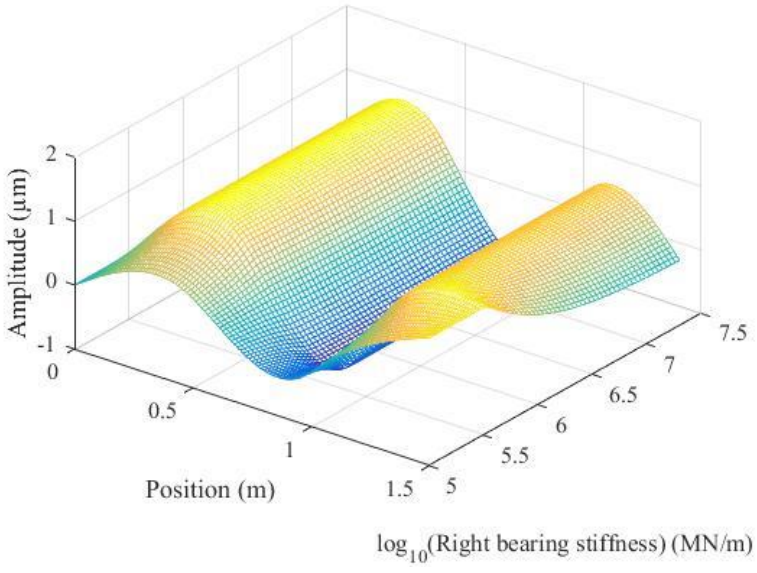


**Figure 47:** Variation of the third mode shape with bearing stiffness

The results obtained by using the following parameter

**Table 5:**Table of calculation parameter

| Parameter | Value |
|---|---|
| Young's modulus | $211\times10^9 N/mm^2$ |
| Poisons' ratio | 0.3 |
| Density | $7810\ Kg/m^3$ |
| G | $81.2\times10^9 N/mm^2$ |
| Equivalent Bearing stiffness | $15.2*10^9 N/m$ |
| Equivalent Bearing damping | $91.4257\ Ns^{-1}m^{-1}$ |

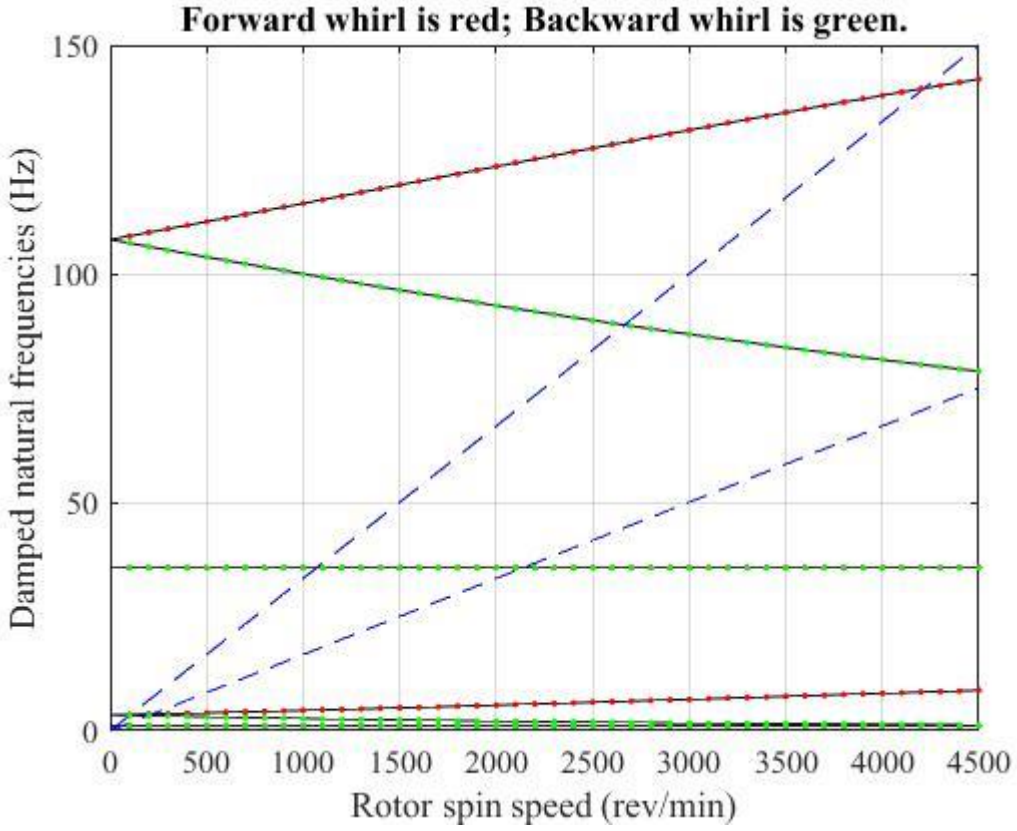


**Figure 48**: Campbell diagram

From the campbell diagram we can extract the frequency F(1)=F1(Ω)and F(2)=F2(Ω).

Where the intersection of the F1(Ω) and F2(Ω) with two straight lines give:

F1=90Hz and $\Omega_1 = 2556\ rev/min$

F2=142.5 HZ and $\Omega_2 = 4056\ rev/min$

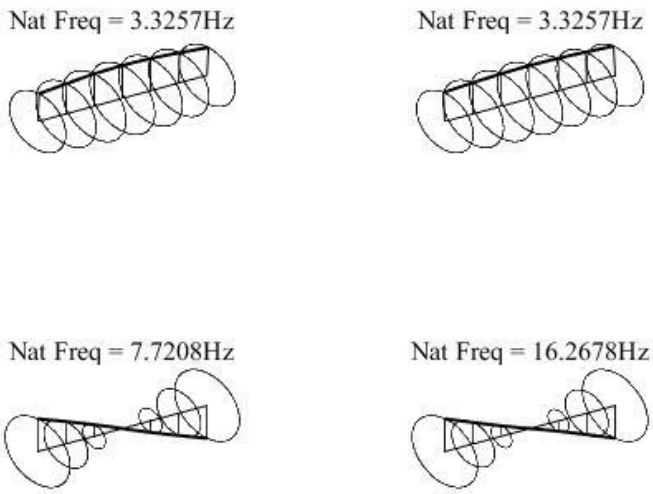


**Figure 49**: Mode shape at 4500 rev-min with metal foam damper

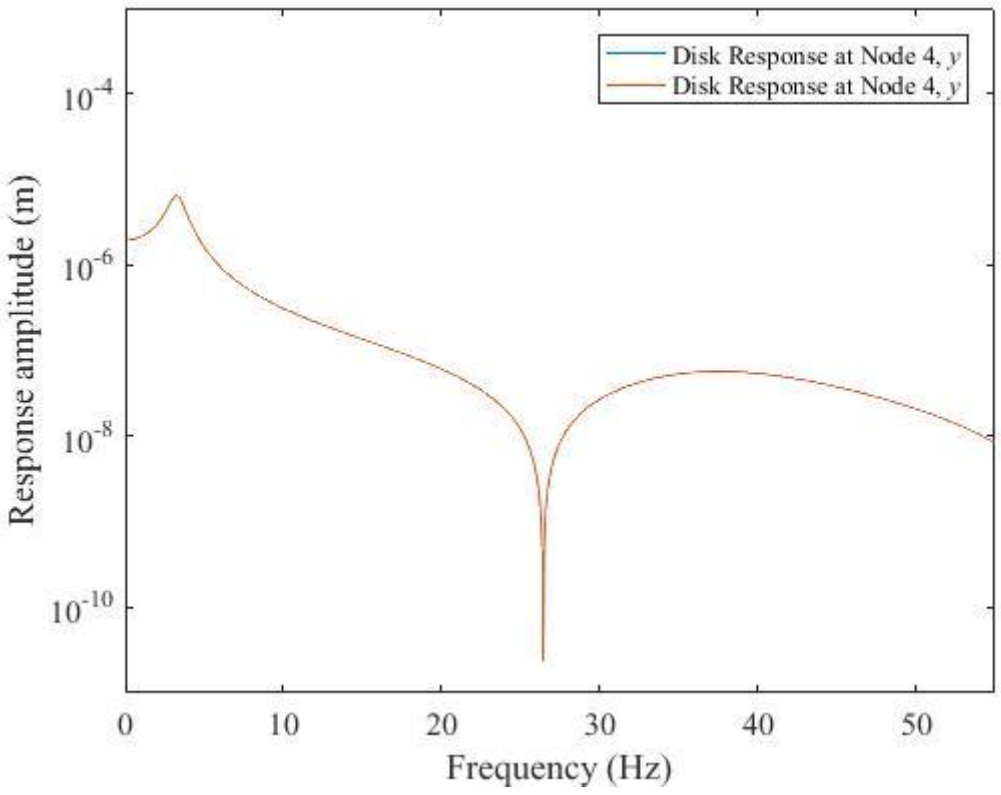


**Figure 50**: Rotor response at node 4 with metal foam damper

Figure 50 represents the variation of the response amplitude with the frequency. We can notice that there is decrease in the response amplitude when we add the metal foam damper to the overall rotor model.

## 3-5 ANALYSE OF THE RESULTS

The figure 42 depicts the response amplitude of the rotor without the usage of metal foam damper. We can notice that at around 10 Hz the amplitude is maximum and reached a value of $10^{-3}$m.

The figure 50 depicts the response amplitude of the rotor with the use of metal foam damper. We can notice the amplitude decreased and reached itsminimum value around $10^{-6}$m because the effect of metal foam damper.

Comparing the two figures, we can notice an attenuation of the amplitude due to the use of the foam damper.

Therefore, the obtained results show that the use of the metal foam in the jeffcott rotor has a good impact in the rotor vibrations.

## 3-6 CONCLUSION

This chapter proposes a new design for ball bearings with metal foam dampers, which aim to reduce rotor vibration amplitudes, minimize transmitted forces into supports, and suppress sound emissions during resonance. The experimental results obtained through dynamic testing of aluminum foam dampers and numerical simulation analysis based on finite element method in MATLAB® show that the proposed metal foam damper design can significantly improve rotor dynamics performance compared to traditional solutions.

The free response of shaft supported by two ball bearings with metal foam damper is presented, the variation of the three first mode shapes with bearings stiffness are computed and shown.

The free response of the rotor is studied with and without the application of the metal foam damper. The dynamic coefficients of the metal foam damper, i.e., the damping and stiffness, are calculated using the half power bandwidth method. The results show that the addition of the metal foam damper has a positive impact on the response of the rotor system. Therefore, it can be concluded that the use of a metal foam damper can effectively minimize the vibrational response amplitudes and transmitted forces during the passage through resonance in a flexible rotor system.

The response amplitude of the rotor at disk location with and without the using of metal foams damper was studied and analysed.

As aresult, we have decreased in the rotor response due to the use of metal foam damper

.

# GENERAL CONCLUSION AND FUTURE WORKS

In this thesis, we have investigated the effectiveness of using an aluminum foam damper to reduce the vibration in a flexible shaft supported by two ball bearings. Our research has led to several key findings.

- ✓ First, we have shown that the equivalent stiffness of the metal foam damper has a significant effect on the response amplitude of the flexible shaft. The stiffness of the damper can be optimized to achieve the desired level of vibration attenuation.
- ✓ Second, we have demonstrated that damping in metal foams is crucial for the effective attenuation of vibration. The aluminum foam specimens used in our experimental study showed significant damping properties, making them an ideal material for vibration control.
- ✓ Third, we have reviewed the main vibration problems in rotating machinery and introduced some technical solutions to control them. By citing relevant literature, we have highlighted the contributions of active, semi-active, and passive vibration control methods.
- ✓ Fourth, we have conducted an experimental study to determine the dynamic characteristics of aluminum foam specimens. Our results have provided valuable insights into the stiffness and damping properties of these materials.
- ✓ Fifth, we have presented an original idea for a new bearing damper made of aluminum foam. This innovative design requires no lubrication or auxiliary systems and takes inspiration from the use of viscoelastic materials in element bearings such as the wire mesh donuts.
- ✓ Finally, we have carried out a numerical simulation analysis using MATLAB® and the finite element method to study the effect of aluminum foam on the vibrational behavior of a flexible shaft. Our results have shown that the use of aluminum foam can significantly reduce vibration amplitudes in the shaft.
- ✓ Another key finding of our research is that the metal foam damper not only helps to reduce vibration amplitudes, but also reduces the transmitted forces. This is an important benefit, as it can help to prolong the life of mechanical components by reducing the stress and wear caused by excessive forces.In fact, the reduction in transmitted forces is directly related to the damping properties of the metal foam. As the foam compresses and expands in response to vibration, it dissipates energy in the form of heat, which reduces the amplitude

of the vibration and the transmitted forces. This effect is particularly important in ball bearing supported shafts, where excessive forces can cause premature wear and failure of the bearings

- ✓ Overall, our research has demonstrated the potential of using aluminum foam dampers for vibration control in rotating machinery. We hope that our findings will inspire further research and contribute to the development of more efficient and reliable mechanical systems.

The objective of this study was to investigate the potential benefits of incorporating a metal foam damper in a ball bearing design to reduce vibration response, transmitted forces, and sound emissions during resonance. The experimental procedure involved obtaining the metal foam sample material, cutting it to the desired dimensions, and configuring it in the vibration calibrator VC 21D. The damping and stiffness of the metal foam damper were then calculated using the Half Power Bandwidth Method, and the obtained properties were used to perform a vibration analysis of the lateral motion of a simple rotor using MATLAB

In conclusion, the use of metal foam dampers has shown great potential for reducing vibration amplitudes and improving the dynamic performance of mechanical systems. Our research has provided valuable insights into the stiffness and damping properties of aluminum foam, and has demonstrated the effectiveness of using aluminum foam dampers to reduce vibration in a flexible shaft supported by two ball bearings.

Our findings suggest that the use of aluminum foam dampers could provide a cost-effective and reliable solution to vibration problems in rotating machinery. By optimizing the design of the damper and tailoring its stiffness and damping properties to the specific application, it may be possible to achieve even greater levels of vibration attenuation. Furthermore, the review of literature on vibration control methods has provided a comprehensive overview of the various techniques available for controlling vibration in mechanical systems. This information can be used as a basis for further research and development of vibration control methods. Overall, our research has contributed to the body of knowledge on vibration control and has demonstrated the potential of using aluminum foam dampers for vibration attenuation in rotating machinery. We hope that our findings will inspire further research and innovation in this area, leading to the development of even more effective and reliable vibration control methods.

In our research, we compared the results of our experimental and numerical studies with and without the metal foam damper. The results showed that the addition of the metal foam damper had a significant impact on the vibration behavior of the flexible shaft. Without the

metal foam damper, the flexible shaft exhibited high levels of vibration amplitude, particularly at resonance frequencies. In contrast, with the metal foam damper in place, the vibration amplitude was significantly reduced, particularly at resonance frequencies. This indicates that the metal foam damper is effective in attenuating vibration and improving the dynamic behavior of the flexible shaft.

In addition, the comparison of the results with and without the metal foam damper showed that the transmitted forces were also significantly reduced with the metal foam damper in place. This indicates that the metal foam damper not only reduces vibration amplitude but also helps to protect the bearings and other components of the system from excessive stress and wear.

Furthermore, future research could also focus on optimizing the design of the metal foam damper, taking into consideration the specific requirements of different applications. The material properties of the foam, such as its stiffness and damping, could be tailored to meet the requirements of specific systems, leading to even better vibration attenuation. Another interesting avenue for future research is the investigation of the use of different types of metal foams, including those with different pore sizes, shapes, and densities. This could lead to the development of even more effective and versatile metal foam dampers that can be used in a wide range of applications.

It is important to note that the use of metal foam dampers is not limited to ball bearing supported shafts. These dampers could be used in a variety of mechanical systems to reduce vibration and improve dynamic performance. Therefore, future research could also focus on investigating the potential of using metal foam dampers in other types of mechanical systems.

In conclusion, our research has opened up new avenues for the use of metal foam dampers in vibration control, and we hope that our findings will inspire further research and innovation in this area. By continuing to explore the potential of metal foam dampers and optimizing their design for different applications, we can develop even more effective and reliable solutions for controlling vibration in mechanical systems.

## REFERENCES

[1] Mohamed, B. E. N. A. D. D. A. (2020). Conception d'un palier fluide intelligent à patins hydrostatiques contrôlés par des valves électrorhéologiques pour contrôler les vibrations de rotors (Doctoral dissertation, Université Ibn Khaldoun-Tiaret-).

[2] Neto, R. R., Bogh, D. L., & Flammia, M. (2006, September). Some experiences on rigid and flexible rotors in induction motors driving critical equipment in petroleum and chemical plants. In 2006 Record of Conference Papers-IEEE Industry Applications Society 53rd Annual Petroleum and Chemical Industry Conference (pp. 1-11). IEEE.

[3] Hartog, J. P. Den, "Vibrag6es nos sistemas Mecanicos", Edgard BlOcher, Ed. Da Universidade de Sao Paulo, 1972.

[4] Vance, J. M., Zeidan, F. Y., & Murphy, B. G. (2010). Machinery vibration and rotordynamics. John Wiley & Sons.

[5] Mohanta, R. K., Chelliah, T. R., Allamsetty, S., Akula, A., & Ghosh, R. (2017). Sources of vibration and their treatment in hydro power stations-A review. Engineering science and Technology, an international journal, 20(2), 637-648.

[6] Sridharan, P., & Kuppuswamy, N. (2014). Mitigation of vibration on bulb turbine in small hydro electric power plants. Int. J. Eng. Tech., 5(6), 4968-79.

[7] Nandi, S., Toliyat, H. A., & Li, X. (2005). Condition monitoring and fault diagnosis of electrical motors—A review. IEEE transactions on energy conversion, 20(4), 719-729.

[8] K.A. Khudabashev, Effect of turn short-circuits in a turbo-generator rotor on its state of vibration, ElektStantsii (Russian) 7 (1961) 40–45.

[9] L.T. Rosenberg, Influence of shorted turns on thermal imbalance in large generators IEEE, PES Summer Meeting, paper A78 (1978) 587–588.

[10] Konstanzer, P., Enenkl, B., Aubourg, P., & Cranga, P. (2008, April). Recent advances in Eurocopter's passive and active vibration control. In Annual Forum Proceedings-American Helicopter Society (Vol. 64, No. 1, p. 854). American Helicopter Society, Inc.

[11] Fang, J., Xu, X., & Xie, J. (2015). Active vibration control of rotor imbalance

in active magnetic bearing systems. Journal of vibration and control, 21(4), 684-700.

[12] Bouzidane, A., & Thomas, M. (2013). Nonlinear dynamic behavior of a flexible shaft supported by smart hydrostatic squeeze film dampers. Journal of tribology, 135(3).

[13] Bouzidane, A., & Thomas, M. (2014). Linear and nonlinear behavior analysis of a flexible shaft supported by hydrostatic squeeze film dampers. International Journal of Engineering Research and Applications, 4(1), 311-316.

[14] Bonneau, O., Arghir, M., & Jolly, P. (2014). Dynamic control of a flexible shaft mounted in adaptive or active bearing. J. Mech. Eng. Autom, 4, 1-7.

[15] Lim, S., Park, S. M., & Kim, K. I. (2005). AI vibration control of high-speed rotor systems using electrorheological fluid. Journal of Sound and Vibration, 284(3-5), 685-703.

[16] San Andrés, L. (2010). Squeeze film dampers: Operation, models and technical issues. Modern Lubrication Theory, Notes, 13.

[17] Vance, J. M., Zeidan, F. Y., & Murphy, B. G. (2010). Machinery vibration and rotor dynamics. John Wiley & Sons.

[18] Xie, X., Yang, D., Ren, M., & Zhang, Z. (2022). Vibration transmission control of a flexible shaft-bearing system using active/passive support. Ocean Engineering, 264, 112450

[19] Roberts, J. B., & Kaya, F. (1987). Vibration control of a flexible transmission shaft by means of a squeeze-film damper: an experimental investigation. Journal of sound and vibration, 113(2), 329-345.

[20] Hesselbach J and Abel-Keilhack C 2002 Active hydrostatic bearing with magnetorheological fluid Proc. 8th Int. Conf. on New Actuators pp 343–6

[21] Guldbakke, J. M., & Hesselbach, J. (2006). Development of bearings and a damper based on magnetically controllable fluids. Journal of Physics: Condensed Matter, 18(38), S2959.

[22] Hamrock, B. J. (1991). Fundamentals of fluid lubrication (Vol. 1255). National Aeronautics and Space Administration, Scientific and Technical Information Program.

[23] Liu, W., Zhao, X., Zhang, T., & Feng, K. (2021). Investigation on the

rotordynamic performance of hybrid bump-metal mesh foil bearings rotor system. Mechanical Systems and Signal Processing, 147, 107076

[24] H. Blok and J. van Rossum, "The Foil Bearing-A New Departure in Hydrodynamic Lubrication," ASLE J. Lubr. Eng, vol. 9, pp. 346-330, 1953.

[25] D. Childs, "The Space Shuttle Main Engine High-Pressure Fuel Turbopump Rotordynamic Instability Problem," Journal of Engineering for Power, vol. 100, no. 1, pp. 48-57, 1978.

[26] P. Samanta, N. C. Murmu, and M. M. Khonsari, "The evolution of foil bearing technology," Tribology International, vol. 135, pp. 305-323, 2019, doi: 10.1016/j.triboint.2019.03.021.

[27] G. Agrawal, "FOIL AIR/GAS BEARING TECHNOLOGY - AN OVERVIEW," in International Gas Turbine & Aemengine Congress & Exhibition Orlando, Florida, 1997: ASME.

[28] C. McAuliffe and P. Dziorny, "BEARING COOLING ARRANGEMENT FOR AIR CYCLE MACHINE," United States Patent 5,113,670 Patent Appl. 562,162, 1992.

[29] L. Xiong, G. Wu, Y. Hou, L. Liu, M. Ling, and C. Z. Chen, "Development of aerodynamic foil journal bearings for a high speed cryogenic turboexpander," Cryogenics, vol. 37, no. 4, pp. 221-230, 1997.

[30] Y. Hou, Z. H. Zhu, and C. Z. Chen, "Comparative test on two kinds of new compliant foil bearing for small cryogenic turbo-expander," Cryogenics, vol. 44, no. 1, pp. 69-72, 2004, doi: 10.1016/j.cryogenics.2003.08.002.

[31] H. Heshmat, J. Walton II, and M. Tomaszewski, "Demonstration of a turbojet engine using an air foil bearing," in ASME Turbo Expo 2005: Power for Land, Sea and Air, Reno- Tahoe, Nevada, USA, ASME, Ed., 2005: ASME.

[32] S. Klusman, "GAS TURBINE ENGINE, MACHINE AND SELF-ALIGNING FOIL BEARING SYSTEM," United States Patent US 9,657,594 B2 Patent Appl. 14/141,399, 2017.

[33] H. Heshmat, J. Walton II, C. Della Corte, and M. Valco, "Oil-Free Turbocharger Demonstration Paves Way to Gas Turbine Engine Applications," in ASME TURBO EXPO 2000, Munich, Germany, ASME, Ed., 2000: ASME.

[34] H. Heshmat, J. Walton II, and M. Tomaszewski, "TURBOJET ENGINE

DEMONSTRATION WITH A HIGH TEMPERATURE AIR FOIL BEARING," in Proceedings of World Tribology Congress III, Washington, D.C., USA, ASME, Ed., 2005: ASME.

[35] R. Bruckner, "AN ASSESSMENT OF GAS FOIL BEARING SCALABILITY AND THE POTENTIAL," in Proceedings of ASME Turbo Expo 2010: Power for Land, Sea and Air, Glasgow, UK, 2010.

[36] J. Walton II, M. Tomaszewski, and H. Heshmat, "THE ROLE OF HIGH PERFORMANCE FOIL BEARINGS IN ADVANCED, OIL-FREE, HIGH-SPEED MOTOR DRIVEN COMPRESSORS," in Proceedings of Fuel Cell Science, Engineering and Technology, Rochester, New York, USA, 2003: ASME.

[37] S. Howard and C. DellaCorte, "Gas Foil Bearings for Space Propulsion Nuclear Electric Power Generation," NASA John H. Glenn Research Center at Lewis Field, Technical Memorandum 2006.

[38] C. Della Corte and O. Pinkus, "Tribological Limitations in Gas Turbine Engines_ A Workshop to Identify the Challenges and Set Future Directions," NASA John H. Glenn Research Center at Lewis Field, Technical Memorandum 2000.

[39] K. Feng, Y. Liu, X. Zhao, and W. Liu, "Experimental Evaluation of the Structure Characterization of a Novel Hybrid Bump-Metal Mesh Foil Bearing," Journal of Tribology, vol. 138, no. 2, 2016, doi: 10.1115/1.4031496.

[40] K. Feng, X. Zhao, C. Huo, and Z. Zhang, "Analysis of novel hybrid bump-metal mesh foil bearings," Tribology International, vol. 103, pp. 529-539, 2016, doi: 10.1016/j.triboint.2016.08.008.

[41] Y.-B. Lee, C. H. Kim, T. H. Kim, and T. Y. Kim, "Effects of Mesh Density on Static Load Performance of Metal Mesh Gas Foil Bearings," Journal of Engineering for Gas Turbines and Power, vol. 134, no. 1, 2012, doi: 10.1115/1.4004142.

[42] H. Ao, H. Jiang, W. Wei, and A. Ulanov. (2005). Study on the Damping Characteristics of MR Damper in Flexible Supporting of Turbo-Pump Rotor for Engine.

[43] M. Zarzour, "Experimental Evaluation of a Metal Mesh Bearing Damper," in

International Gas Turnine & Aeroengine Congress & Exhibition, Indianapolis, Indiana, 1999: Transactions of the ASME.

[44] A. Okayasu, T. Ohta, T. Azuma, T. Fujita, and H. Aoki, "Vibration problem in the LE-7 LH2 turbopump," presented at the AIAA/SAE/ASME/ASEE 26th Joint Propulsion Conference, Orlando, FL, 1990.

[45] C. DellaCorte, A. R. Zaldana, and K. C. Radil, "A Systems Approach to the Solid Lubrication of Foil Air Bearings for Oil-Free Turbomachinery," Journal of Tribology, vol. 126, no. 1, pp. 200-207, 2004, doi: 10.1115/1.1609485.

[46] E. M. Al-Khateeb, "DESIGN, MODELING AND EXPERIMENTAL INVESTIGATION OF WIRE MESH VIBRATION DAMPERS," DOCTOR OF PHILOSOPHY, Texas A&M University,
3051578, 2002.

[47] L. San Andrés, T. A. Chirathadam, and T.-H. Kim, "Measurement of Structural Stiffness and Damping Coefficients in a Metal Mesh Foil Bearing," Journal of Engineering for Gas Turbines and Power, vol. 132, no. 3, 2010, doi: 10.1115/1.3159379.

[48] K. Gjika, P. Mahadevan, and A. Costeux, "Turbocharger Synchronous Vibration Control on High Speed Balancer: Test and Prediction," Journal of Engineering for Gas Turbines and Power, vol. 136, no. 7, 2014, doi: 10.1115/1.4026600.

[49] K. Gjika, A. Costeux, G. LaRue, and J. Wilson, "Ball bearing turbocharger vibration management: application on high speed balancer," Mechanics & Industry, vol. 21, no. 6, 2020, doi: 10.1051/meca/2020091.

[50] Yalcintas M. and Dai H., (1999), Smart Materials and Structures, 8, pp.560-573, Magnetorheological and electrorheological materials in adaptive structures and their performance comparison.

[51] Nikolajsen JL and Hoque MS. An electroviscous damper for rotor applications. J Vib Acoust 1990; 112: 440–443.

[52] Morishita S and Mitsui J. Controllable squeeze film damper (an application of electro-rheological fluid). J Vib Acoust 1992; 114: 354–357.

[53] Tichy JA. Behavior of a squeeze film damper with an electrorheological fluid. Tribol Trans 1993; 36: 127–133.

[54] Yao G, Guang M and Yang Q. Electro-rheological multilayer squeeze film damper and its application to vibration control of rotor system. J Vib Acoust 2000; 122: 7–11.

[55] Lim S, Park S-M and Kim K-I. AI vibration control of high-speed rotor systems using electrorheological fluid. J Sound Vib 2005; 284: 685–703.

[56] Peng J and Zhu K-Q. Effects of electric field on hydrodynamic characteristics of finite-length ER journal bearings. Tribol Int 2006; 39: 533–540.

[57] Sun Y and Thomas M. Control of torsional rotor vibrations using an electrorheological fluid dynamic absorber. J Vib Control 2010. DOI: 1077546309359759.

[58] Abed, A., Bouzidane, A., Thomas, M., & Zahloul, H. (2017). Performance characteristics of a three-pad hydrostatic squeeze film damper compensated with new electrorheological valve restrictors. Proceedings of the Institution of Mechanical Engineers, Part J: Journal of Engineering Tribology, 231(7), 889-899.

[59] Benadda, M., Bouzidane, A., Thomas, M., & Guilbault, R. (2020). Dynamic behavior analysis of a rigid rotor supported by hydrostatic squeeze film dampers compensated with new electrorheological valve restrictors. Industrial Lubrication and Tribology, 72(5), 611-619.

[60] Breńkacz, Ł., Witanowski, Ł., Drosińska-Komor, M., & Szewczuk-Krypa, N. (2021). Research and applications of active bearings: A state-of-the-art review. Mechanical Systems and Signal Processing, 151, 107423.

[61] Forte, P., Paternò, M., & Rustighi, E. (2004). A magnetorheological fluid damper for rotor applications. International Journal of Rotating Machinery, 10(3), 175-182.

[62] Wang, J., Zhang, J., Ma, L., & Yu, Y. (2019). Study on the effect mechanism of MRD to rotor system. Applied Sciences, 9(11), 2247.

[63] Zhu, C. (2005). A disk-type magneto-rheological fluid damper for rotor system vibration control. Journal of sound and vibration, 283(3-5), 1051-1069.

[64] Wang, J., Meng, G., Feng, N., & Hahn, E. J. (2005). Dynamic performance and control of squeeze mode MR fluid damper–rotor system. Smart Materials and Structures, 14(4), 529.

[65] J. Banhart, "Manufacture, characterization and application of cellular metals and metals foams," Progress in material science 46 (6), pp. 559-632, 2001.

[66] Costanza, G.,Gusmano G,Montanari,R.,Tata, M.E., "Manufacturing routes and applications of metal foams," La metallurgia italiana 95 (2), pp. 31-35, 2003.

[67] Matsushita, T. Fujibayashi, S., Kokubu, T., "Titanium foam for bone tissue engineering. In: mettalic foam bone , process modification and characterization and properties," Metallic Foam Bone. Woodhead Publishing, pp. 111-130, 2017.

[68] Costanza, G.,Dodbiba,G.,Tata, ME, "optimisation of the process parameter for the manufacturing of open cell iron foams with high energy absorption," Procedia structural integrity2, pp. 2227-2282, 2016.

[69] Singh, G., Pandey,P.M, "Uniform and graded open cell ordered foams fabricated by rapid manufacturing : surface morphology, Mechanical properties and energy absorption capacity," Materials science and Engineering A, vol. 761, no. (22), 2019.

[70] Costanza, G., Tata, ME, "Recycling of exhaust batteries in lead-foams electrode.," Rewas2013 Enabling materials Resource Sustainbility. Hoboken;Wiley, pp. 272-278, 2013.

[71] WAN, Tan, LIU, Yuan, ZHOU, Canxu, et al. , "Fabrication, properties, and applications of open-cell aluminum foams: A review," Journal of Materials Science & Technology,, vol. 62, pp. 11-24, 2021.

[72] ASHBY, Michael F., EVANS, Tony, FLECK, Norman A., et al, Metal foams: a design guide, Elsevier, 2000..

[73] Luo, Y., Yu, S., Liu, J., Zhu, X.,&Luo, Y, "Compressive property and energy absorption characteristic of open-cell SiCp/AlSi9Mg composite foams.," Journal of Alloys and Compounds, vol. 499, no. 2, p. 227–230., 2010.

[74] Rajak, D. K., Kumaraswamidhas, L. A., & Das, S, "An energy absorption behaviour of foam filled structures," Procedia Materials Science, vol. 5, p. 164–172., 2014.

[75] Rajak, D. K., Kumaraswamidhas, A., & L., & Das, S, "Energy absorption capabilities of aluminium foam-filled square.," Advanced Materials Letters, vol. 6, no. 1, p. 80–85., 2015.

[76] ASHBY, Michael F., EVANS, Tony, FLECK, Norman A., et al, Metal foams: a design guide, Elsevier, 2000..

[77] Rajak, D. K., Kumaraswamidhas, L. A., & Das, S. , "Technical overview of aluminium alloy foam.," *Reviews on Advanced Materials Science.,* Vols. 48,, p. 68–86., 2017.

[78] Ruan, D., Lu, G., Chen, F. L.,&Siores, E, "Compressive behaviour of aluminium foams at low and medium strain rates.," *Composite Structures,*, vol. 57, no. (1–4), p. 331–336., 2002.

[79] Paul, A., & Ramamurty, U., "Strain rate sensitivity of a closed-cell aluminum foam.," *Materials Science and Engineering: A,* vol. 281, no. 1–2, p. 1–7., 2000.

[80] Patel, A., Das, S., & Prasad, B. K. ,, "Compressive deformation behaviour of Al alloy (2014)–10wt.% SiCp composite: Effects of strain rates and temperatures.," *Materials Science and Engineering: A,* vol. 530, p. 225–232., 2011.

[81] Hall, I. W., Guden, M., & Yu, C.-J., "Crushing of aluminum closed cell foams: Density and strain rate effects," *Scripta Materialia,* vol. 43, no. 6, p. 515–521., 2000.

[82] Davies, G. J.,&Zhen, S., "Metallic foams: Their production, properties and applications," *Journal of Materials Science,*, vol. 18, no. 7, p. 1899–1911., 1983.

[83] Yang XH, Kuang JJ, Lu TJ, Han FS, Kim T, "A simplistic analytical unit cell based model for the effective thermal conductivity of high porosity open-cell metal foams.," *J Phys D Appl Phys,* vol. 46, p. 255302., 2013.

[84] Yang, Xiaohu, Tianjian Lu, and Tongbeum Kim., "Effective thermal conductivity modelling for closed-cell porous media with analytical shape factors.," *Transport in porous media,* vol. 100, no. 2, pp. 211-224, 2013.

[85] Yang XH, Lu TJ, Kim T, "An analytical model for permeability of isotropic porous media," *Phys Lett A* , vol. 378, p. 2308–2311, 2014.

[86] Bhattacharya A, Calmidi VV, Mahajan RL, "Thermophysical properties of high porosity metal foams.," *International Journal of Heat Mass Transfer* , vol. 45, p. 1017–1031, 2002.

[87] Yang, Xiaohu, Jiabang Yu, Zengxu Guo, Liwen Jin, and Ya-Ling He, "Role

of porous metal foam on the heat transfer enhancement for a thermal energy storage tube," *Applied Energy*, vol. 239, pp. 142-156, 2019.

[88] Zhao, C. Y., Lu, T. J., Hodson, H. P., & Jackson, J. D, "The temperature dependence of effective thermal conductivity of open-celled steel alloy foams.," *Materials Science and Engineering: A*, vol. 367, no. 1-2, p. 123–131., 2004.

[89] L. DAHIL, A. KARABULUT, S. BASPINAR, "Damping Properties of Open Pore Aluminum Foams Produced By Vacuum Casting And NaCl Dissolution Process," METALURGIJA, pp. 489-492, 2013.

[90] J.F. Ramírez, M. Cardona, J.A. Velez, I. Mariaka, J.A. Isaza, E. Mendoza, S. Betancourt, P. Fernández-Morales, "Numerical modeling and simulation of uniaxial compression of aluminum foams using FEM and 3D-CT images," Procedia Materials Science, pp. 227-231, 2014.

[91] Shunjie Yin, Nassif Rayess, "characterization of polymer-metal foam hybrid for use in vibration dampening and isolation," procedia materials science, pp. 311-316, 2014.

[92] Massimo Golettia, Valerio Mussia, Andrea Rossia, Michele Monnob, "Procedures for damping properties determination in metal foams to improve FEM modeling," Procedia Materials Science, vol. 4, p. 233 – 238, 2014.

[93] Beshoy Morkos, Surya Venkata Sumanth Dochibhatla, Joshua D. Summers, "Effects of Metal Foam Porosity, Pore Size and Ligament Geometry on Fluid Flow," Journal of Thermal Science and Engineering Applications, p. 1.4039302, July 2017.

[94] LAMANNA, Emanuele, GUPTA, Nikhil, CAPPA, Paolo, et al. Evaluation of the dynamic properties of an aluminum syntactic foam core sandwich. Journal of Alloys and Compounds, 2017, vol. 695, p. 2987-2994.

[95] Lenko Stanev, Mihail Kolev, Boris Drenchev, Ludmil Drenchev, "Open-Cell Metallic Porous materials obtained through space Holders—Part II Structure and Properties.," Journal of Manufacturing Science and Engineering, vol. 139, pp. 050802-1, MAY 2017.

[96] Choudhry, V. V. (2004). Experimental evaluation of wire mesh for design as a bearing damper (Doctoral dissertation, Texas A&M University).

[97] RAJAK, Dipen Kumar et GUPTA, Manoj., "An Insight Into Metal Based Foams.," Singapore Springer,, vol. 10, pp. 978-981., 2020.

[98] Friswell, Michael I., John ET Penny, Seamus D. Garvey, and Arthur W. Lees. Dynamics of rotating machines. Cambridge university press, 2010.

[99] Kang, Y., Shih, Y.-P., and Lee, A.-C. (1992), Investigation on the steady-state responses of asymmetric rotors, Journal of Vibration and Acoustics 114,194—208.

[100] Harris, T. A. (2001). Rolling Bearing Analysis, Fourth Edition (John Wiley and Son, New York).

[101] Kramer, E. (1993). Dynamics of Rotors and Foundations (Springer-Verlag, Berlin, Germany).

[102] Bouzidane, Ahmed, and Marc Thomas. "Equivalent stiffness and damping investigation of a hydrostatic journal bearing." Tribology transactions 50, no. 2 (2007): 257-267.

## APPENDIX A: SOFTWARE EXAMPLE OF SIMPLE JEFFCOTT ROTOR

```
% File name: Example_05_09_01.m
%
% Example 5.9.1
%
% This example has isotropic bearings
% A model with 6 Timoshenko beam elements
%
clear
close all
% Set the material parameters
E = 211e9;
G = 81.2e9;
rho = 7810;
damping_factor = 0; % no damping in shaft
% Consider a model with 6 equal length elements
% Shaft is 1.5m long
model.node = [1 0.0; 2 0.25; 3 0.5; 4 0.75; 5 1.0; 6 1.25; 7 1.50];
% Assume shaft type 2 - Timoshenko with gyroscopic effects included
% Solid shaft with 50mm outside diameter
shaft_od = 0.05;
shaft_id = 0.0;
model.shaft = [2 1 2 shaft_od shaft_id rho E G damping_factor; ...
2 2 3 shaft_od shaft_id rho E G damping_factor; ...
2 3 4 shaft_od shaft_id rho E G damping_factor; ...
2 4 5 shaft_od shaft_id rho E G damping_factor; ...
2 5 6 shaft_od shaft_id rho E G damping_factor; ...
2 6 7 shaft_od shaft_id rho E G damping_factor];
% Disk 1 at node 3 has diameter of 280mm and thickness of 70mm
% Disk 2 at node 5 has diameter of 350mm and thickness of 70mm
% Note inside diameter of disk is assumed to be the outside diameter
% of the shaft
disk1_od = 0.28;
disk2_od = 0.35;
disk_thick = 0.07;
model.disc = [1 3 rho disk_thick disk1_od shaft_od; ...
1 5 rho disk_thick disk2_od shaft_od];
% Constant stiffness short isotropic bearing (1NM/m) with no damping
% Bearings at the ends of the shaft - nodes 1 and 7
bear_stiff = 1e6;
model.bearing = [3 1 bear_stiff bear_stiff 0 0; ...
3 7 bear_stiff bear_stiff 0 0];
% Draw the rotor
figure(1), clf
picrotor(model)
% Plot the Campbell diagram
% ========================
% Define the rotor spin speed range
Rotor_Spd_rpm = 0:100:4500.0;
Rotor_Spd = 2*pi*Rotor_Spd_rpm/60; % convert to rad/s
% Calculate the eigensystem for the range of rotor spin speeds
[eigenvalues,eigenvectors,kappa] = chr_root(model,Rotor_Spd);
% Plot Campbell diagram
figure(2)
NX = 2;
damped_NF = 1; % plot damped natural frequencies
plotcamp(Rotor_Spd,eigenvalues,NX,damped_NF,kappa)
% Plot the modes and orbits at 4000 rev/min
% ========================================
% Calculate the eigensystem at 4000 rev/min
Rotor_Spd_rpm = 4000;
```

```
Rotor_Spd = 2*pi*Rotor_Spd_rpm/60; % convert to rad/s
[eigenvalues,eigenvectors,kappa] = chr_root(model,Rotor_Spd);
% Plot the first 4 eigenvectors and annotate with corresponding
% eigenvalue
figure(3)
subplot(221)
plotmode(model,eigenvectors(:,1),eigenvalues(1))
subplot(222)
plotmode(model,eigenvectors(:,3),eigenvalues(3))
subplot(223)
plotmode(model,eigenvectors(:,5),eigenvalues(5))
subplot(224)
plotmode(model,eigenvectors(:,7),eigenvalues(7))
% Plot the orbits at the disks for the first 6 eigenvectors
% Note that the axes command is used here for different subplots -
% the MATLAB command subplot could also have been used
figure(4)
outputnode = [3 5];
axes('position',[0.2 0.53 0.2 0.2 ])
plotorbit(eigenvectors(:,1),outputnode,'Mode 1',eigenvalues(1))
axes('position',[0.39 0.53 0.2 0.2 ])
plotorbit(eigenvectors(:,3),outputnode,'Mode 2',eigenvalues(3))
axes('position',[0.58 0.53 0.2 0.2 ])
plotorbit(eigenvectors(:,5),outputnode,'Mode 3',eigenvalues(5))
axes('position',[0.2 0.25 0.2 0.2 ])
plotorbit(eigenvectors(:,7),outputnode,'Mode 4',eigenvalues(7))
axes('position',[0.39 0.25 0.2 0.2 ])
plotorbit(eigenvectors(:,9),outputnode,'Mode 5',eigenvalues(9))
axes('position',[0.58 0.25 0.2 0.2 ])
plotorbit(eigenvectors(:,11),outputnode,'Mode 6',eigenvalues(11))
```

## APPENDIX B: CALCULATION OF MAPS OF CRITICAL SPEEDS AND ASSOCIATED MODE SHAPES.

```
% File name:   Example_06_10_01.m
%
% Example of Jeffcott rotor 6.10.1
%
% Calculation of maps of critical speeds and associated mode shapes.
% In this example the bearing stiffness is changed.
%


clear
format shorte
close all

set(0,'defaultaxesfontsize',12)
set(0,'defaultaxesfontname','Times New Roman')
set(0,'defaulttextfontsize',12)
set(0,'defaulttextfontname','Times New Roman')




% set the material parameters
E = 211e9;
Poisson = 0.3;
G = E/(2*(1+Poisson));
rho = 7810;
damping_factor = 0;    % no damping in shaft


% Consider the model with 6 equal length elements
% Shaft is 1.5m long
model.node = [1 0.0; 2 0.25; 3 0.5; 4 0.75; 5 1.0; 6 1.25; 7 1.50];

% Assume shaft type 2 - Timoshenko with gyroscopic effects included
% Solid shaft with 50mm outside diameter
shaft_od = 0.025;
shaft_id = 0.0;
model.shaft = [2 1 2 shaft_od shaft_id rho E G damping_factor; ...
               2 2 3 shaft_od shaft_id rho E G damping_factor; ...
               2 3 4 shaft_od shaft_id rho E G damping_factor; ...
               2 4 5 shaft_od shaft_id rho E G damping_factor; ...
               2 5 6 shaft_od shaft_id rho E G damping_factor; ...
               2 6 7 shaft_od shaft_id rho E G damping_factor];

% Disk at node 4 has diameter of 250mm and thickness of 40mm
% Note inside diameter of disk is assumed to be zero - this could be set
% as the outside diameter of the shaft
disk_od = 0.250;
disk_thick = 0.04;
model.disc = [1 4 rho disk_thick disk_od 0.0];

% constant stiffness and damping short bearing
% various options
% bearings at nodes 1 and 5
Bearing_LHcase = [1e7 1e7  0   0];
Bearing_RHcase = [1e7 1e7  0   0]; % this will be varied later
```

```
model.bearing = [3 1 Bearing_LHcase; ...
                 3 7 Bearing_RHcase];


% draw the rotor
figure(1), clf
picrotor(model)




% calculate critical speeds for different right bearing stiffnesses
% use the iterative method
% we only want the forward whirling critical speeds

Nk = 60;  % number of bearing stiffness values to consider
RH_bearing_k = logspace(5,7.3,Nk);  % define bearing stiffness values

nnode = size(model.node,1);
ndof = 4*nnode;

% to get a nice plot we need to use the shape functions to obtain a
smoother
% mode shape

z = model.node(:,2);  % axial node positions
n_xi = 20;  % number of points within an element
xi = (0:n_xi).'/n_xi; % points within element
N1 = ones(n_xi+1,1) - 3*xi.^2 + 2*xi.^3;  % shape functions
N2 = xi - 2*xi.^2 + xi.^3;
N3 = 3*xi.^2 - 2*xi.^3;
N4 = -xi.^2 + xi.^3;

zplot = [];
for inode = 1:nnode-1
Le = z(inode+1) - z(inode);
   zplot = [zplot; z(inode)*ones(n_xi+1,1)+Le*xi];
end

% parameters for critical speed calculations

NX = 1;
damped_NF = 1;
number_criticals = 6;
max_iterations = 20;
convergence_tol = 1e-6;

% initialise the critical speed map calculation and loop through bearing
% stiffness values

critical_freq_map_rpm = zeros(number_criticals,Nk);
critical_mode_map = zeros((nnode-1)*(n_xi+1),number_criticals,Nk);

for i=1:Nk

% set the bearing stiffness
    Bearing_RHcase = RH_bearing_k(i)*[1 1  0   0];
    model.bearing = [3 1 Bearing_LHcase; ...
                     3 7 Bearing_RHcase];% it was  3 5
```

```
% calculate critical speeds
    [critical_speeds,mode_shapes] =
crit_spd(model,NX,damped_NF,number_criticals,max_iterations,convergence_tol
);
    critical_freq_map_rpm(:,i) =
critical_speeds(1:number_criticals)*60/(2*pi);

% normalise mode shapes and then use the shape functions to produce
% smooth mode shapes in the x direction only
for ic=1:number_criticals
        [mx,index] = max(abs(mode_shapes(1:4:28,ic)));
mode_ic = mode_shapes(:,ic)/mode_shapes(4*index-3,ic);
        mode_xi = [];
for inode = 1:nnode-1
            Le = z(inode+1) - z(inode);
            xx = [N1 Le*N2 N3 Le*N4]*real(mode_ic([4*inode-3 4*inode
4*inode+1 4*inode+4]));
            mode_xi = [mode_xi; xx];
end
        critical_mode_map(:,ic,i) = mode_xi;
end

end



% plot variation of critical speeds
figure(2), clf
semilogx(RH_bearing_k,critical_freq_map_rpm(2:2:number_criticals,:))
xlabel('Right bearing stiffness (MN/m)')
ylabel('Critical speed (rev/min)')
legend('First critical','Second critical','Third critical')


% plot the variation of mode shapes
zplot = zplot*ones(1,Nk);
yplot = ones((nnode-1)*(n_xi+1),1)*log10(RH_bearing_k);

figure(3), clf
xplot = squeeze(real(critical_mode_map(:,2,:)));
mesh(zplot,yplot,xplot)
view(37.5,45)
xlabel('Position (m)')
ylabel('log_{10}(Right bearing stiffness) (MN/m)')
zlabel('Amplitude (µm)')

figure(4), clf
xplot = squeeze(real(critical_mode_map(:,4,:)));
mesh(zplot,yplot,xplot)
view(37.5,45)
xlabel('Position (m)')
ylabel('log_{10}(Right bearing stiffness) (MN/m)')
zlabel('Amplitude (µm) ')

figure(5), clf
xplot = squeeze(real(critical_mode_map(:,6,:)));
mesh(zplot,yplot,xplot)
view(37.5,45)
xlabel('Position (m)')
ylabel('log_{10}(Right bearing stiffness) (MN/m)')
zlabel('Amplitude (µm)')
```

```
%*****************************************************
% added by me
% plot the modes at a given speed
%*****************************************************
% Response to foundation excitation with constant stiffness bearings.
% determine case (a), icase = 1 (spinner), or case (b) (forced)

icase = menu('Example 6.5.1 - forcing through the foundations',...
'case (a) - frequency response',...
'case (b) - time response');
% define the unbalance force at node 3
% 1 = case (a) is isotropic bearings, 2 = case (b) is anisotropic

if icase == 1  % case (a) - frequency response
    force_mag = 1e-5;
    model.force = [4 0 force_mag 0 force_mag];
else% case (b) - forced time response to pulse
force_mag = 1e-3;
    pulse_duration = 0.025;
model.force = [5 0 force_mag 0 force_mag pulse_duration];
end
% plot the response to foundation excitation

Rotor_Spd_rpm = 3000.0;
Rotor_Spd = 2*pi*Rotor_Spd_rpm/60;  % convert to rad/s

if icase==1 % case (a) plot the frequency response

    omega_Hz = 0:0.05:55;
    omega = 2*pi*omega_Hz;  % convert to rad/s

    [response] = freq_fdn(model,Rotor_Spd,omega);

    figure(8), clf
    outnode = [3.1; 5.2];
    plotfrf(omega,response,outnode)

    figure(9), clf
    outnode = [3.1; 5.2];
    plotfrf(omega,response,outnode)

else% case (b) plot the time response

% plot time response

    dt = 0.00006;
    npts = 65536;
    [response,force,time] = time_fdn(model,Rotor_Spd,dt,npts);

    figure(10), clf
    plot(time,force)
    xlabel('Time (s)')
    ylabel('Foundation displacement pulse')

    figure(11), clf
    outdof = [10 18];  % output the y displacment at nodes 3 and 5
    plot(time,1000*response(outdof,:))
    xlabel('Time (s)')
    ylabel('Response displacement (mm)')
    legend('Node 3, {\ity}','Node 5, {\ity}')
```

```
% work out frequency response for pulse

    dt = 0.001;
    npts = 16384;
    nr = 10;
    [response,force,time] = time_fdn(model,Rotor_Spd,dt,npts,nr);

    [fft_out,omega_fft] = fftscale(response,time);
    [fft_force,omega_force] = fftscale(force,time);

    figure(12), clf
    semilogy(omega_fft,abs(fft_out(outdof,:)))
    xlabel('Frequency (Hz)')
    ylabel('Response amplitude (m)')
    legend('Disk Response at Node 3, {\ity}','Disk Response at Node 5,
{\ity}')
    axis([0 50 1e-8 1e-3])

    figure(13), clf
    semilogy(omega_force,1e-3*abs(fft_force))
    xlabel('Frequency (Hz)')
    ylabel('Foundation displacement amplitude (m)')
    axis([0 55 1e-7 1e-5])


    figure(14), clf
    outputnode = [4 7];
    subplot(221), ifreq = 225;
    plotorbit(fft_out(:,ifreq),outputnode,['Orbit at '
num2str(omega_fft(ifreq)) 'Hz'])
    subplot(222), ifreq = 235;
    plotorbit(fft_out(:,ifreq),outputnode,['Orbit at '
num2str(omega_fft(ifreq)) 'Hz'])
    subplot(223), ifreq = 672;
    plotorbit(fft_out(:,ifreq),outputnode,['Orbit at '
num2str(omega_fft(ifreq)) 'Hz'])
    subplot(224), ifreq = 767;
    plotorbit(fft_out(:,ifreq),outputnode,['Orbit at '
num2str(omega_fft(ifreq)) 'Hz'])

% plot the modes at a given speed

Rotor_Spd_rpm = 3000;
Rotor_Spd = 2*pi*Rotor_Spd_rpm/60;  % convert to rad/s
[eigenvalues,eigenvectors,kappa] = chr_root(model,Rotor_Spd);

figure(15)
subplot(221)
plotmode(model,eigenvectors(:,1),eigenvalues(1))
subplot(222)
plotmode(model,eigenvectors(:,3),eigenvalues(3))
subplot(223)
plotmode(model,eigenvectors(:,5),eigenvalues(5))
subplot(224)
plotmode(model,eigenvectors(:,7),eigenvalues(7))


% plot orbits

figure(16)
```

```
outputnode = [3 5];
axes('position',[0.2 0.53 0.2 0.2 ])
plotorbit(eigenvectors(:,1),outputnode,'Mode 1',eigenvalues(1))
axes('position',[0.39 0.53 0.2 0.2 ])
plotorbit(eigenvectors(:,3),outputnode,'Mode 2',eigenvalues(3))
axes('position',[0.58 0.53 0.2 0.2 ])
plotorbit(eigenvectors(:,5),outputnode,'Mode 3',eigenvalues(5))
axes('position',[0.2 0.25 0.2 0.2 ])
plotorbit(eigenvectors(:,7),outputnode,'Mode 4',eigenvalues(7))
axes('position',[0.39 0.25 0.2 0.2 ])
plotorbit(eigenvectors(:,9),outputnode,'Mode 5',eigenvalues(9))
axes('position',[0.58 0.25 0.2 0.2 ])
plotorbit(eigenvectors(:,11),outputnode,'Mode 6',eigenvalues(11))
end
```

## APPENDIX C: CALCULATES THE MASS, STIFFNESS AND DAMPING MATRICES FOR THE BEARINGS

```
function [Cb,Kb,K1b,zero_dof] = bearasym(model)
%
%  function bearasym.m
%
%     [Mb,Cb,Kb,zero_dof] = bearasym(model)
%
% calculates the mass, stiffness and damping matrices for the bearings
% for the asymetrical rotor case - bearings must be symetrical
%
% zero_dof indicates the degrees of freedom that should be constrained
% for stiff bearings (bearing types 1 and 2)

Node_Def = model.node;
Bearing_Def = model.bearing;

% determine the number of degrees of freedom and initialise matrices

[no_node,ncol_node] = size(Node_Def);
ndof = 4*no_node;
[nbearing,ncol_bearing] = size(Bearing_Def);
Cb  = zeros(ndof,ndof);
Kb  = zeros(ndof,ndof);
K1b = zeros(ndof,ndof);
zero_dof = [];

% go through each bearing, and deciding on bearing type include model

for i = 1:nbearing

    Bearing_Type = round(Bearing_Def(i,1));
if (Bearing_Type<1) | (Bearing_Type>4)
        disp(['>>>> Error - bearing type ' num2str(Bearing_Type) ' not
implemented - bearing ignored'])
end
Kb1 = zeros(4,4);
    K1b1 = zeros(4,4);
    Cb1 = zeros(4,4);

if Bearing_Type == 1       % short, stiff bearing - pinned boundary
condition
        n1 = Bearing_Def(i,2);
        zero_dof = [zero_dof 4*n1-3 4*n1-2];
end

if Bearing_Type == 2       % long, stiff bearing - clamped boundary
condition
        n1 = Bearing_Def(i,2);
        zero_dof = [zero_dof 4*n1-3:4*n1];
end

if Bearing_Type == 3       % constant stiffness and damping, diagonal, no
rotations
if ncol_bearing<6, disp('>>>> Error - too few columns in bearing definition
matrix for bearing type 3'), end
if Bearing_Def(i,3)~=Bearing_Def(i,4), disp('>>>> Error - bearings must be
symmetric'), end
```

```
if Bearing_Def(i,5)~=Bearing_Def(i,6), disp('>>>> Error - bearings must be
symmetric'), end
        Kb1 = diag( [Bearing_Def(i,3) Bearing_Def(i,4) 0 0] );
        Cb1 = diag( [Bearing_Def(i,5) Bearing_Def(i,6) 0 0] );
        K1b1(1,2) = -Bearing_Def(i,5); K1b1(2,1) = Bearing_Def(i,5);
end

if Bearing_Type == 4       % constant stiffness and damping, diagonal
if ncol_bearing<10, disp('>>>> Error - too few columns in bearing
definition matrix for bearing type 4'), end
if Bearing_Def(i,3)~=Bearing_Def(i,4), disp('>>>> Error - bearings must be
symmetric'), end
if Bearing_Def(i,5)~=Bearing_Def(i,6), disp('>>>> Error - bearings must be
symmetric'), end
if Bearing_Def(i,7)~=Bearing_Def(i,8), disp('>>>> Error - bearings must be
symmetric'), end
if Bearing_Def(i,9)~=Bearing_Def(i,10), disp('>>>> Error - bearings must be
symmetric'), end
        Kb1 = diag( [Bearing_Def(i,3) Bearing_Def(i,4) Bearing_Def(i,5)
Bearing_Def(i,6)] );
        Cb1 = diag( [Bearing_Def(i,7) Bearing_Def(i,8) Bearing_Def(i,9)
Bearing_Def(i,10)] );
        K1b1(1,2) = -Bearing_Def(i,7); K1b1(2,1) = Bearing_Def(i,7);
        K1b1(3,4) = -Bearing_Def(i,9); K1b1(2,1) = Bearing_Def(i,9);
end

    nnode = Bearing_Def(i,2);
    dof = (4*nnode-3):4*nnode;
    Kb(dof,dof) = Kb(dof,dof) + Kb1;
    Cb(dof,dof) = Cb(dof,dof) + Cb1;
    K1b(dof,dof) = K1b(dof,dof) + K1b1;

end
```

## APPENDIX D: CALCULATES THE CRITICAL SPEEDS FOR THE ROTOR SYSTEM

```
function [critical_speeds,mode_shapes] =
crit_spd(model,NX,damped_NF,number_criticals,max_iterations,convergence_tol
,initial_estimates)
%
%  function  crit_spd.m
%
%   [critical_speeds,mode_shape] = crit_spd(model,NX,damped_NF,
%      number_criticals,max_iterations,convergence_tol,initial_estimates)
%
% This functions calculates the critical speeds for the rotor system
% either using the direct approach (for constant stiffness bearings) or
% by iteration (possible for all cases). The critical speeds are defined
% when the rotor spin speed equals a natural frequency
%
%   NX                  shaft order to calculate unbalance
%                       (=1 for unbalance, which is default)
%
%   damped_NF           determines whether the damped natural frequencies
%                       (default, damped_NF=1) or undamped natural
%                       frequencies (damped_NF=0) are used
%
%   number_criticals    number of criticals to compute (default=5)
%
%   max_iterations      maximum iterations to try (default=20)
%
%   convergence_tol     relative change in critical speed from one
%                       iteration to next for convergence (default=1e-6)
%
%   initial_estimates   initial estimate of critical speeds - only used
%                       for iterative method and critical speeds closest
%                       to these initial estimates are obtained
% first sort out which method to use
%
%  imethod = 1    direct
%  imethod = 2    iterative, choose eigenvalue by number
%  imethod = 3    iterative, choose eigenvalue by closeness to current


% only methods 1 and 2 implemented so far
% =======================================


if nargin==7,
    imethod = 3;
    number_criticals = length(initial_estimates);
end
if nargin==6, imethod = 2; end
% check to see if there are any speed dependent bearings
Bearing_Def = model.bearing;
[nbearing,ncol_bearing] = size(Bearing_Def);
const_bearing = 1;
for i=1:nbearing
    bearing_type = Bearing_Def(i,1) ;
if (bearing_type==7) | (bearing_type==8)
        const_bearing = 0;
end
end
if (nargin<6)
```

```
if const_bearing
        imethod = 1;
else
        imethod = 2;
end
end

% add in defaults
if nargin < 2, NX = 1; end
if nargin < 3, damped_NF = 1; end
if nargin < 4, number_criticals = 5; end
if nargin < 5, max_iterations = 20; end
if nargin < 6, convergence_tol = 1e-6; end


% make sure NX is within a reasonable range
NX = abs(NX);
NX = max([NX 0.2]);


Node_Def = model.node;
[nnode,ncol_node] = size(Node_Def);
ndof = 4*nnode;

% The direct method

if imethod==1

    [M0,C0,C1,K0,K1] = rotormtx(model);
    [Mb,Cb,Kb,zero_dof] = bearmtx(model,0);
    dof = 1:ndof;
    dof(zero_dof) = [];
    nzero = length(zero_dof);
    ncdof = ndof - nzero;
    jot = sqrt(-1);
    MM = -(NX^2)*(M0 + Mb) + jot*NX*C1;
    CC = jot*NX*(C0 + Cb) + K1;
    KK = K0 + Kb;
    AA = [zeros(ncdof,ncdof) eye(ncdof,ncdof); -MM(dof,dof)\KK(dof,dof) -
MM(dof,dof)\CC(dof,dof)];
if nargout<=1
        eigenvalues = sort(eig(AA));
end
if nargout==2
        [eigenvectors,eigenvalues] = eig(AA);
[eigenvalues,isort] = sort(diag(eigenvalues));
eigenvectors = eigenvectors(:,isort);
        mode_shapes = zeros(ndof,number_criticals);
        mode_shapes(dof,:) =
eigenvectors(1:ncdof,(1:2:2*number_criticals));
end
if damped_NF
        critical_speeds = abs(real(eigenvalues(1:2:2*number_criticals)));
else
        critical_speeds = abs(eigenvalues(1:2:2*number_criticals));
end

end
```

```
if imethod==2

% obtain model of rotor
    [M0,C0,C1,K0,K1] = rotormtx(model);

% calculate critical speeds - first sort out zeroed DoF
    Rotor_Spd = 2*pi*500/60;  % start with initial guess of 500 rev/min
    [Mb,Cb,Kb,zero_dof] = bearmtx(model,Rotor_Spd);
    dof = 1:ndof;
    dof(zero_dof) = [];
    nzero = length(zero_dof);
    ncdof = ndof - nzero;
M = M0 + Mb;
    K = K0 + Kb + Rotor_Spd*K1;
    C = C0 + Cb + Rotor_Spd*C1;
    AA = [zeros(ncdof,ncdof) eye(ncdof,ncdof); -M(dof,dof)\K(dof,dof) -
M(dof,dof)\C(dof,dof)];
eigenvalues_initial = sort(eig(AA));

    critical_speeds = zeros(number_criticals,1);
for icritical = 1:number_criticals
        ieig = 2*icritical-1;
        rel_change = 1;
        iteration = 0;
if damped_NF>0.5
            critical_i = abs(imag(eigenvalues_initial(ieig)))/NX;
else
            critical_i = abs(eigenvalues_initial(ieig))/NX;
end
%  disp([icritical iteration 30*critical_i/pi])
while (rel_change>convergence_tol) & (iteration<max_iterations)
            [Mb,Cb,Kb,zero_dof] = bearmtx(model,critical_i);
            M = M0 + Mb;
            K = K0 + Kb + critical_i*K1;
            C = C0 + Cb + critical_i*C1;
            AA = [zeros(ncdof,ncdof) eye(ncdof,ncdof); -
M(dof,dof)\K(dof,dof) -M(dof,dof)\C(dof,dof)];
            eigenvalues = sort(eig(AA));
            critical_i_old = critical_i;
if damped_NF>0.5
                critical_i = abs(imag(eigenvalues(ieig)))/NX;
else
                critical_i = abs(eigenvalues(ieig))/NX;
end
if critical_i_old == 0
                rel_change = 2*convergence_tol;
else
                rel_change = abs( (critical_i -
critical_i_old)/critical_i_old );
end
            iteration = iteration + 1;
%     disp([icritical iteration 30*critical_i/pi])
end
        critical_speeds(icritical) = critical_i;
end

% Calculate the eigenvectors corresponding to the critical speeds if
% required

if nargout == 2
        mode_shapes = zeros(ndof,number_criticals);
for icritical = 1:number_criticals
```

```
            [Mb,Cb,Kb,zero_dof] =
bearmtx(model,critical_speeds(icritical));
            M = M0 + Mb;
            K = K0 + Kb + critical_speeds(icritical)*K1;
            C = C0 + Cb + critical_speeds(icritical)*C1;
            AA = [zeros(ncdof,ncdof) eye(ncdof,ncdof); -
M(dof,dof)\K(dof,dof) -M(dof,dof)\C(dof,dof)];
            [eigenvectors_i,eigenvalues] = eig(AA);
[eigenvalues,isort] = sort(diag(eigenvalues));
eigenvectors_i = eigenvectors_i(:,isort);
            mode_shapes(dof,icritical) =
eigenvectors_i(1:ncdof,2*icritical-1);
end
end

end
if imethod==3

% obtain model of rotor
    [M0,C0,C1,K0,K1] = rotormtx(model);

% calculate critical speeds - first sort out zeroed DoF
    Rotor_Spd = 2*pi*500/60;  % assume non-zero speed, just in case of
fluid bearings
    [Mb,Cb,Kb,zero_dof] = bearmtx(model,Rotor_Spd);
    dof = 1:ndof;
    dof(zero_dof) = [];
    nzero = length(zero_dof);
    ncdof = ndof - nzero;

    critical_speeds = zeros(number_criticals,1);
for icritical = 1:number_criticals
        rel_change = 1;
        iteration = 0;
        critical_i = abs(initial_estimates(icritical));
while (rel_change>convergence_tol) & (iteration<max_iterations)
            [Mb,Cb,Kb,zero_dof] = bearmtx(model,critical_i);
            M = M0 + Mb;
            K = K0 + Kb + critical_i*K1;
            C = C0 + Cb + critical_i*C1;
            AA = [zeros(ncdof,ncdof) eye(ncdof,ncdof); -
M(dof,dof)\K(dof,dof) -M(dof,dof)\C(dof,dof)];
            eigenvalues = sort(eig(AA));
            critical_i_old = critical_i;
if damped_NF>0.5
critical_est = abs(imag(eigenvalues))/NX;
else
critical_est = abs(eigenvalues)/NX;
end
            [delta_c,index_c] = min( abs( critical_est -
initial_estimates(icritical) ) );
            critical_i = critical_est(index_c);
if critical_i_old == 0
                rel_change = 2*convergence_tol;
else
                rel_change = abs( (critical_i -
critical_i_old)/critical_i_old );
end
            iteration = iteration + 1;
%     disp([icritical iteration 30*critical_i/pi])
end
        critical_speeds(icritical) = critical_i;
end
```

```
% Calculate the eigenvectors corresponding to the critical speeds if
% required

if nargout == 2
        mode_shapes = zeros(ndof,number_criticals);
for icritical = 1:number_criticals
            [Mb,Cb,Kb,zero_dof] =
bearmtx(model,critical_speeds(icritical));
            M = M0 + Mb;
            K = K0 + Kb + critical_speeds(icritical)*K1;
            C = C0 + Cb + critical_speeds(icritical)*C1;
            AA = [zeros(ncdof,ncdof) eye(ncdof,ncdof); -
M(dof,dof)\K(dof,dof) -M(dof,dof)\C(dof,dof)];
            [eigenvectors_i,eigenvalues] = eig(AA);
[eigenvalues,isort] = sort(diag(eigenvalues));
eigenvectors_i = eigenvectors_i(:,isort);
if damped_NF>0.5
critical_est = abs(imag(eigenvalues))/NX;
else
critical_est = abs(eigenvalues)/NX;
end
            [delta_c,index_c] = min( abs( critical_est -
critical_speeds(icritical) ) );
            mode_shapes(dof,icritical) = eigenvectors_i(1:ncdof,index_c);
end
end

end
```